CALIBRATION OF COMBINED BENDING-TORSION FATIGUE RELIABILITY RESEARCH MACHINES AND RELIABILITY DATA REDUCTION

by

Jeffrey Bentley McConnell

A Thesis Submitted to the Faculty of the

DEPARTMENT OF AEROSPACE AND MECHANICAL ENGINEERING

In Partial Fulfillment of the Requirements
For the Degree of

MASTER OF SCIENCE
WITH A MAJOR IN MECHANICAL ENGINEERING

In the Graduate College

THE UNIVERSITY OF ARIZONA

1 9 7 3

STATEMENT BY AUTHOR

This thesis has been submitted in partial fulfillment of requirements for an advanced degree at The University of Arizona and is deposited in the University Library to be made available to borrowers under rules of the Library.

Brief quotations from this thesis are allowable without special permission, provided that accurate acknowledgment of source is made. Requests for permission for extended quotation from or reproduction of this manuscript in whole or in part may be granted by the head of the major department or the Dean of the Graduate College when in his judgment the proposed use of the material is in the interests of scholarship. In all other instances, however, permission must be obtained from the author.

SIGNED: Jeffrey McConnell

APPROVAL BY THESIS DIRECTOR

This thesis has been approved on the date shown below:

D. B. Kececioglu

D. B. KECECIOGLU
Professor of Aerospace and Mechanical Engineering

August 7, 1973
Date

ACKNOWLEDGMENTS

The author wishes to express his sincere appreciation to Dr. Dimitri B. Kececioglu, Professor of Aerospace and Mechanical Engineering, The University of Arizona, whose help and guidance were invaluable in the preparation of this report.

TABLE OF CONTENTS

			Page
LIST OF ILLUSTRATIONS			viii
LIST OF TABLES			xi
ABSTRACT			xiii
CHAPTER			
1	INTRODUCTION		1
2	DESCRIPTION OF COMBINED BENDING-TORSION FATIGUE RELIABILITY RESEARCH MACHINES		13
	A.	General Description of Fatigue Machines	13
	B.	General Description of the Instrumentation	16
	C.	Detailed Description of Fatigue Machines and Instrumentation	17
		The Test Specimen	17
		The Collet Assembly	17
		Electric Motor	17
		Flexible Couplings	19
		Gear Box	19
		Method of Torquing	19
		Loading Frame	20
		Instrumentation	20
3	CALIBRATION OF RESEARCH MACHINES		29
	A.	Calibration Requirements	29
	B.	Bending Calibration	31
		1. Visicorder output from bending strain gages on toolholder versus true stress in toolholder	31
		Description of Test	31
		Test Setup	31
		Test Procedure	34
		The Data Reduction	36

TABLE OF CONTENTS--Continued

	Page
2. Visicorder output from bending strain gages in specimen groove versus true stress in specimen groove	41
Description of Test	41
Test Setup	42
Test Procedure	43
Data Reduction	43
2a. Experimental determination of the average stress concentration factor in specimen groove	48
3. Torque interaction into bending bridge output	50
Description of Test	50
Test Setup	51
Test Procedure	54
Data Reduction	54
4. Relationship between toolholder bending stress and specimen groove bending stress	60
4a. Toolholder strain gage output versus specimen strain gage output	62
Description of Test	62
Test Setup	62
Test Procedure	63
Data Reduction	63
4b. Toolholder bending stress versus specimen bending stress	69
Data-taking Procedure	73
C. Torque Calibration	77
1. Torque load versus Visicorder output	77
Description of Test	77
Test Setup.	77
Data Reduction	77
2. Bending interaction into the torque bridge output	83
Description of Test	83
Test Setup	83
Test Procedure	84
Data Reduction	84
2a. Effect of bending on torque bridge output - additional test	91
Description of Test	91
Test Setup	91
Test Procedure	91
Data Reduction.	92

TABLE OF CONTENTS--Continued

Page

D. Axial Effects 95

1. Effect of axial load on bending bridge output. 95
Description of Test 95
Test Setup. 96
Data Reduction 96
2. Measurement of the axial stress . . . 97
2a. Measurement of the axial stress as a function of bending load 97
Description of Test 97
Test Setup. 97
Test Procedure 98
Data Reduction 98
2b. Measurement of the axial stress as a function of torque load 101
Description of Test 101
Test Procedure 101
Data Reduction 102

E. Summary of Calibration Results 102

4 RESEARCH DATA REDUCTION 109

A. Conversion of Visicorder Outputs to Stress Levels 109
B. Reduction of Endurance Strength Data for $r_s = \infty$ and $r_s = 0.90$ 110
C. Generation of S-N Diagrams Using Distributional Stress Levels and Mean Cycles-to-Failure 117
D. Generation of Theoretical S-N Diagram . . 120
E. Comparison of Theoretical and Experimental S-N Curves 121

5 STRESS CONCENTRATION AND NOTCH SENSITIVITY EFFECTS 126

A. Stress Concentration 126
B. Notch Sensitivity Survey 127
C. Proposed Notch Sensitivity Determination 135

6 CONCLUSIONS 137

7 RECOMMENDATIONS 140

TABLE OF CONTENTS--Continued

		Page
APPENDIX A	DATA REDUCTION RESULTS FOR $r_s = \infty$	142
APPENDIX B	DATA REDUCTION RESULTS FOR $r_s = 0.7$ AND $r_s = 0.9$	148
APPENDIX C	OPERATING CHECKLIST FOR COMBINED BENDING-TORSION FATIGUE RESEARCH MACHINES	154
APPENDIX D	PROCEDURE FOR OPERATING COMBINED BENDING-TORSION FATIGUE RESEARCH MACHINES WITH COMBINED BENDING AND TORQUE LOADS	158
APPENDIX E	CALIBRATION OF NEW TORQUE GAGES FOR MACHINE #3, JUNE 1969	160
APPENDIX F	MAINTENANCE CHECKLIST FOR COMBINED BENDING TORSION FATIGUE RESEARCH MACHINES . .	167
SYMBOLS	. . . .	168
REFERENCES	. . . .	171

LIST OF ILLUSTRATIONS

Figure		Page
1	Mabie-Gjesdahl Fatigue Testing Machine . . .	9
2	Calibration Flow Chart	12
3	Combined Bending-torsion Fatigue Reliability Research Machine - Front View	14
4	Combined Bending-torsion Fatigue Reliability Research Machine - Top View	15
5	Loading Frame Analysis and Test Specimen . .	18
6	Bending Load Lever Arm	21
7	Strain Gage and Slip-Ring Arrangement . . .	22
8	Bending Moment Instrumentation	24
9	Torque Instrumentation	25
10	Torsional Stresses for One Gage	26
11	Test Setup for the Bending Cantilever Calibration	32
12	Test Setup for Torque Interaction into Bending Bridge Output.	52
13	Torque Interaction into Bending - Machine #1	57
14	Torque Interaction into Bending - Machine #2	58
15	Specimen Groove Output Versus Toolholder Output - Machine #1	66
16	Specimen Groove Output Versus Toolholder Output - Machine #2	67
17	Specimen Groove Output Versus Toolholder Output - Machine #3	68

LIST OF ILLUSTRATIONS--Continued

Figure		Page
18	Free Body Diagram of Toolholder	70
19	Laboratory Setup of Lever Arm, Pivot Point, Resisting Moment Measurement Experiment . . .	72
20	Scale Graduations of Measurement Experiment	75
21	Torque Output Versus Pan Weight - Machine #1	79
22	Torque Output Versus Pan Weight - Machine #2	80
23	Torque Output Versus Pan Weight - Machine #3	81
24	Bending Interaction into Torque - Machine #1	86
25	Bending Interaction into Torque - Machine #2	87
26	Bending Interaction into Torque - Machine #3	90
27	Bending Interaction into Torque at High Torque Level - Machine #2	94
28	Axial Output Versus Bending Load - Machine #1	100
29	Axial Output Versus Torque Load - Machine #1	104
30	Pan Weight Versus True Bending Stress for Endurance Strength for $r_s = \infty$	115
31	Pan Weight Versus True Bending Stress for Endurance Strength for $r_s = 0.90$	116
32	Applied Bending Stress Distributions for Stress Ratio of ∞	118
33	Applied Bending Stress Distribution for a Stress Ratio of 0.70 and Endurance Strength for a Stress Ratio of 0.90.	119
34	Fatigue Strength Versus Mean Cycles-to-Failure and Endurance Strength for $r_s = \infty$, 0.70, and 0.90, and the Theoretical S-N Diagram for $r_s = \infty$	122

LIST OF ILLUSTRATIONS--Continued

Figure		Page
35	Three-dimensional Distributional Goodman Fatigue Strength Surface Based on Research Results Reported here for 10^7 Cycles of Life	124
36	Notch Sensitivity of Normalized Steel Specimens	129
37	Notch Sensitivity of Quenched and Tempered Alloy Steel Specimens	130
38	Curves of Notch Sensitivity Versus Radius for Steels, Bending or Axial Loading. . . .	131
39	The Fatigue Notch Factor	132
40	Notch Sensitivity Charts for Steels and 245-T Wrought Aluminum Alloys Subjected to Reversed Bending or Reversed Axial Loads. .	133
41	Notch Sensitivity Curves for Materials in Reversed Torsion	134
42	Bending Interaction into Torque - Machine #3, June 1969	162
43	Torque Output Versus Pan Weight - Machine #3, June 1969	165

LIST OF TABLES

Table		Page
1	Instrumentation	27
2	Toolholder Output Versus Pan Weight Data for Bending Bridge Calibration	37
3	Toolholder Output Versus Pan Weight Data in Incremental Form for Bending Bridge Calibration in Terms of Change in Toolholder Output Divisions for 10.27 lbs. of Pan Weight	39
4	Calibration Specimen Groove Strain Gage Output Versus Pan Weight Data	44
5	Reduction of Machine #2 Data Given in Table 4	45
6	Reduction of Machines #1 and #3 Data Given in Table 4	47
7	Torque Output Versus Bending Output Data from Torque into Bending Interaction Calibration	55
8	Toolholder Versus Groove Bridge Output Data for Quasi-Static Calibration of Groove Stress	64
9	Table 8 Visicorder Divisions Converted to Strain in Toolholder and Specimen Groove	65
10	Torque Output Versus Pan Weight Data for Torque Bridge Calibration	78
11	Torque Reduction Table from the Results of Table 10	82
12	Bending Output Versus Torque Output Data for Bending into Torque Interaction Calibration	85
13	Bending Output Versus Torque Output Data at High Torque Level for Bending into Torque Interaction Calibration	93

LIST OF TABLES--Continued

Table		Page
14	Axial Output Versus Bending Output for Axial to Bending Interaction Calibration . . .	99
15	Axial Output Versus Torque Output for Axial Load into Torque Interaction Calibration . . .	103
16	The Calibration Coefficients for Each Research Machine	105
17	Stress Levels and Visicorder Divisions for $r_s = 3$ and Machine #1	108
18	Torque Output Versus Pan Weight Data for New Torque Gages, Machine #3, June 1969	161
19	Bending Output Versus Torque Output Data for New Torque Gages, Machine #3, June 1969 . . .	164

ABSTRACT

The combined bending-torsion fatigue reliability research machines, conceived, designed, and built at The University of Arizona are described. Three such machines are presently in operation at The University of Arizona. The calibration of these machines is presented in depth. Fatigue data generated with these machines for SAE 4340 steel grooved specimens subjected to reversed bending and steady torque loading are given. The data reduction procedure is presented. Finally, some comments are made about notch sensitivity and stress concentration as applied to combined fatigue.

CHAPTER 1

INTRODUCTION

The calibration effort and data reduction techniques for the Combined Bending-Torsion Fatigue Reliability Research Machines are presented here. Because of the complexity of the problem of determining the true bending stress and the true shear stress present in the groove of the test specimen, eight distinct calibrations had to be performed on each machine. A description of each calibration test, the test setup, the procedure, the data, and the data reduction are given for each calibration test. Then the need for each test is presented in Section 3.E where a calibration flow chart was developed to aid in the data reduction procedure. Specific calibration parameters for each machine were determined and their needs demonstrated. The calibration equations in bending were shown to be

$$\sigma_{out_{TH}} = K_{GR-TH} K_{BGR} \sigma_{true_{GR}}$$

$$\sigma'_{out_{TH}} = \sigma_{out_{TH}} + K_{T/B} \tau_{out_{TH}}$$

$$N_{vis_B} = \frac{N_{cal}\ N_a\ G\ R_{cal}}{E\ R_{gage}} \sigma'_{out_{TH}}$$

and the calibration equations in torque were shown to be

$$\tau_{true_{GR}} = \frac{\sigma_{true_{GR}}}{r_s \sqrt{3}}$$

$$\tau_{out_{TH}} = \frac{1}{K_{ts}} \frac{1}{K_T} \frac{C_{TH}}{J_{TH}} \frac{J_{GR}}{C_{GR}} \tau_{true_{GR}}$$

$$\tau'_{out_{TH}} = \tau_{out_{TH}} + K_{B/T} \sigma_{out_{TH}}$$

$$N_{vis_T} = \frac{N_{cal} \, N_a \, G \, R_{cal}}{E \, R_{gage}} \tau_{out_{TH}}$$

In addition, the static stress concentration factor for the notched specimen was determined to be 1.28.

For data reduction, the calibration flow chart was generalized and computerized. The data reduction program as well as all the data generated to date are presented. Sample calculations for the data reduction technique are given. Cycles-to-failure data reduction is not included in this report, and is the subject of another report.

The results of the data reduction are briefly presented in the form of S-N curves.

Lastly, the problem of notch sensitivity is discussed and a proposal made.

Prior to this research effort, the basic methodology for designing reliability into mechanical components by consideration of the interference of their stress-strength distributions was discussed by Kececioglu and Cormier [1]. Included in this paper was a discussion of Monte Carlo techniques for determining stress and strength distributions, given the distributions of the factors affecting them.

Freudenthal [2] wrote a paper in which structural unreliability was considered to be the probability, or risk, of failure. The safety factor was shown to be a distribution function which is the quotient of the strength to the stress, where both strength and stress are considered as statistical variables. Freudenthal, Garrelts, and Shinozuka [3] prepared a comprehensive report, along the same lines, which discussed in more detail the mathematical techniques required, the appropriate statistical distributions involved, and problems which remained to be solved. Several example problems in structural reliability were worked out, and an extensive bibliography was given. These efforts concentrated on simple fatigue and structural reliability.

The Battelle Memorial Institute and its Mechanical Reliability Research Center presented studies [4,5] which described some of the fundamental problems in mechanical reliability and suggested methods for their solution.

Mittenbergs [4] discussed the fundamental aspects of reliability engineering as they pertain to mechanical devices. He stated that the failure modes of mechanical elements were basically:

1. Deformation
2. Fracture
3. Instability.

He also asserted that many factors combine to determine the reliability of a mechanical part under such failure modes. The interaction of strength and load distributions was discussed. The Sixth Progress Report of the Mechanical Reliability Research Center [5] summarized a two-year research effort. This extensive research effort contained a thorough discussion of mechanical reliability, and attempted to quantify the relationships of various factors on such phenomena as creep and fatigue. An extensive bibliography was included.

The IIT Research Institute conducted a program in "Methods for Prediction of Electro-Mechanical System Reliability," [6]. The program was concerned with three major areas:

1. The study of prime mechanisms of failure in mechanical design. Specific items included fatigue, surface fatigue, wear, creep, and corrosion.
2. The application of failure mechanism and design information for the reliability evaluation of specific mechanical parts. Parts

included were gears, bearings, springs, and shafts.

3. The determination of mechanical system reliability in terms of individual part reliability figures.

A paper by M. J. Bratt, G. Reethof, and G. W. Weber of the Large Jet Engine Department, General Electric Company, entitled "A Model for Time Varying and Interfering Stress-Strength Probability Density Distributions with Considerations for Failure Incidence and Property Degradation" [7], provided a computer approach towards the solution of the time variant strength distribution case.

An extension of this study was made by Lipson, Sheth, and Disney [8], who conducted an extensive literature survey, gathered available fatigue data, and developed an analysis of the stress-strength interference theory using the Weibull distribution extensively.

The above works provided some interesting and valuable contributions to the problem of designing specified reliabilities into mechanical components. However, a number of important aspects of this problem remained to be investigated. The problem of time-variant stress and strength distributions needed further treatment. The effects of various factors, which are themselves distributions, on the distributions of the failure-governing stress and strength had yet to be fully explored. The development of a formal engineering design methodology for designing mechanical components had yet to be developed. Finally, much of the work in mechanical reliability theory suffered from a lack of statistically adequate data, due to a lack of test results on a large number of identical mechanical components.

The purpose of the current investigation is to fill in the gaps in the above-mentioned areas, with the following specific objectives:

1. Develop a formal engineering methodology for designing into mechanical components, subjected to combined-stress fatigue which involves time-dependent strength distributions, specified reliabilities.
2. Explore the methods of functions of random variables as applied to structural reliability.
3. Explore the methods available for determining failure-governing stress and strength distributions and develop new ones.
4. Explore the methods available for calculating the reliability once the failure-governing stress and strength distributions are known and develop new ones.
5. Develop and fabricate fatigue testing machines for reliability research, so that the explored

and developed methodologies described above can be demonstrated.

6. Pursue a test program with a statistically significant number of test specimens to obtain data from which these methodologies can be demonstrated.

A literature survey was made in order to locate fatigue testing machines to generate the desired, combined bending-torsion fatigue data. "References on Fatigue," was surveyed from 1955 to 1963 [9]. The only paper of interest was the "Symposium on Large Fatigue Testing Machines and Their Results" [10]. No testing machines capable of handling combined steady torque and reversed bending moment were found in the paper. Other references [11,12] were reviewed; information concerning combined-stress fatigue machines was not found.

"The Proceedings of the Society for Experimental Stress Analysis" [13] from 1945 to 1960 and "Experimental Mechanics" [14] from 1961 to December 1965 were reviewed in an attempt to locate a combined steady torque and reversed bending moment testing machine. Several fatigue testing machines were found, but only one was of direct interest to the NASA contract, a testing machine built by Mabie and Gjesdahl [15]. This machine used the four-square principle for applying a steady torque while the rotating beam principle was used to produce the bending moment.

The four-square principle is not a new principle for developing steady torque. Industrial corporations, such as gear manufacturers, speed reducer manufacturers, and coupling manufacturers, all use this principle to evaluate their products [16].

In the Mabie-Gjesdahl Machine this principle was used to develop a maximum steady torque of 6,000 in-lb; however, the machine was only operated at a maximum of about 2,000 in-lb of torque [15, p. 86]. At this loading the machine produced a high pitch whine [17], a result of the pitch line velocity of the spur gears being 3,000 to 4,000 feet per minute [18].

The pre-set torque could not be maintained. The steady torque, four-square principle was coupled with a reversed bending moment, as shown in Figure 1. The desired bending moment was applied to the test piece so as to simulate a simply-supported beam. Through the use of a hydraulic cylinder and associated equipment the required bending moment load was developed [17]. A reduction in bending moment occurred during testing as a result of hydraulic cylinder leakage. The bending moment was constant along the length of the test piece for a specific value of the bending load. The machine was designed for 5,000 in-lb and operated at a maximum of about 3,200 in-lb

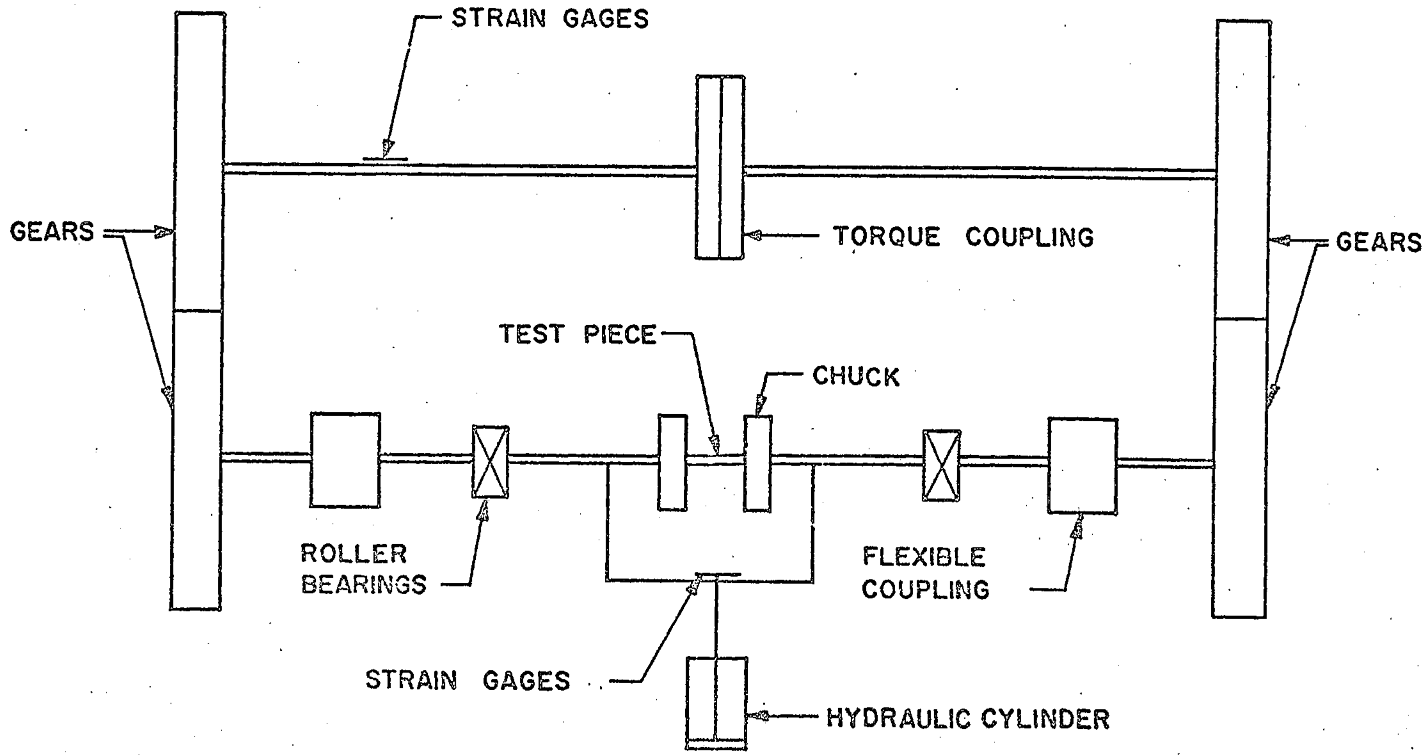

Fig. 1.--Mabie-Gjesdahl Fatigue Testing Machine

of bending moment. The reversed bending moment was gained through the rotating of the test piece in the four-square mechanism.

The Mabie-Gjesdahl test machine operated at 1,200 rpm. The machine was driven by a 3 hp, 1,200 rpm induction motor [19]. Mabie [17] furnished two assembly drawings [20,21] and additional design information as to the problem areas in his test machine. Mabie indicated that the disadvantages of this machine were that it was difficult to hold the torque and bending moment, and noise and vibration were present. However, the machine did not dissipate energy to apply torque to the specimen and operated on a proven principle.

The exact instrumentation on the Mabie-Gjesdahl test machine is not known. However, the torque values were measured and checked only in a static situation. The bending moment values were checked and related to the pressure gage on the hydraulic equipment. The load was applied statically and the pressure noted. Strain gages were used for the static torque measurements and also for the bending load. The bending load strain gages were mounted on the loading bar.

The test machine was calibrated dynamically with suitably mounted strain gages and slip-ring and brush assemblies. The exact equipment is not known. Correlation of these dynamic tests was made to the stresses obtained through calculations and an 8-12% error was noted [15]. Correspondence with Mabie [22] indicated that the commercially purchasable components exceeded $5,000.00.

With these thoughts in mind, test machines similar to the Mabie-Gjesdahl principle were conceived, designed and built at The University of Arizona, starting the fall of 1965.

Three combined bending-torsion fatigue reliability research machines are presently in operation at The University of Arizona. A research program is being conducted for the National Aeronautics and Space Administration under the direction of Dr. Dimitri Kececioglu at The University of Arizona, Tucson, Arizona, and Mr. Vincent R. Lalli at the NASA Lewis Research Center, Cleveland, Ohio. The description of these test procedures, test data and their reduction presented here are part of this research effort. The objective of this report is to obtain the calibration parameters presented in Figure 2. The experimental tests which must be run to determine these parameters are described. The data reduction technique is also given. The problem of stress concentration in the notch of the test specimens and the associated notch sensitivity are discussed, and recommendations for future work are made.

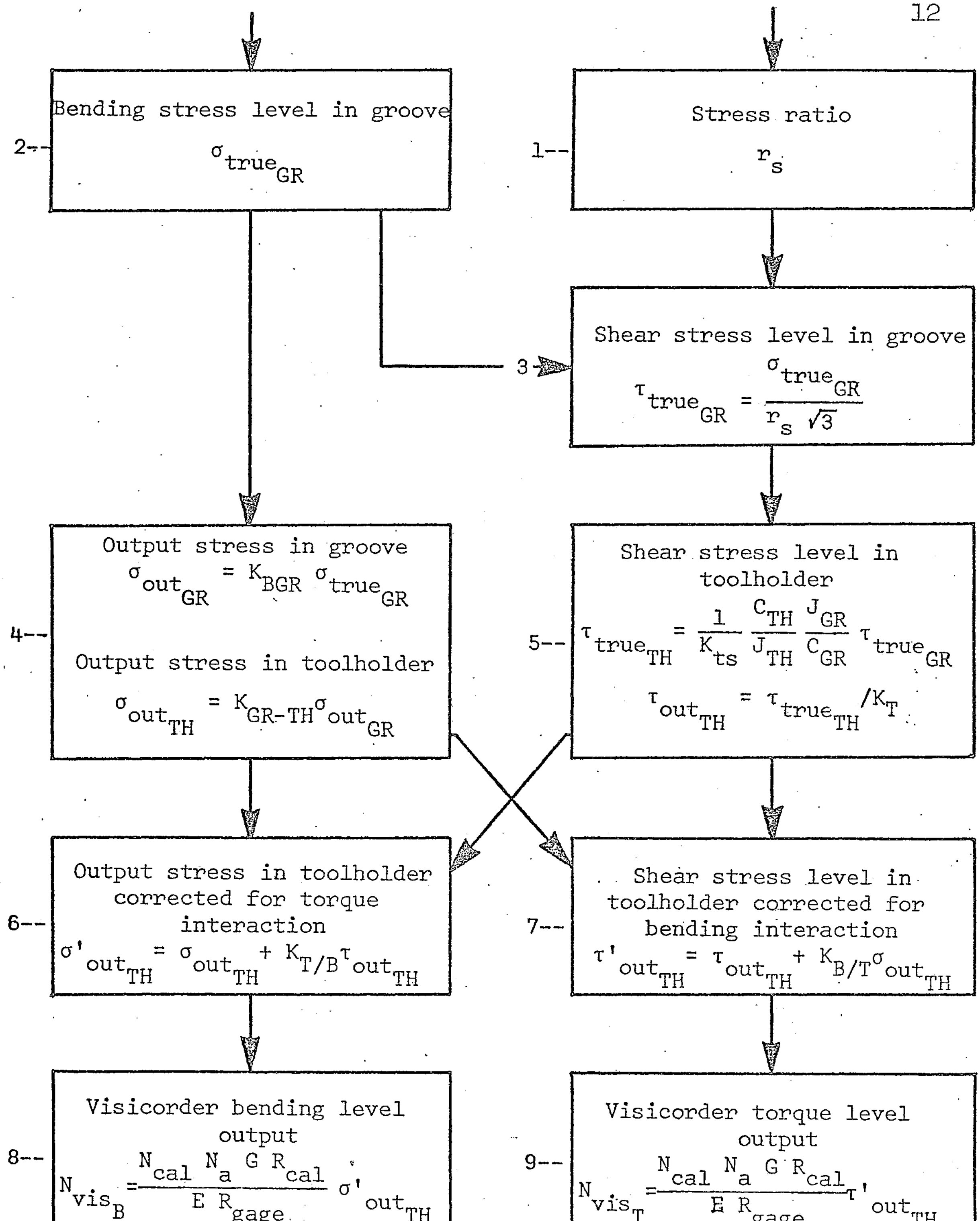

Fig. 2.--The Calibration Flow Chart

CHAPTER 2

DESCRIPTION OF COMBINED BENDING-TORSION FATIGUE RELIABILITY RESEARCH MACHINES

The combined bending-torsion fatigue reliability research machines are designed to simulate a shaft in service. The objective of the immediate research program is to examine the fatigue life of specimens made of SAE 4340 steel under combined loadings. The specimens are subjected to reversed bending and steady torque applied to a rotating specimen with a stress concentration, which produce combined bending-torsion stress, or combined-stress, fatigue.

A. General Description of Fatigue Machines

Each fatigue machine consists of a two-section, rotating shaft with a test specimen locked in the center, as shown in Figures 3 and 4. The horizontal shaft is coupled at each end to allow for relatively free deflection when the specimen is loaded. A seven and one-half horsepower, 1,800 rpm motor powers the shaft. The bending load is applied to the specimen by means of two yokes, one each on two bearings located symmetrically about the

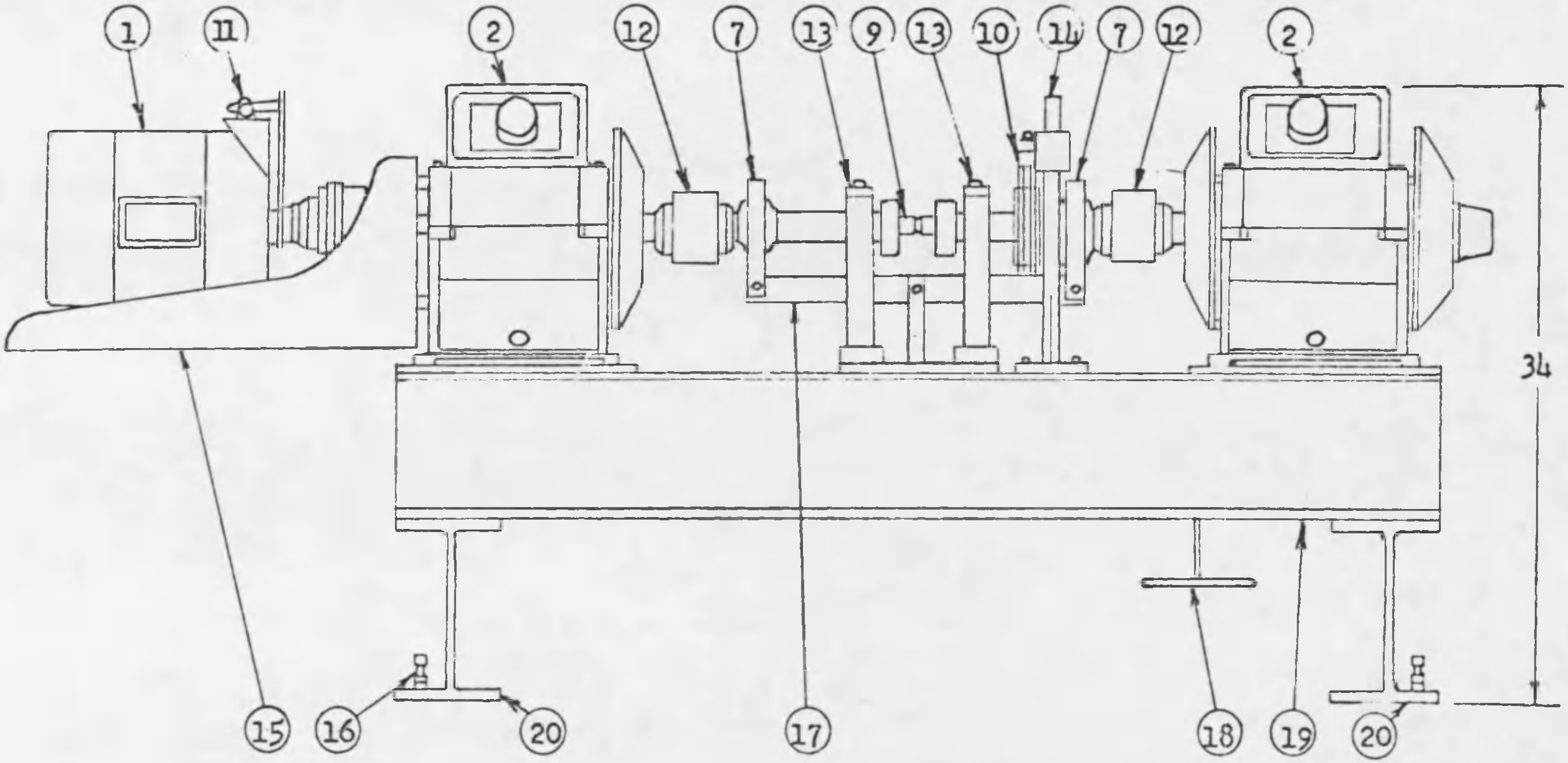

1. Motor
2. Gearboxes
7. Loading Frame Bearing
9. Test Specimen
10. Slip Rings and Brushes
11. Counter
12. Coupling
13. Safety Bridge
14. Brush Holder
15. Motor Bracket
16. Mount Bolts
17. Loading Frame
18. Weights
19. Machine Mount
20. Floor Mounts

Fig. 3.--Combined Bending-torsion Fatigue Reliability Research Machine - Front View

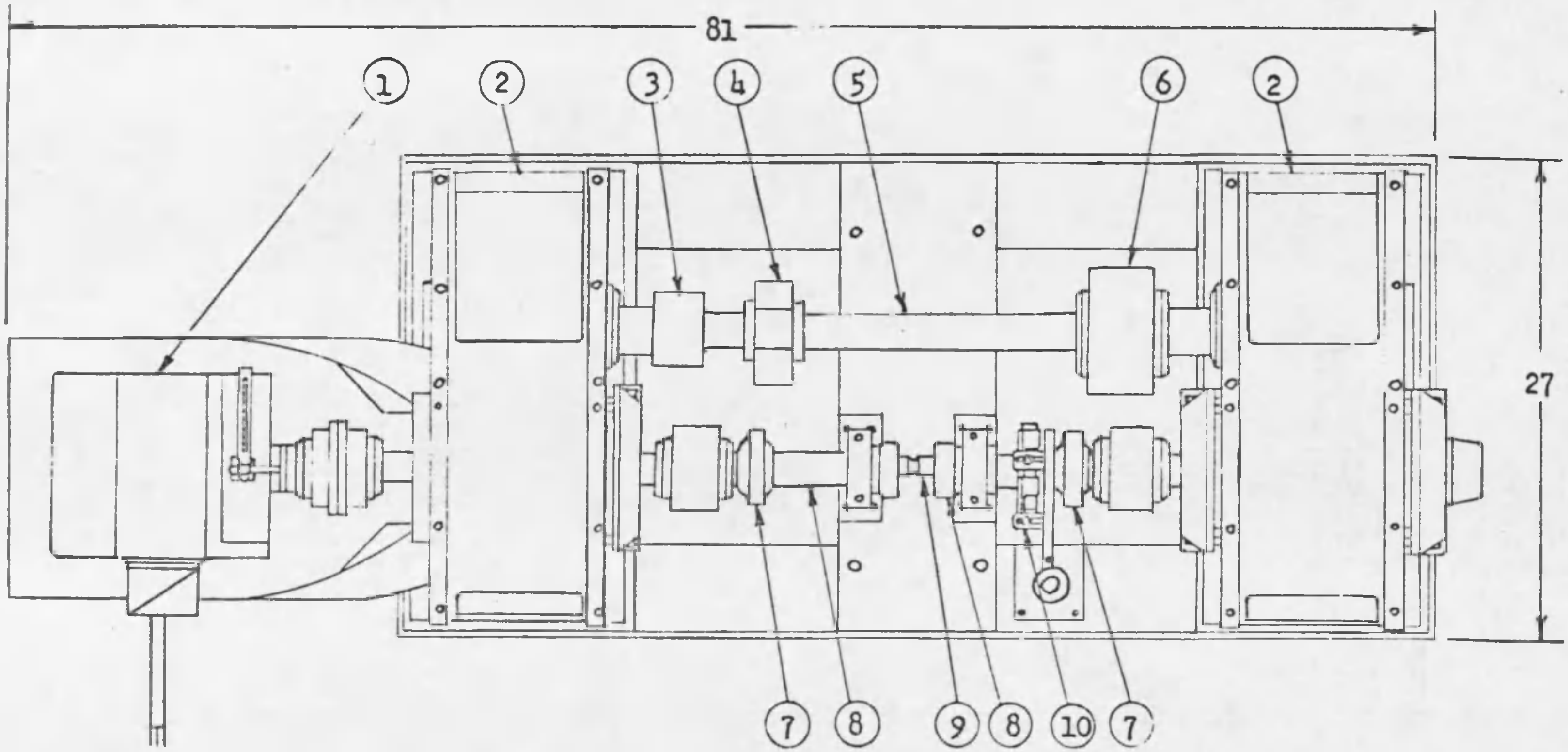

1. Motor
2. Gearboxes
3. Coupling
4. Infinite Indexer
5. Backshaft
6. Coupling
7. Loading Frame Bearing
8. Straight Shank Toolholder
9. Test Specimen
10. Slip-Rings and Brushes

Fig. 4.--Combined Bending-torsion Fatigue Reliability Research Machine - Top View

specimen on two commercial toolholders. Below the shaft, the yokes are connected by a horizontal link, which concentrates the load at a single vertical link in the center. The vertical link is then connected to either a long or a short loading lever arm. These loading arms make possible the application of a great range of bending stresses in the specimen groove, by means of pan weight applied at the end of the loading arm. One pound of pan weight is approximately equal to two thousand psi in the groove. The torque is applied by means of a commercial Infinit-Indexer which is located on the back shaft of the machine.

B. General Description of the Instrumentation

Strain gages are located on one side of the main shaft, or toolholder, immediately adjacent to the specimen. There are two four-gage bridges -- one for bending and one for torque. Next to the gages is a slip-ring brush assembly which electrically connects the rotating shaft with the stationary instrumentation. The output is amplified and permanently recorded photographically by means of a Minneapolis-Honeywell Visicorder.

C. Detailed Description of Fatigue Machines and Instrumentation

The Test Specimen

The test specimen, shown in Figure 5, is six inches long and is composed of SAE 4340 steel. Its major diameter is 0.750 inches. A stress concentration factor is incorporated in the center by means of a groove, giving a minor diameter of 0.500 inches. The radius of the groove is 0.150 inches. A keyway is located at each end of the specimen for the positive application of the torque.

The Collet Assembly

The specimen is rigidly held in the drive shaft with a collet-type toolholding fixture. This makes it possible to rapidly install and remove specimens. The Balas toolholder, Part No. S16-8"-C12, with collet, Part No. c-12, was used for this purpose. The holder was altered slightly so that the test specimen key would fit properly. The key prevents relative motion between the specimen and the collet, thus enabling the positive transmission of torque.

Electric Motor

The fatigue machine is powered by a General Electric, induction, squirrel cage, 440-volt, three-phase, Type K, Tri-Clad, 700-line motor. This motor has a NEMA 213T frame. It fulfills the design requirements of 7.5

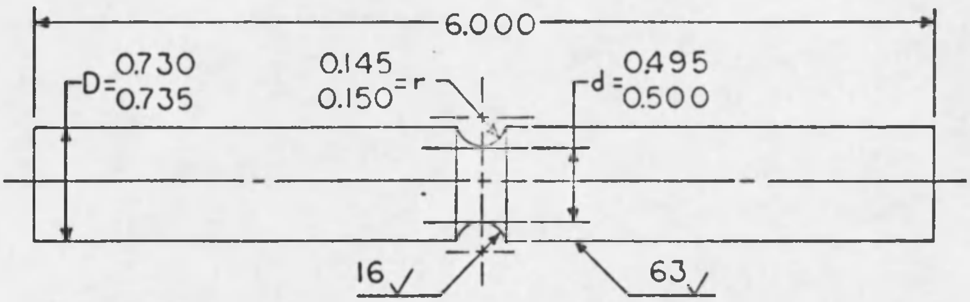

a) UANASA TEST SPECIMEN
6700-B-D02

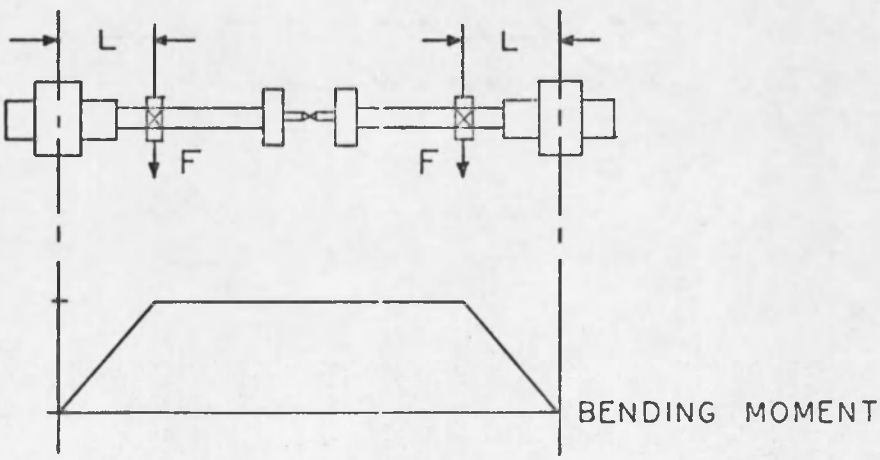

b) LOADING FRAME ANALYSIS

Fig. 5.--Loading Frame Analysis
and Test Specimen

horsepower, 1,800 rpm, 440-volt, 3-phase motor. The control system consists of a magnetic starter with an off-on push button and the proper fuses.

Flexible Couplings

Sier-Bath, all steel, flexible couplings are used because of their ability to transmit torque and allow relative movement of shafts holding the test specimen for proper transmission of the bending moment. In addition, they are small in size and relatively low in cost. There are two Sier-Bath couplings located at either end of the two halves of the front shaft and a larger one on the back shaft. They are shrunk-fit on the shafts.

Gear Box

A Falk Corporation gear reducer box is used. It has a mechanical horsepower rating of 210 horsepower and a thermal rating of 272 horsepower, with cooling fans. Its speed is 1,800 rpm, and it has a AGMA gear ratio of 1.84.

Method of Torquing

The torque is applied to the specimen by means of a HDUI-200 Infinit-Indexer made by the Harmonic Drive Division of United Show Machinery Corporation, Beverly, Massachusetts. The Infinit-Indexer has a flexible circular gear rotating within a slighly elliptical flexible, spline-like, outer gear. At the major axis the gear teeth do not mesh. When the shaft turns, the inner gear advances very slightly with respect to the outer gear inducing a steady torque. The torque level is adjusted by turning a large hexagonal shell on the outside housing of the Indexer with respect to the shaft.

Loading Frame

The loading frame is capable of producing a 3,540 in-lb bending moment in the specimen groove. There are two bearings located on each side of the front shaft. They are spherical, roller bearings with a tapered inside diameter capable of a maximum of 3° misalignment. The bearings require adapter sleeves and are SKF from service catalogue No. 450. The bearing housings are D/N UANASA-6700-E-006 type and are press fitted on to the bearings. Below the front shaft is located a T-shaped frame which joins the bearing housings to the essentially horizontal, loading lever arm. The specifications of the lever are given in Figure 6.

Instrumentation

Strain gages are used on the toolholder to monitor the bending and torque loads. They are not located in the specimen groove, but rather on the toolholder directly behind the collets as shown in Figure 7. The reason for this is two-fold:

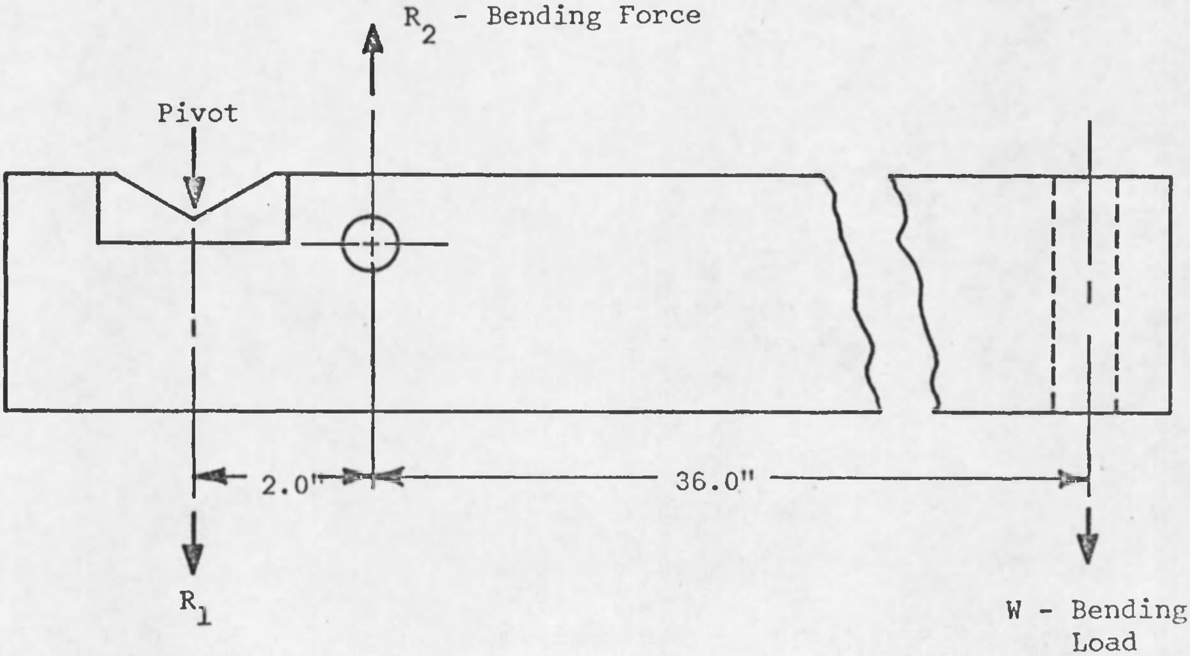

Fig. 6.--Bending Load Lever Arm

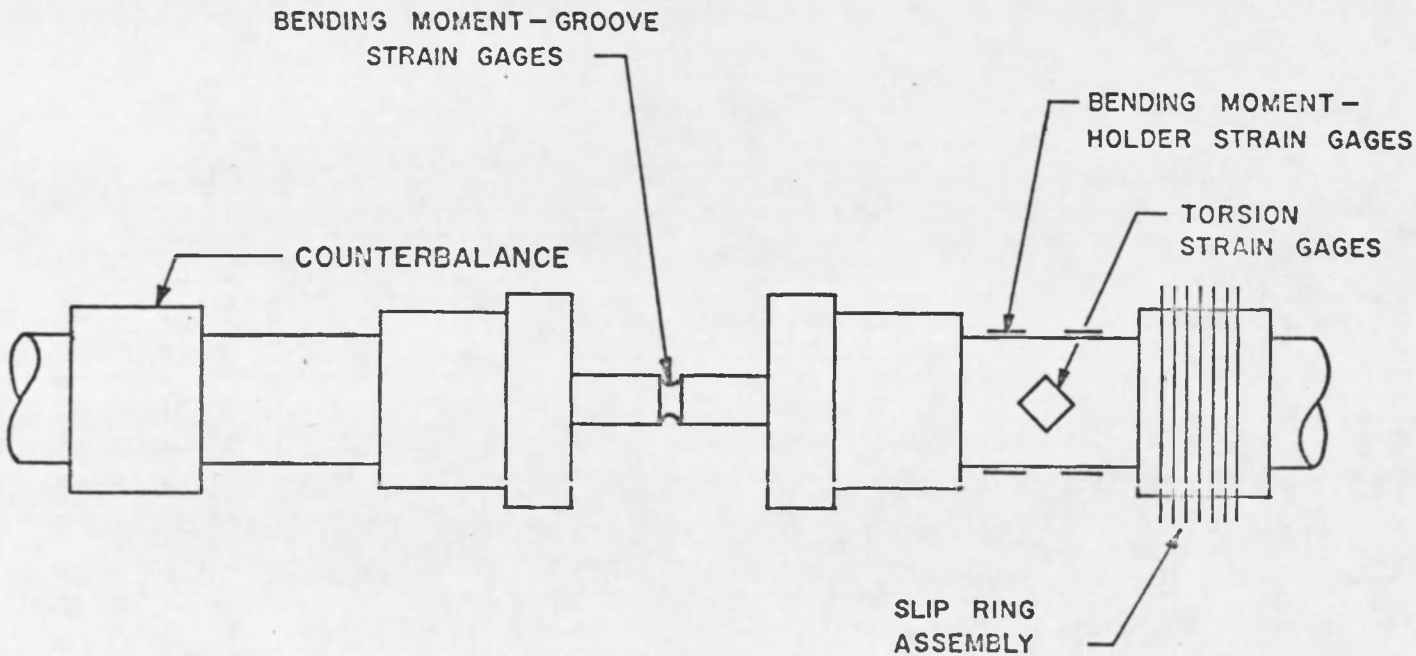

Fig. 7.--Strain Gage and Slip-Ring Arrangement

1. It is extremely difficult to mount strain gages in the limited space of the specimen groove.
2. Since the specimens are not reusable, the gages are not reusable also.

The positioning and electrical circuitry for the four-gage bending bridge is given in Figure 8. The strain gage bridge arrangement for torque is shown in Figure 9. Torque is measured by the method shown in Figure 10. These are double-gages, 90° apart and all in one piece. They are so mounted on the toolholder surface that the two gages make 45° with the toolholder axis of rotation. Table 1 contains the specifications of all the gages, as well as of the other electrical components. The slip-ring assembly is located adjacent to the strain gages, as shown in Figure 7. The slip-ring and brushes used are Breeze AJ-8005-A8 type. The slip-rings are counterbalanced with an aluminum collar of equal weight and nearly equal dimensions located on the other toolholder, as shown in Figure 7. The amplifiers, galvanometers and recorder are matched units consisting of a Honeywell Model 119 carrier amplifier, M1650 galvanometers and a Model 906 C-1 recorder (Visicorder). This is the equipment used to amplify and record the output from the bending and torque gages.

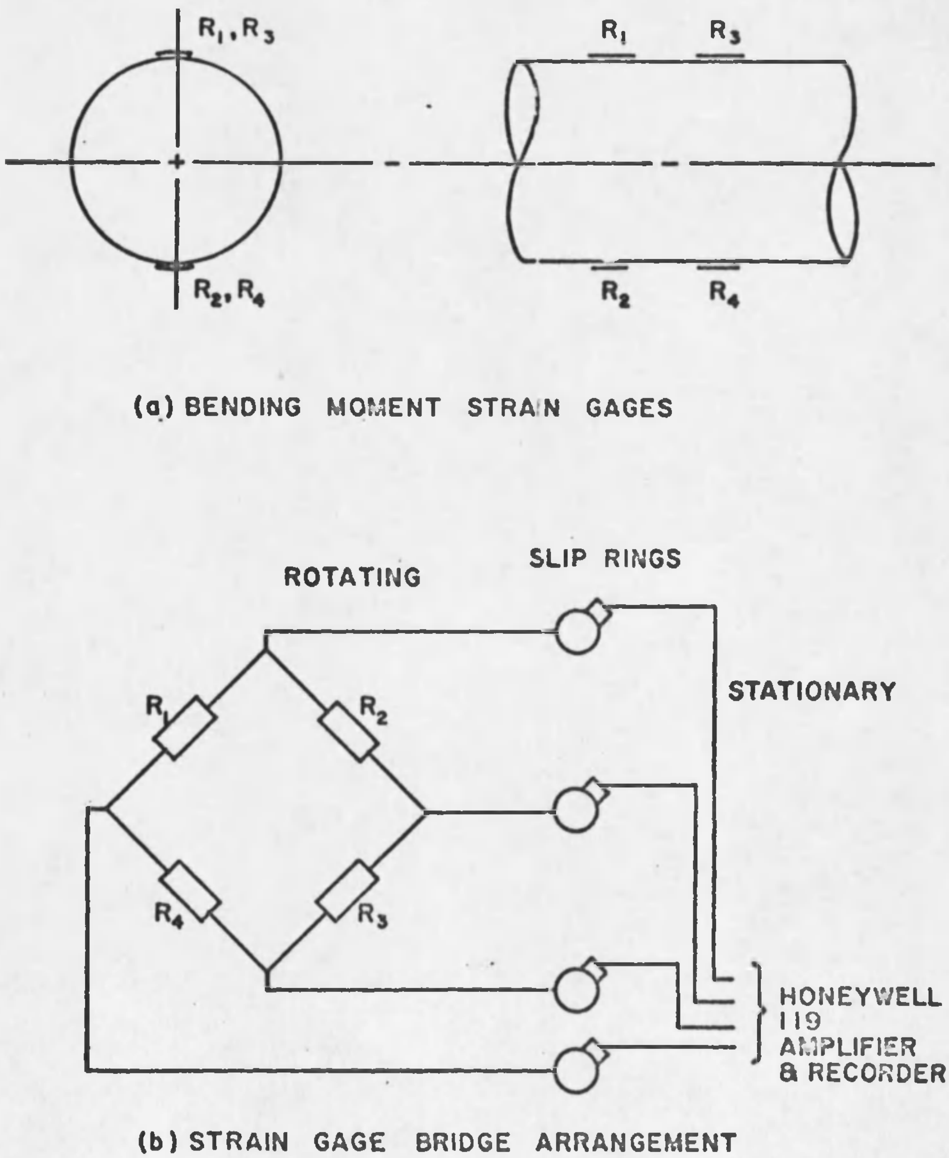

Fig. 8.--Bending Moment Instrumentation

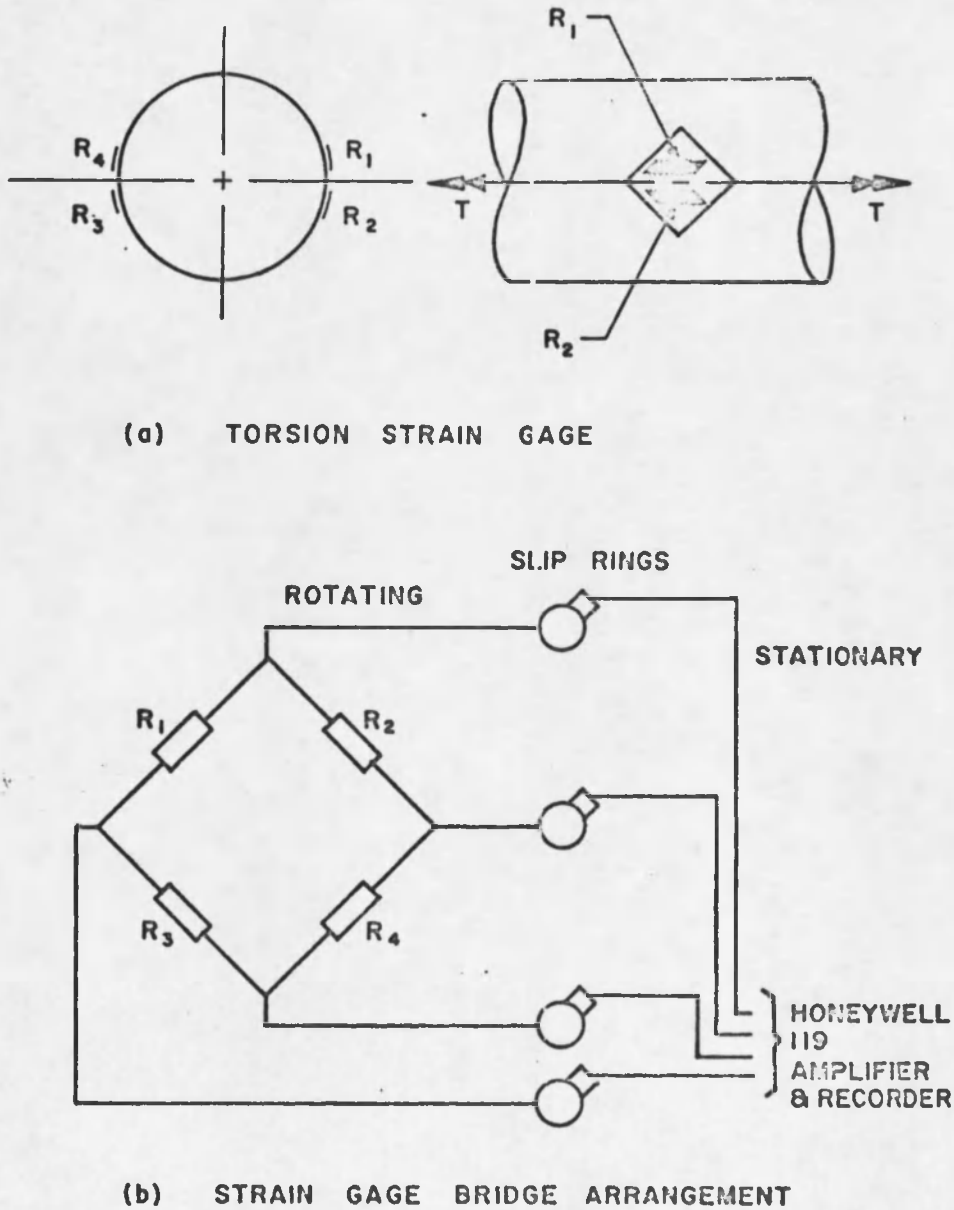

Fig. 9.--Torque Instrumentation

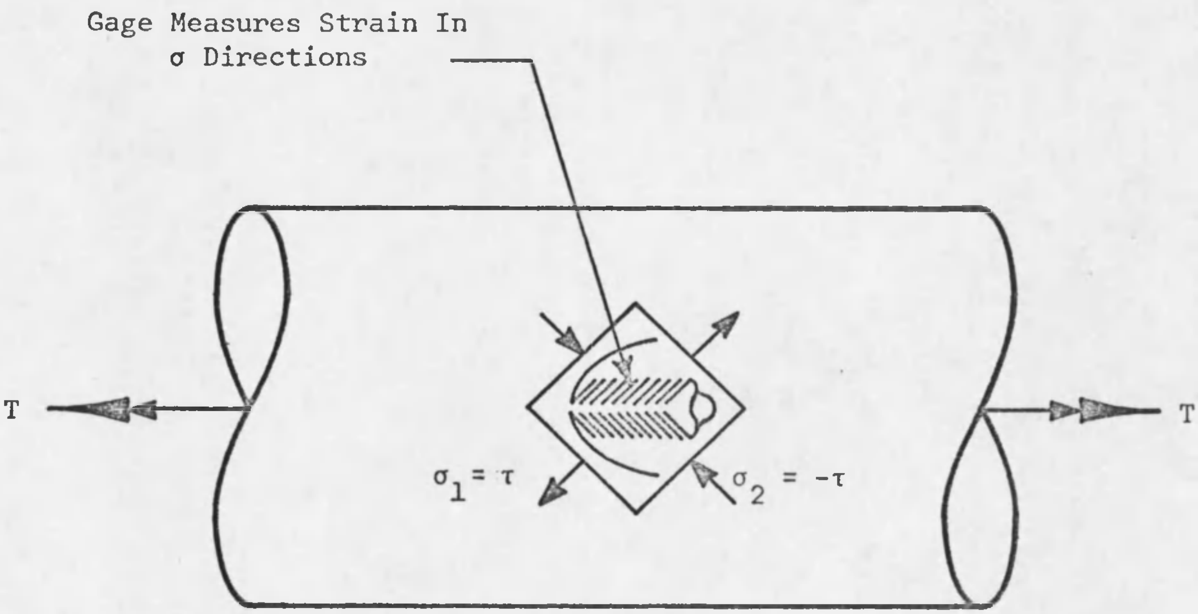

Fig. 10.--Torsional Stresses for One Gage

Table 1. Instrumentation

Name	Part Number	Manufacturer	Catalogue Number	Quantity	Remarks
Metalfilm strain gages with leads	324B-190	The Budd Co. Instruments Division	BG 2400	4	Bending moment-shank of tool-holder
Metalfilm strain gages with leads	3 x 4 - M15E-240	"	"	2	Bending moment groove of speci-men
Metalfilm strain gages with leads	C6-121-R2VC	"	"	2	Torque-shank of Toolholder
Slip rings and brushes	AJ-8005-A8	Breeze Cor-poration, Inc.	66SR	1	Transfer of data
Visicorder	906 C-1	Honeywell	D-2009	1	With grid line system, 14 mag-netic assembly channels

Table 1. Instrumentation--Continued

Name	Part Number	Manufacturer	Catalogue Number	Quantity	Remarks
Galvanometer	M1650	Honeywell	D-2007	6	0-5000 cps
Amplifier	119	"	D-2005	6	Carrier and linear/integrating system with carrier channels 0-5000 cps

CHAPTER 3

CALIBRATION OF RESEARCH MACHINES

A. Calibration Requirements

It was desired that the bending stress and shear stress in the specimen groove be accurately known for each specimen. These two stresses cannot be monitored directly because it is not possible to locate strain gages directly in the specimen groove since each fatigue failure would destroy the gages. This would necessitate replacement of the gages after each test run. Therefore the shear and bending stresses must be determined indirectly through the use of strain gages located on the toolholder shaft adjacent to the specimen.

The complete calibration procedure takes into account the following complications:

1. Since the strain gages are located on the toolholder rather than in the specimen groove, the groove stress must be calibrated against the strain gage output.
2. The specimen contains a groove, which introduces an additional unknown, the stress concentration factor. This value can either

be taken from published data or determined through additional calibration.

3. The torque and bending gages may be damaged during installation and require calibration against a standard.
4. The torque and bending gages may be slightly misaligned during installation, and there may be interference or interaction between the torque and bending outputs.
5. There may be an axial force present in the specimen due to the geometry of the couplings and the loading frame. This axial force could be a function of the torque or the bending load, or both.

The above suggests that the following calibrations be performed:

1. Calibration of the bending gages in terms of bending stress versus Visicorder output.
2. Calibration of the bending stress in the specimen groove versus Visicorder output.
3. Torque interaction into the bending bridge.
4. Toolholder strain gage bending output versus specimen strain gage bending output.
5. Calibration of the torque gages in terms of shear stress versus Visicorder output.

6. Bending interaction into the torque bridge.
7. Axial interaction into bending of the specimen groove gages.
8. Measurement of any axial force from torque and bending moment.

These calibrations are explained in detail on the following pages.

B. Bending Calibration

1. Visicorder output from bending strain gages on toolholder versus true stress in toolholder

Description of Test

This involved the calibration of the Visicorder output in bending against the true bending stress. The true bending stress was obtained by introducing a known bending moment at the toolholder strain gages. In order that the bending moment at the gages be accurately known, it was desirable that the test setup be as simple as possible in order that the error introduced was small when calculating the bending moment, and, subsequently, the bending stress.

Test Setup

The laboratory setup is shown in Figure 11. The slip-ring side of the toolholder was removed from one of the fatigue machines. The toolholder was locked down,

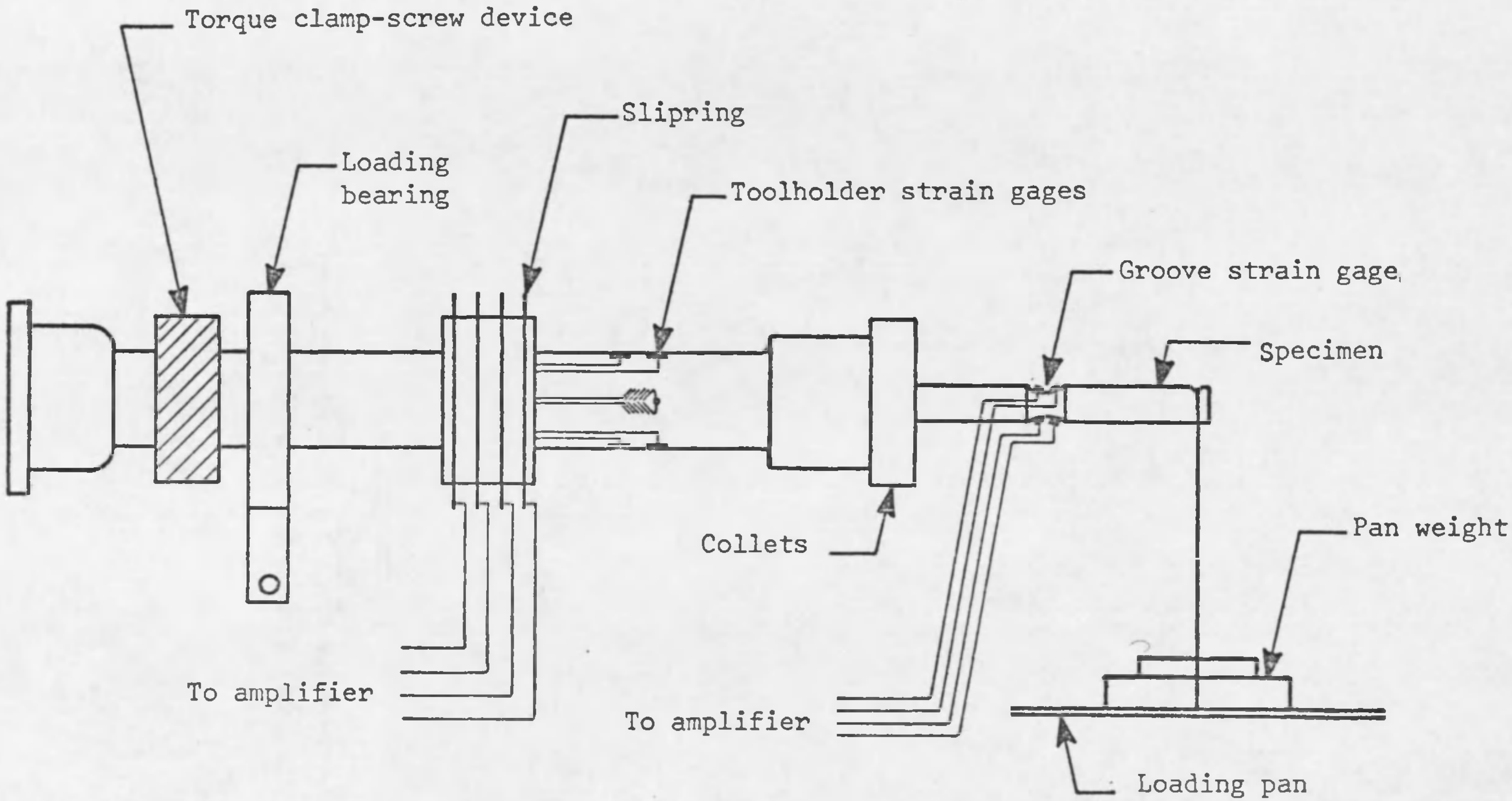

Fig. 11.--Test Setup for the Bending Cantilever Calibration

cantilever fashion, at the coupling end of the shaft. This was accomplished by gripping the toolholder shaft with a torque clamp-screw device between the loading bearing housing and the coupling. The screw end of the torque device was then locked in a vise on a laboratory table, thus securing the toolholder in a horizontal position. Next, a small notch was machined near the end of a test specimen, and the specimen was installed in the collet of the toolholder. The purpose of the notch was to hold the wire which supports the loading pan in position. Therefore, the specimen was positioned so that the notch was on top.

Electrical connection between the toolholder bridge and the amplifier was made with the use of thin uninsulated wire which was wedged between the silver plates and the di-electric on the appropriate arms of the slip-ring assembly. The opposite end of the wires were soldered to the correct leads of a bending bridge amplifier cable, after having been removed from the brush terminals of one of the fatigue machines.

The toolholder was removed from the clamp-screw device and placed in a vertical position, resting on the coupling. This insured that there was no bending on the strain gages while the electrical equipment was zeroed and balanced. The Visicorder was zeroed and the bending bridge balanced according to the standard laboratory procedure. A five-hundred-thousand ohm calibration resistance was used for twenty-five Visicorder calibration divisions. These calibration divisions were established left and right of zero bending in accordance with standard procedures.

Next, the toolholder shaft was again clamped in the cantilever position, this time making sure that the bending gages were located directly on the top and bottom of the toolholder. This was accomplished in two ways:

(1) A visual check to see that the gages were in the proper positions.

(2) With the toolholder gripped loosely and free to rotate, the shaft was moved slightly to see where the Visicorder bending output peaks and then clamped in that position.

It was necessary to have the gages aligned in this manner because the bending load was to be applied vertically, and this was the only position in which the bending gages will record full output. Finally, a stout wire was hung in the specimen notch and was attached to a loading pan.

Test Procedure

Weight was added to the loading pan in ten-pound increments until sixty pounds was reached. Then weight was removed in ten-pound increments until zero pan weight was again reached. The static strain gage output was monitored at each bending level. The Visicorder output was carefully watched to see that the Visicorder output returned to the same level each time zero pan weight was reached. This insured that there was no electrical drift occurring in the amplifier. Since the lever arm distance for application of the bending moment to the toolholder gages was about seven inches and the maximum pan weight was sixty pounds, the bending moment only reached about 420 inch pounds. This was a good deal below the operating bending moment and therefore the amplifier strain gage system was extremely sensitive in this low range of operation. Because of the great sensitivity it was necessary to alter the test plan for some runs because of bending zero drift and other small problems. The sequence of the pan weights was not important as long as at least twelve data points were taken. After changing the pan weight, a wait of up to ten minutes was sometimes necessary before taking the Visicorder run in order for the electrical system to reach equilibrium. This test procedure was applied to the toolholder arms of all three fatigue machines.

It was important that the lever arm distance, the distance between the loading wire and the geometric center of the toolholder gages, be recorded before the test system was torn down.

The Data Reduction

The standard procedure for reducing data of the kind presented in Table 2 is to plot toolholder output versus pan weight and fit a straight line to the points; then convert the pan weight axis to true bending stress at the toolholder and the output axis to apparent bending stress. However, these data were reduced using an analytical incremental method. This method determines the average increase in Visicorder output per unit increase in pan weight. This is the slope of the above-mentioned curve. Since strain gage outputs are linear and are zero for zero load, it was not necessary to calculate the bending moment produced by the dead weight of the toolholder, thus eliminating a major source of error.

Looking at the data, it can be seen that the pan weights were not taken in ten-pound increments as previously stated. When the weights were calibrated against a standard, they were all found to be 10.27 pounds. These same weights were used throughout the entire calibration program.

Table 2. Toolholder Output Versus Pan Weight Data for Bending Bridge Calibration

	MACHINE #1		MACHINE #2		MACHINE #3	
Data Point Number	Tool-holder Output div.	Pan Weight lbs.	Tool-holder Output div.	Pan Weight lbs.	Tool-holder Output div.	Pan Weight lbs.
1	2.2	0	3.5	0	2.4	0
2	13.9	30.81	6.8	10.27	14.4	30.81
3	25.6	61.62	10.3	20.54	23.6	61.62
4	17.8	41.08	13.5	30.81	18.6	41.08
5	9.9	20.54	17.2	41.08	22.4	51.35
6	21.3	51.35	21.0	51.35	7.0	10.27
7	5.8	10.27	24.9	61.62	10.8	20.54
8	2.1	0	20.8	51.35	3.0	0
9	9.7	20.54	17.1	41.08	10.7	20.54
10	17.3	41.08	13.4	30.81	22.1	51.35
11	25.1	61.62	10.0	20.54	18.5	41.08
12	21.2	51.35	6.0	10.27	26.1	61.62
13	13.3	30.81	2.1	0	14.4	30.81
14	5.8	10.27			6.7	10.27
15	2.0	0			2.7	0
16	5.6	10.27			18.1	41.08
17	17.1	41.08			25.8	61.62
18	24.8	61.62			6.5	10.27
19	13.2	30.81			14.3	30.81
20	21.0	51.35			10.4	20.54
21	9.5	20.54			21.8	51.35
22	1.7	0			2.5	0

Visicorder Calibration Resistances:
- Machine #1 - 500 kΩ at 24.9 divisions
- Machine #2 - 500 kΩ at 25.2 divisions
- Machine #3 - 500 kΩ at 25.0 divisions

First, the data were retabulated in incremental form as shown in Table 3. Note that the size of the strain increments is roughly constant, not a function of pan weight; and therefore, the assumption that the data are linear is a good one.

The arithmetic average of the data was determined for each machine. These averages have the units Visicorder divisions per 10.27 pounds. They had to be converted to true stress per Visicorder output stress, a useful calibration parameter, which was the slope of the desired curve. The toolholder ouput can be converted to incremental output bending stress by

$$\Delta\sigma_o = \frac{E\ R_{gage}}{N_a\ G\ R_{cal}} \cdot \frac{\Delta N_{vis}}{N_{cal}} \tag{1}$$

where $\Delta\sigma_o$ = incremental output bending stress,

E = Young's Modulus for SAE 4340 steel = 30×10^6 psi,

R_{gage} = resistance of the bending gage = 190Ω,

N_a = number of active arms in the strain gage bridge = 4,

G = gage factor = 3.23,

R_{cal} = the calibration resistance = 500 kΩ,

ΔN_{vis} = the incremental Visicorder output,

N_{cal} = the Visicorder calibration divisions.

Table 3. Toolholder Output Versus Pan Weight Data in Incremental Form for Bending Bridge Calibration in Terms of Change in Toolholder Output Divisions for 10.27 Lbs. of Pan Weight

Data Point Increment	Machine #1	Machine #2	Machine #3
1-2	3.90	3.3	4.00
2-3	3.90	3.5	3.96
3-4	3.90	3.2	3.85
4-5	3.95	3.7	3.80
5-6	3.80	3.8	3.85
6-7	3.87	3.9	3.80
7-8	3.70	4.1	3.90
8-9	3.60	3.7	3.85
9-10	3.80	3.7	3.60
10-11	3.90	3.4	3.60
11-12	3.90	4.0	3.80
12-13	3.95	3.9	3.90
13-14	3.75		3.85
14-15	3.80		4.00
15-16	3.60		3.85
16-17	3.83		3.85
17-18	3.85		3.86
18-19	3.86		3.90
19-20	3.90		3.90
20-21	3.83		3.80
21-22	3.90		3.86
Average	3.838	3.683	3.850

The resulting output stresses for each machine were:

$$\Delta\sigma_{o_1} = 135.9 \text{ psi},$$

$$\Delta\sigma_{o_2} = 129.9 \text{ psi},$$

$$\Delta\sigma_{o_3} = 135.6 \text{ psi}.$$

where the subscripts indicate the machine numbers. These values were the apparent increase in bending strain when a 10.27 pound weight was loaded on the pan. It remained to calculate the actual bending stress increase for 10.27 pounds of pan weight. The equation was:

$$\Delta\sigma_T = \frac{L\Delta WC}{I}$$

where $\Delta\sigma_T$ = incremental actual bending stress,

L = lever arm distance,

ΔW = incremental pan weight = 10.27 pounds,

C = radius of the toolholder = 1.0 inch,

I = moment of inertia of the toolholder cross-section = 0.74 in^4.

The lever arm distances for each of the three machines were:

L_1 = 8.745 in,

L_2 = 8.199 in,

L_3 = 8.237 in.

Performing the calculations, the true stresses for each machine per 10.27 pounds of pan weight were:

$$\Delta\sigma_{T_1} = 140.0 \text{ psi},$$

$$\Delta\sigma_{T_2} = 131.5 \text{ psi},$$

$$\Delta\sigma_{T_3} = 132.2 \text{ psi}.$$

Forming the ratio, $K_{BTH} = \dfrac{\Delta\text{OUTPUT (apparent) STRESS}}{\Delta\text{TRUE STRESS}}$

$$K_{BTH_1} = 0.967,$$

$$K_{BTH_2} = 0.902,$$

$$K_{BTH_3} = 0.972.$$

These parameters will not be used directly in the calibration procedure presented in Section 3-E but have a variety of uses in the daily operation of the fatigue machine. This parameter can be used to determine true stress at the toolholder gages and is extremely useful to have on hand.

2. Visicorder output from bending strain gages in specimen groove versus true stress in specimen groove

Description of Test

In a previous section, it was pointed out that the fatigue test specimen does not ordinarily contain strain gages in the groove. But for calibration purposes, two test specimens with bending gages in the grooves were prepared. Before these specimens can be used in the calibration of the fatigue machines, their bridge outputs must first be compared with the analytically determined true bending stress in the specimen groove.

Since this calibration is identical in nature to the toolholder strain gage calibration presented in the previous section, the same test setup was used. Indeed, it was possible to run the two tests simultaneously.

Test Setup

Instead of using an ordinary test specimen in the bending cantilever test setup, the specimen with the gages in the groove was used. It was locked in the collet with the bending strain gages on the toolholder and in the groove lined up. Once again, a notch was machined at the extreme end of the test specimen in order to guide the loading wire and maintain a constant lever arm.

A second amplifier cable was removed from the brush terminals of a fatigue machine and positioned near the cantilever system. Thin wire leads were connected from the strain gage terminals to the cable in the proper arrangement for a two-gage bridge. The amplifier is designed to accommodate a two-gage bridge as well as a four-gage bridge. All connections were soldered and insulated.

Test Procedure

The test procedure was identical to that in Section 3-B-1; however, instead of monitoring just the toolholder output, the groove output was also recorded. The calibration resistance used for the groove amplifier channel was 30 kΩ with the Visicorder set at 25.0 divisions. Upon completion of the test, both lever arm distances were recorded.

Data Reduction

A glance at the data in Table 4 shows that the groove outputs for Machines #1 and #3 are not presented in form of Visicorder divisions. The reason for this is that at the time of the tests, some difficulty was being experienced in balancing the specimen groove bending bridge with the Honeywell amplifier. Therefore, a static strain indicator was briefly substituted for the amplifier and Visicorder. The strain indicator allows for the setting of the gage factor and bridge size and then gives strain directly in microinches per inch.

The data from Machine #2 were reduced by the incremental method which was presented in Section 3-B-1. The change in Visicorder output for each 10.27 pound pan weight increment was determined. The changes in output were then averaged. The results are given in Table 5.

Table 4. Calibration Specimen Groove Strain Gage Output Versus Pan Weight Data

	MACHINE #1		MACHINE #2		MACHINE #3	
Data Point Number	Groove Output μin/in	Pan Weight lbs.	Groove Output div.	Pan Weight lbs.	Groove Output μin/in	Pan Weight lbs.
1	39670	0	0.1	0	39655	0
2	40190	30.81	2.3	10.27	40174	30.81
3	40703	61.62	4.6	20.54	40695	61.62
4	40357	41.08	6.9	30.81	40346	41.08
5	40015	20.54	9.4	41.08	40518	51.35
6	40539	51.35	11.6	51.35	39825	10.27
7	39838	10.27	14.2	61.62	39998	20.54
8	39668	0	11.4	51.35	39655	0
9	40013	20.54	9.1	41.08	39998	20.54
10	40357	41.08	7.0	30.81	40516	51.35
11	40697	61.62	4.8	20.54	40345	41.08
12	40527	51.35	2.5	10.27	40785	61.62
13	40182	30.81	0	0	40172	30.81
14	39834	10.27			39825	10.27
15	39661	0			39655	0
16	39834	10.27			40345	41.08
17	40351	41.08			40687	61.62
18	40691	61.62			39824	10.27
19	40181	30.81			40171	30.81
20	40522	51.35			39995	20.54
21	39005	20.54			40514	51.35
22	39661	0			39654	0

Visicorder Calibration Resistance:
Machine #2 - 30 kΩ at 25.0 divisions

Table 5. Reduction of Machine #2 Data Given in Table 4

Data Point Increment	Change in Toolholder Output in Divisions per 10.27 lbs. of Pan Weight
1-2	2.2
2-3	2.3
3-4	2.3
4-5	2.5
5-6	2.2
6-7	2.6
7-8	2.8
8-9	2.3
9-10	2.1
10-11	2.2
11-12	2.3
12-13	2.5
Average	2.358 divisions

The incremental output stress in the groove was then calculated as follows:

$$\Delta\sigma_{o_2} = \frac{E\ R_{gage}}{N_a\ G\ R_{cal}}\ \frac{\Delta N_{vis}}{N_{cal}}$$

where

$E = 30 \times 10^6$ psi,

$R_{gage} = 120\Omega$,

$N_a = 2$,

$G = 2.08$,

$R_{cal} = 20\ k\Omega$,

$N_{cal} = 25.0$ divisions,

$\Delta N_{vis} = 2.358$ divisions,

$\Delta\sigma_{o_2} = 2718$ psi.

For Machines #1 and #3, the static strain gage indicator outputs were averaged for each pan weight level. Then the incremental output strains were determined and averaged. The results are given in Table 6. The result is an overall average of the increase in strain in the groove for a 10.27 pound increase in pan weight. This average is then converted to incremental output stress.

$$\Delta\sigma_{o_1} = E\Delta\epsilon_{o_1}/2 = (30 \times 10^6)(170.7 \times 10^{-6})/2 = 2560 \text{ psi}$$

$$\Delta\sigma_{o_3} = E\Delta\epsilon_{o_3}/2 = (30 \times 10^6)(172.7 \times 10^{-6})/2 = 2589 \text{ psi}$$

The next step was to determine the true bending stress in the groove analytically using

Table 6. Reduction of Machines #1 and #3 Data Given in Table 4

	MACHINE #1		MACHINE #3	
Pan Weight lbs.	Average Strain μin/in	ΔStrain μin/in	Average Strain μin/in	ΔStrain μin/in
0	39666.3	169.0	39654.7	170.0
10.27	39835.3	175.7	39824.7	172.0
20.54	40011.0	173.3	39996.7	175.6
30.81	40184.3	170.7	40172.3	173.0
41.08	40355.0	174.3	40345.3	171.7
51.35	40529.3	170.7	40516.0	173.0
61.62	40697.0		40689.0	
Average		170.7		172.7

$$\sigma_{GR} = \frac{MC}{I}. \tag{2}$$

But the use of this equation is deferred until the next section, (3-B-2a), because of the complication which is introduced by the presence of stress concentration in the groove. This stress concentration factor, not yet determined so far, must be included in Equation 2.

2a. Experimental determination of the average stress concentration factor in specimen groove

There are two unknowns: K_t, the stress concentration factor for the specimen groove, and K_{BGR}, the Visicorder output stress versus true stress curve slope. Since the procedure in Section 3-B-2b was the only experimental test, it was necessary to somehow extract both of these unknowns from this single test. A rigorous determination of K_t and K_{BGR} is not theoretically possible, but it was felt that even a less precise development is more desirable than resorting to tabulare values of theoretical stress concentration factors.

The method used for determining K_t and K_{BGR} was the following: For each machine, the incremental output bending stress in the groove was set equal to the incremental true stress

$$\Delta\sigma_O = \Delta\sigma_T$$

or,

$$\Delta\sigma_o = K_t \frac{\Delta WLC}{I}.$$

Solving for K_t

$$K_t = \frac{\Delta\sigma_o I}{WLC}. \qquad (3)$$

The solution of Equation 3 for each machine gives

$$K_{t_1} = 1.240$$

$$K_{t_2} = 1.160$$

$$K_{t_3} = 1.445$$

Since the same specimen was used for each of the three tests, the stress concentration factor must be the same. Its value was taken to be the arithmetic average of the three values. Therefore, the effective static stress concentration factor for all specimens is 1.28. This is a static stress concentration factor because the calibration procedure used was static in nature.

Next, it was necessary to allow for variation from machine to machine. This is reflected in the value of K_{BGR} for each machine. First, $\Delta\sigma_T$ was calculated using the newly determined value of K_t, or

$$\Delta\sigma_T = K_{ave} \frac{\Delta WLC}{I}.$$

Then K_{BGR} was calculated using the experimental results from Section 3-B-2,

$$K_{BGR} = \frac{\Delta \text{Output Stress}}{\Delta \text{True Stress}}.$$

The results for each machine were

$$K_{BGR_1} = 0.967$$

$$K_{BGR_2} = 0.902$$

$$K_{BGR_3} = 0.972$$

K_{BGR} will be used in the data reduction technique of Section 4-E.

3. Torque interaction into bending bridge output

Description of Test

For the bending strain gages on the toolholder to perform satisfactorily, they must be in the proper position on the shaft and must have the correct orientation. No matter how much care is taken, due to human error during installation, the gages will always be slightly out of position. The effect of such misalignment is interaction of the torque load with the bending bridge output. The extent of this interaction and its direction must be determined. The procedure used was to maintain a constant bending load and vary the applied torque. A setup was used, whereby the change in the bending bridge output was only due to torque interaction.

Test Setup

Because of its simplicity, a cantilever-type setup was again used. A torque arm was needed to apply torque to the toolholder. This device was a standard test specimen with a steel bar welded perpendicular to the specimen at the groove. The bar was approximately thirty inches long and has a small hole near the far end through which a wire was strung to support a loading pan, as shown in Figure 12. The toolholder was cantilevered in exactly the same way as in previously described calibrations. Once again, the toolholder bending gages should be directly on the top and bottom of the shaft for full bridge output.

In this test, it was necessary to monitor bending and torque toolholder outputs; therefore, two amplifier cables were used and were connected to the slip-ring by fine wires in the manner described in the earlier calibrations.

Next the specimen with the torque arm was placed in the toolholder collet. A key was placed in the keyway on the specimen so that the collet could support the torque without the specimen slipping. The specimen was then tightened in the collet with the loading pan, and the torque arm was placed in a position slightly above the horizontal. The reason for this was that the torque arm

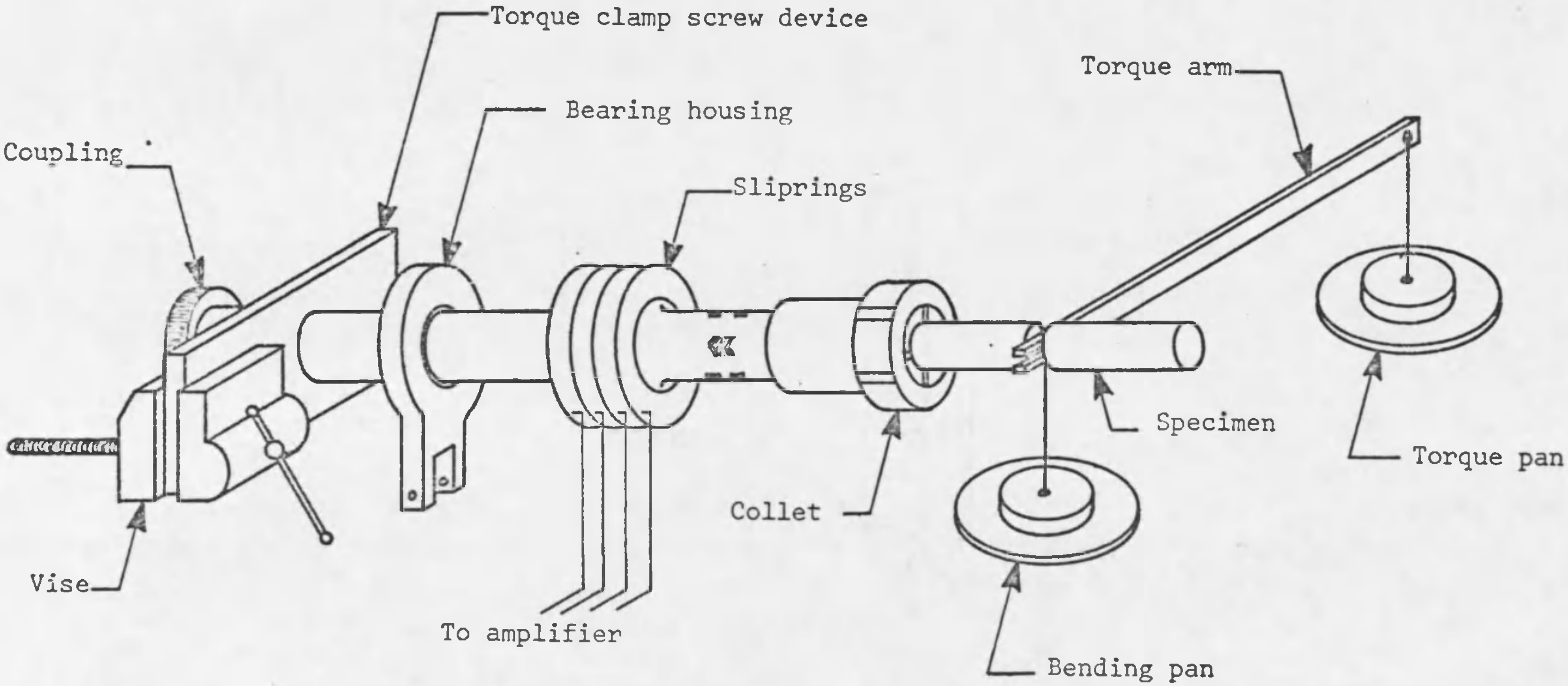

Fig. 12.--Test Setup for Torque Interaction into Bending Bridge Output

deformed elastically during loading. Using a level, the torque arm was positioned so that it was about one-half a degree above the horizontal in the no-load configuration and one-half a degree below the horizontal when the maximum load was applied. It should be noted that the error introduced by the change in lever arm distance due to elastic deformation of the torque arm is a function of the cosine of the change of the angle and is negligible.

Once the torque arm was positioned with respect to the toolholder, the entire assembly was removed from the screw device and placed with the toolholder in the vertical position. Then the torque and bending bridges were balanced; the Visicorder outputs zeroed, and the calibration resistances (five hundred thousand ohms for bending and three hundred four thousand ohms for torque, and the calibration divisions (twenty-five divisions for bending and forty-five divisions for torque) were set on the Visicorder. Then the assembly was returned to the test configuration. Next a bending load pan was suspended directly below the specimen groove. Also a torque load pan was hung from the end of the torque arm. A plane connecting the two pans must be perpendicular to the longitudinal axis of the toolholder and specimen. This was checked through plumb lines and squares. Four ten-pound weights were added to the bending pan and the test setup was ready for torque interaction calibration.

Test Procedure

Weight was removed in ten-pound increments from the bending pan and added to the torque pan. Both the bending and the torque channels were monitored. When the weights were changed, there was a tendency for the torque arm to vibrate. This was dampened with the use of the hand. It was necessary at times to wait as long as ten minutes between data points, depending on how much drift there was in the amplifier and how long the amplifier took to reach equilibrium. When all the weight was in the torque pan, the weights were removed, ten pounds at a time, and placed in the bending pan. When all the weights were back in the bending pan, the two Visicorder outputs for zero torque pan weight were compared. If they were identical, then it was concluded that no amplifier drift occurred during the data-taking period and the data were good. If they did not compare favorably, then the data were scrapped, and the test was re-run. At least two good sets of up-and-down runs are needed for calibration purposes.

Data Reduction

The calibration data are presented in Table 7. After the test for Machine #3 was run, the Visicorder

Table 7. Torque Output Versus Bending Output Data from Torque into Bending Interaction Calibration

	MACHINE #1		MACHINE #2		MACHINE #3	
Data Point Number	Torque Output div.	Bending Output div.	Torque Output div.	Bending Output div.	Torque Output div.	Bending Output div.
1	8.8	11.6	5.6	17.6		
2	41.9	10.0	14.9	18.3		
3	8.8	11.8	23.8	18.5		
4	41.7	10.2	32.4	18.9		
5	33.9	10.6	40.4	19.0		
6	25.7	11.1	32.5	18.6		
7	17.4	11.6	23.9	18.3		
8	8.8	12.0	14.9	18.0		
9	17.3	11.5	5.7	17.6		
10	25.3	11.3	14.9	17.9	See Data	
11	34.0	10.8	23.7	18.1	Reduction	
12	41.9	10.4	32.3	18.3	in Section	
13	8.8	10.9	40.3	18.8	4-B-3	
14			32.4	18.5		
15			23.8	18.2		
16			14.9	17.9		
17			5.6	17.6		
18			5.3	12.9		
19			14.5	13.1		
20			23.4	13.3		
21			32.2	13.6		
22			40.2	13.8		
23			32.2	13.6		
24			23.5	13.5		
25			14.6	13.2		
26			5.3	12.8		

Visicorder Calibration Resistances:

Machine #1 - Bending 500 kΩ at 25.0 divisions
Torque 304 kΩ at 45.0 divisions

Machine #2 - Bending 500 kΩ at 25.0 divisions
Torque 30 kΩ at 44.7 divisions

Machine #3 - Bending 500 kΩ at 25.0 divisions
Torque 304 kΩ at 45.0 divisions

output was closely inspected. It was found that there was no measurable change in the bending bridge output with torque load. Therefore, it was not necessary to carry the reduction any further; it was immediately concluded that there is no detectable torque interaction into bending for Machine #3.

The data from Machines #1 and #2 were reduced graphically. First, the torque bridge output in divisions was plotted versus the bending bridge output in divisions, as shown in Figures 13 and 14; then a straight line was fitted to the points. Next, the slope of the curve was determined by selecting two points for the curve, and the rates of change were determined. For Machine #2, there are two sets of data and two slopes. The average slope was used. From Figure 13:

Machine #1

Point A - (10.0, 11,912)

Point B - (40.0, 10,425)

$$\Delta N_{vis_{torque}} = 30 \text{ div}$$

$$\Delta N_{vis_{bending}} = - 1.487 \text{ div}$$

From Figure 14:

Machine #2

Point A - (36.35, 18.70)

Point B - (5.00, 17.72)

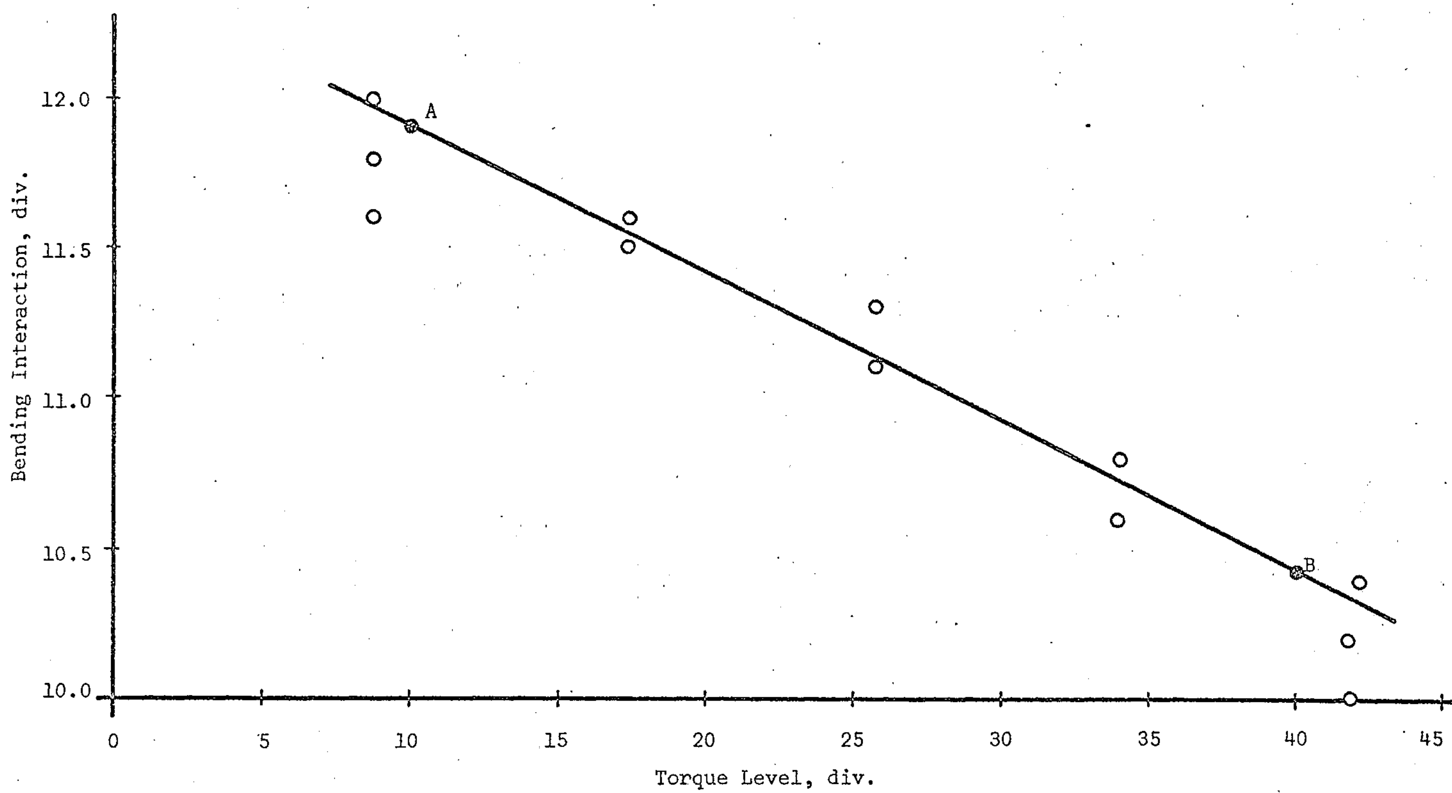

Fig. 13.--Torque Interaction into Bending - Machine #1

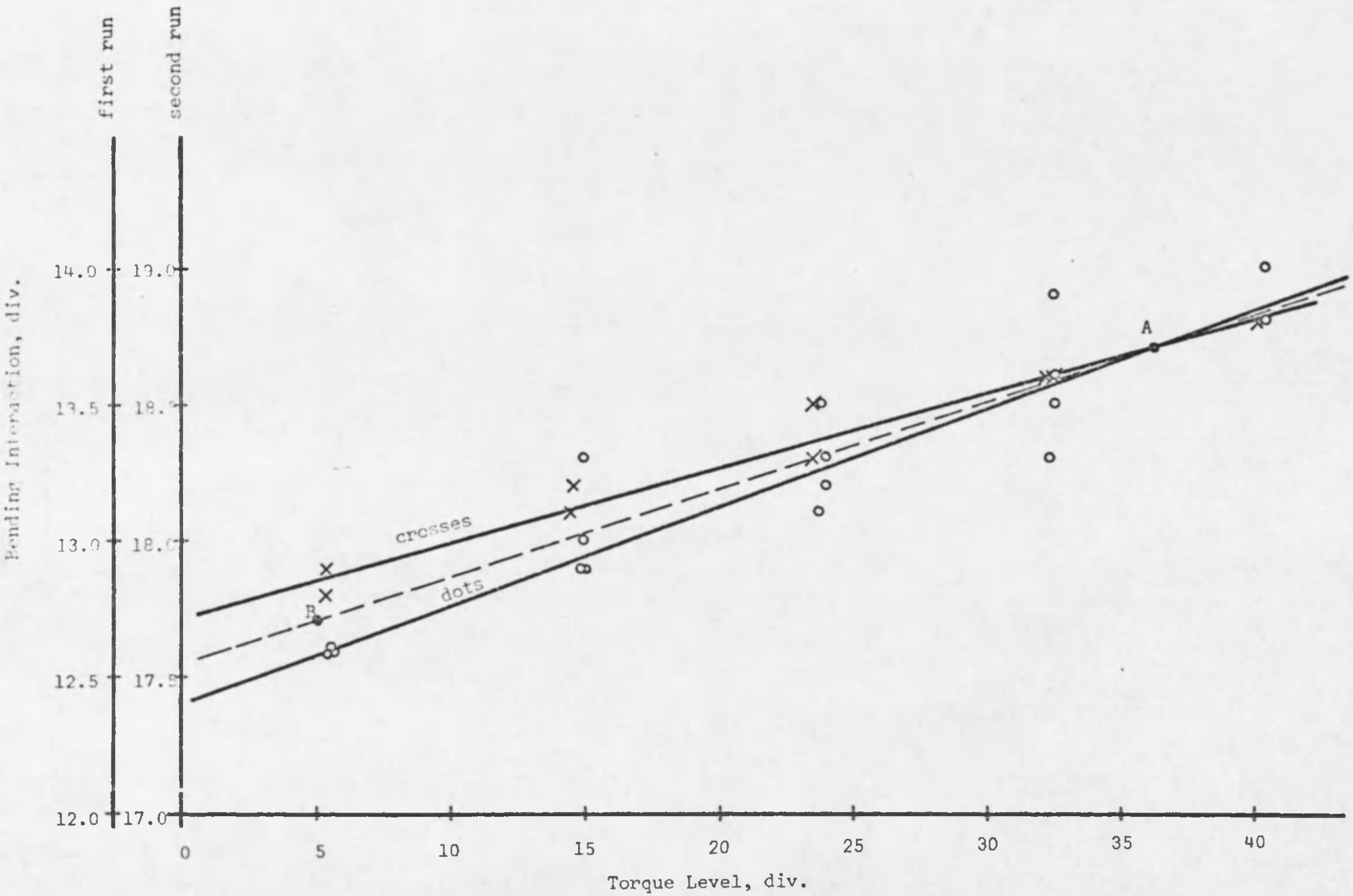

Fig. 14.--Torque Interaction into Bending - Machine #2

$$\Delta N_{vis_{torque}} = 31.25 \text{ div.}$$

$$\Delta N_{vis_{bending}} = 0.98 \text{ div.}$$

Next, the Visicorder outputs in divisions were converted to strain, using Equation 1. The conversions to strain gave:

$$\Delta\epsilon_{B_1} = 1.75 \ \mu\text{in/in}$$

$$\Delta\epsilon_{T_1} = - 31.9 \ \mu\text{in/in}$$

$$\Delta\epsilon_{B_2} = 1.15 \ \mu\text{in/in}$$

$$\Delta\epsilon_{T_2} = 33.5 \ \mu\text{in/in}$$

Conversion to stress instead of strain could have been used also where the subscript denotes torque or bending for Machines #1 or #2. For torque, the parameters are:

$$R_{gage} = 120\Omega$$

$$N_a = 4$$

$$G = 2.06$$

$$R_{cal} = 304 \text{ k}\Omega$$

The slopes in terms of strain would be:

$$S_1 = - \frac{1.75}{31.9} = - 0.0548 = K_{T/B_1}$$

$$S_2 = \frac{1.15}{33.5} = 0.0343 - K_{T/B_2}.$$

Since stress is equal to the strain multiplied by Young's Modulus, the slope of the bending stress versus shear stress curve is identical to the strain curve slope. This slope is given the designation $K_{T/B}$ and will be used in the calibration procedure described later. Since there must be no interaction into bending for zero torque load, a plot of bending stress interaction versus shear stress could be constructed by drawing a line through the origin with the slope $K_{T/B}$ and labeling the axes appropriately.

Note that the interaction for Machine #1 is negative, the interaction for Machine #2 is positive, and the interaction for Machine #3 is zero.

4. Relationship between toolholder bending stress and specimen groove bending stress

All previous tests involved the calibration of only the bending strain gage bridge outside of the fatigue machine. In this test, the bending bridge will be calibrated in the fatigue machine.

For an approximate analysis, it can be assumed that the bending moment along the toolholder shaft between the two loading bearings is constant. This would be true if the toolholder were weightless. Then the relationship between toolholder bending moment and specimen groove bending moment is

$$M_{toolholder} = M_{groove}$$

The bending stresses are given by

$$\sigma_{TH} = \frac{M_{TH}C_{TH}}{I_{TH}}$$

$$\sigma_{GR} = \frac{M_{GR}C_{GR}}{I_{GR}}$$

Combining these gives

$$\frac{\sigma_{TH}I_{TH}}{C_{TH}} = \frac{\sigma_{GR}I_{GR}}{K_f C_{GR}}.$$

Solving for the bending stress in the specimen groove, the groove stress is obtained as

$$\sigma_{GR} = K_f \frac{C_{GR}}{C_{TH}} \frac{I_{TH}}{I_{GR}} \sigma_{TH}.$$

However, in a more sophisticated analysis, the dead weight of the toolholder must be considered. Two approaches are given. In Section 3-B-4a, an experimental analysis is conducted. The results of these tests are applied to the calibration procedure presented later. The second approach is analytical and is presented in Section 3-B-4b.

4a. Toolholder strain gage output versus specimen strain gage output

Description of Test

This test involves the calibration of the bending bridge of the toolholder against the bending bridge of the specimen groove.

Test Setup

For this calibration to have any usefulness, the setup must be the normal running mode of the fatigue machines. Therefore, a specimen with bending gages in the groove was installed in the toolholder collets according to the actual test procedure which is used in running specimens. For the full procedure, the laboratory checklist given in Appendix C should be consulted. The leads from the specimen were soldered directly to an amplifier, leaving some play in the leads so that the shaft can be rotated by hand a few times without causing the leads to wrap tightly around the specimen. The normal brush and slip-ring arrangement was used for monitoring the toolholder output.

The strain gage bridges were zeroed and balanced according to the checklist procedure. The toolholder shaft was rotated until the specimen groove gages were along the neutral axis, when balancing the bridge. The toolholder gages will then be randomly oriented, which is perfectly all right since the loading frame is blocked up (see checklist procedure). The calibration resistances were 190 kΩ for the toolholder and 11 kΩ for the groove bridges, while the Visicorder calibration divisions were both 25 divisions.

Test Procedure

A "quasi-static" test was run by rotating the fatigue machine shaft by hand rather than being turned full speed or left at rest, while readings were taken.

Weights were placed in the loading pan in two-and-one-half-pound increments until fifteen pounds of total weight was reached. Then the weights were removed from the loading pan at the same rate until the pan weight was zero. At each level, the toolholder shaft was rotated a few times by hand while the Visicorder recorded the outputs from both bending bridges. It was made sure that both outputs showed an upper and lower peak so that the total bending width could be determined. At least twelve data points were taken.

The test was repeated for the other two fatigue machines.

Data Reduction

The calibration data are given in Table 8. The graphical reduction technique of the data was used.

Table 8. Toolholder Versus Groove Bridge Output Data for Quasi-static Calibration of Groove Stress

	MACHINE #1		MACHINE #2		MACHINE #3	
Data Point Number	Toolholder Output div.	Groove Output div.	Toolholder Output div.	Groove Output div.	Toolholder Output div.	Groove Output div.
1	21.6	16.2	20.0	31.1	25.0	26.8
2	25.1	18.6	23.9	36.2	28.6	41.8
3	29.1	21.7	27.2	41.3	32.0	47.3
4	33.1	24.2	30.3	45.3	39.1	57.0
5	36.1	26.1	37.6	56.0	21.6	31.9
6	40.3	29.3	36.6	52.8	25.1	36.3
7	43.9	31.7	34.7	50.7	28.2	40.9
8	39.9	29.3	30.0	44.6	32.4	46.2
9	35.9	26.4	27.7	40.6	40.0	56.0
10	32.7	23.9	23.7	34.3	21.7	31.3
11	29.2	21.5	20.1	30.5	25.2	36.3
12	25.7	18.9	23.1	34.8	28.8	41.3
13	22.0	16.4	27.0	39.9	32.0	46.6
14	25.8	19.2	30.0	43.6	35.3	50.3
15	28.8	21.3	33.9	49.3		
16	33.3	24.3	36.2	52.2		
17	36.1	26.7				
18	40.2	29.3				
19	44.0	31.7				

Visicorder Calibration Resistances:

Machine #1 - Toolholder 200 kΩ at 24.9 divisions
Groove 22.22 kΩ at 24.9 divisions

Machine #2 - Toolholder 190 kΩ at 24.8 divisions
Groove 11 kΩ at 24.6 divisions

Machine #3 - Toolholder 190 kΩ at 25.0 divisions
Groove 11 kΩ at 25.0 divisions

For each set of data, a plot of toolholder output in divisions was made, as shown in Figures 15, 16, and 17. Straight lines were drawn to fit the data. Two points were selected on each line and the $\Delta N_{vis_{toolholder}}$ and $\Delta N_{vis_{groove}}$ were determined. Next, the outputs were converted from divisions to strain by using Equation 1 with Young's Modulus removed. The results are given in Table 9. Lastly, the slopes of the toolholder bending strain versus

Table 9. Table 8 Visicorder Divisions Converted to Strain in Toolholder and Specimen Groove

	ΔN_{vis} Toolholder div.	$\Delta \epsilon_{Toolholder}$ μin/in	ΔN_{vis} groove div.	$\Delta \epsilon_{groove}$ μin/in
Machine #1	22.2	32.85	15.75	1620
Machine #2	40.0	62.40	59.0	3145
Machine #3	10.7	16.55	15.0	786

groove bending strain plots were determined and given the designation K_{GR-TH}, with the following results:

$$K_{GR-TH_1} = 0.0203$$

$$K_{GR-TH_2} = 0.0198$$

$$K_{GR-TH_3} = 0.0215$$

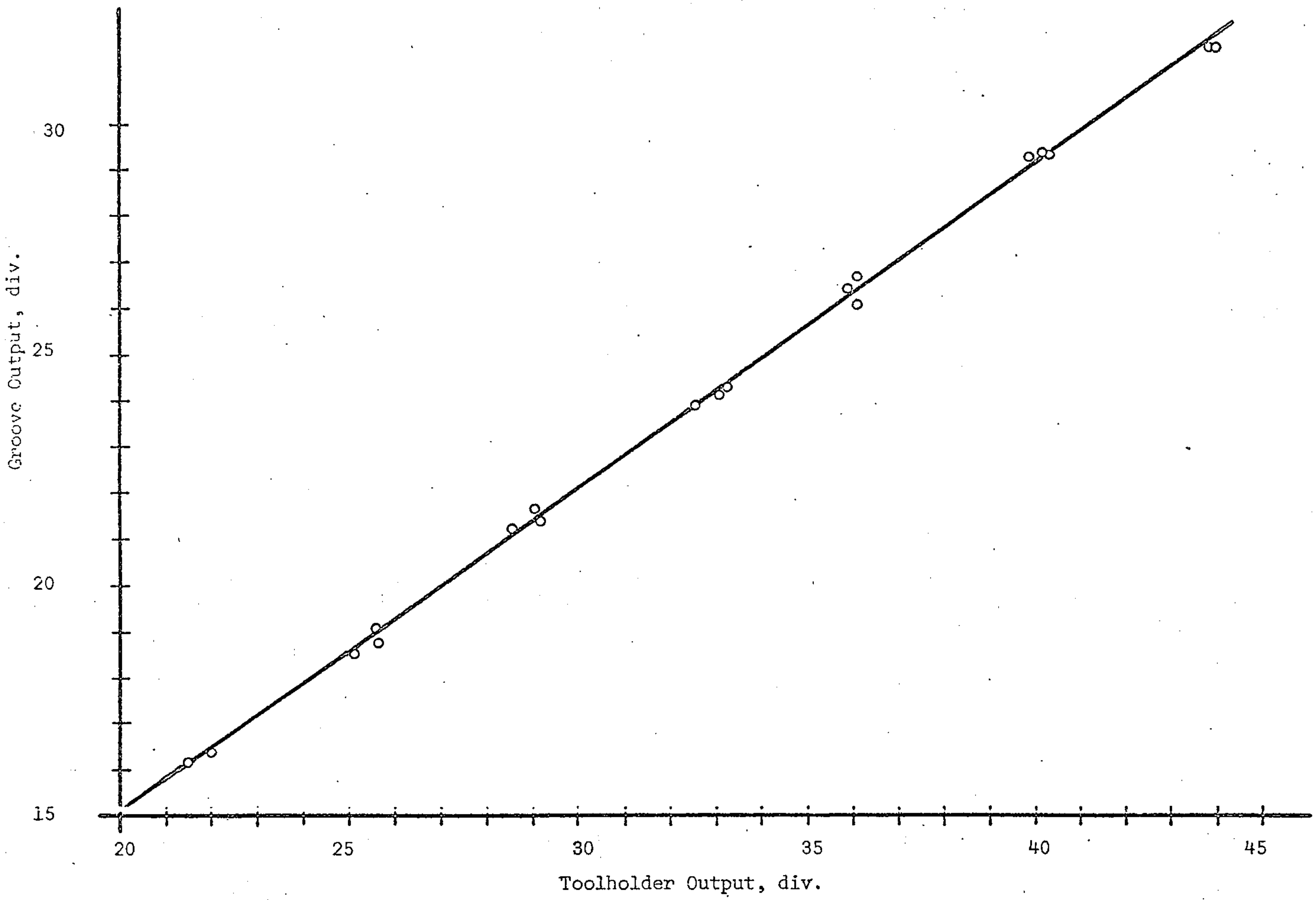

Fig. 15.--Specimen Groove Output Versus Toolholder Output - Machine #1

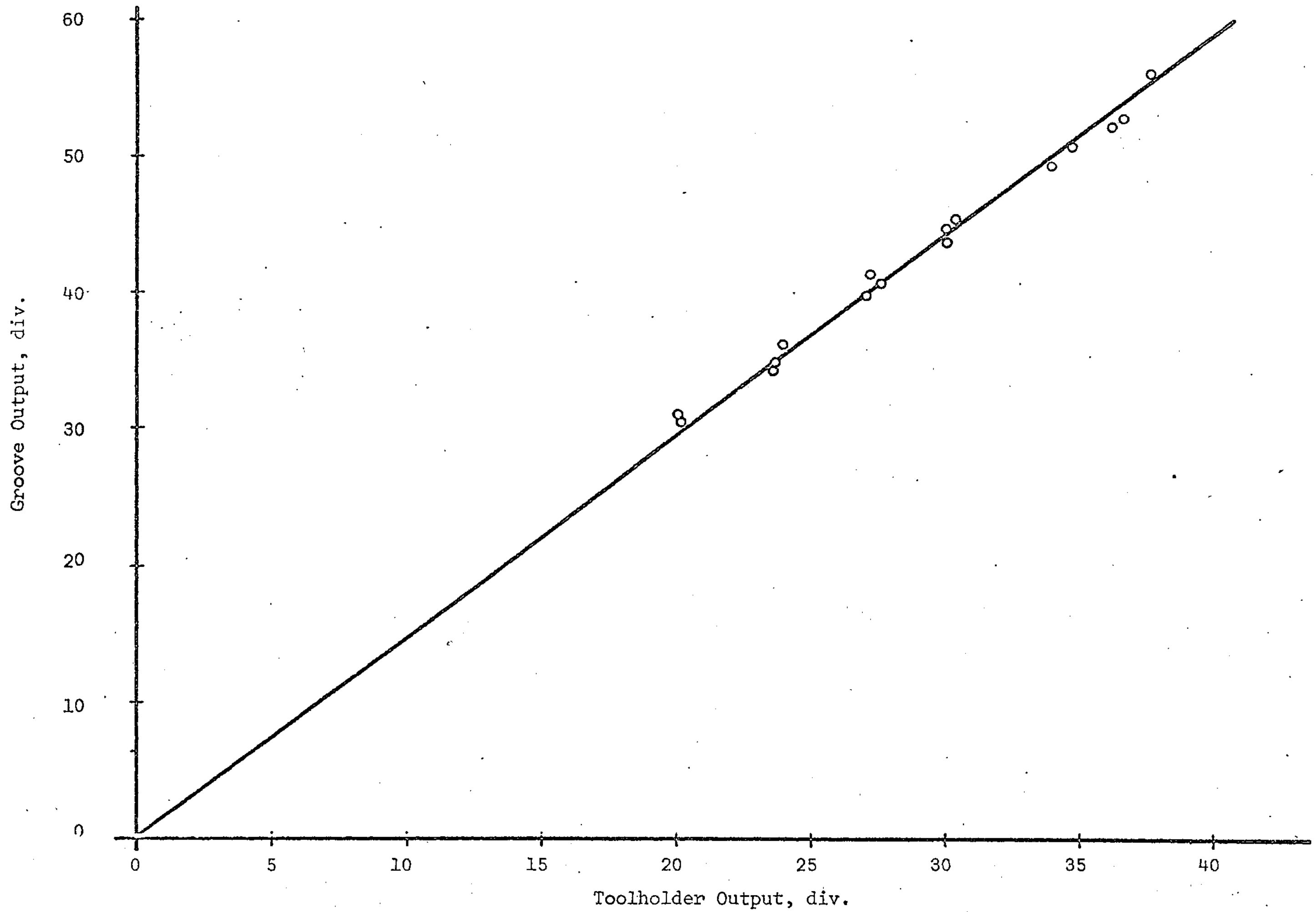

Fig. 16.--Specimen Groove Output Versus Toolholder Output - Machine #2

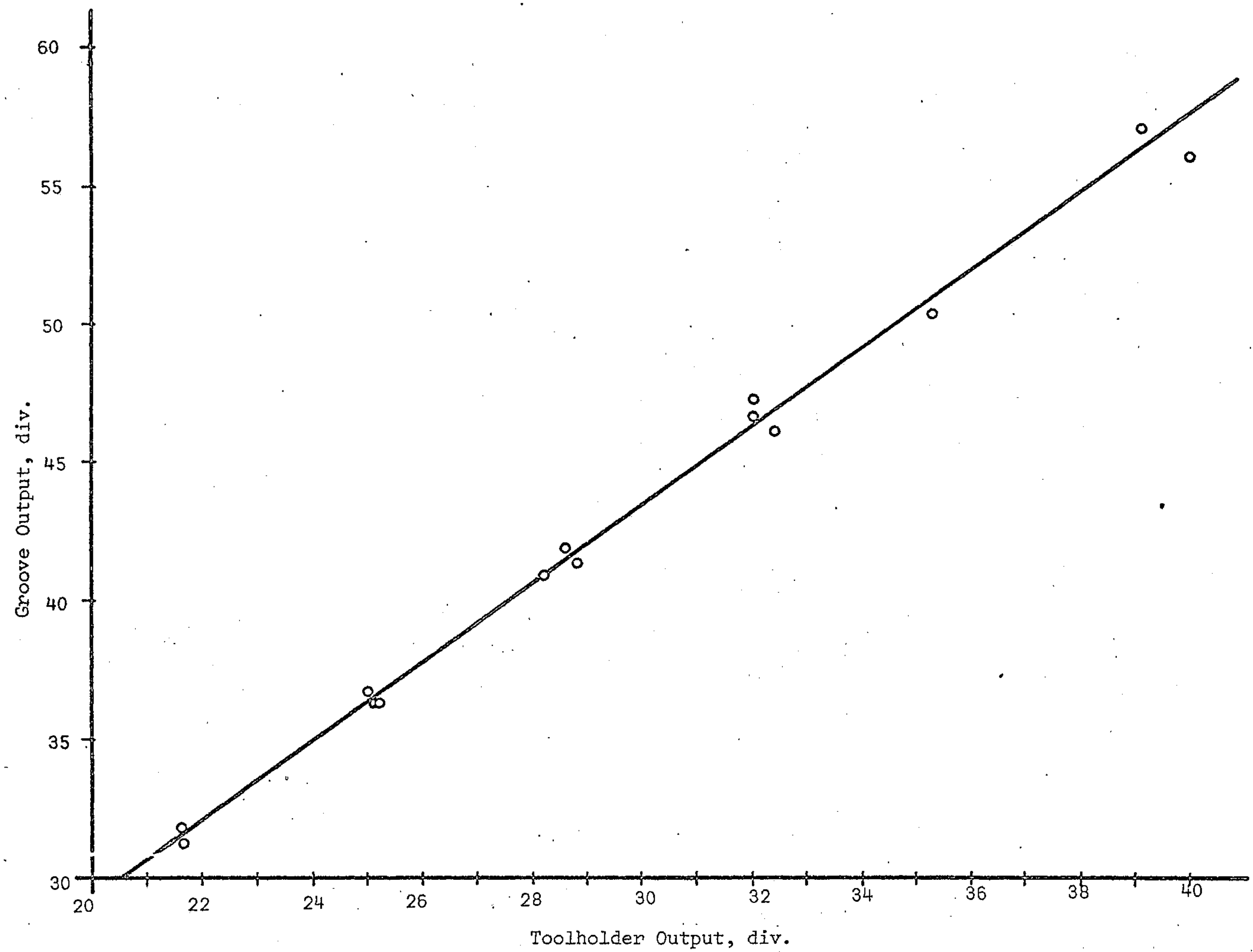

Fig. 17.--Specimen Groove Output Versus Toolholder Output - Machine #3

Note again that the stress curve slope is identical to the strain curves slope. These parameters will be used in the calibration procedure presented in Section 4-E.

4b. Toolholder bending stress versus specimen bending stress

In early calculations, it was assumed the bending moment along the toolholder was essentially constant between the strain gages and the specimen groove. While the assumption was acceptable during the design phases of the project, later calibration required more accurate knowledge of the change in bending moment between the strain gages and the specimen groove.

Ideally, it would be best to construct a mathematical model of the toolholder; in other words, completely describe the physical system in terms of point forces and loading functions. This involves the drawing of a free body diagram of the front shaft, so that a bending moment diagram can be calculated as a function of pan weight. In addition to being able to get the correct stress in the specimen groove for the increase in bending moment, it also becomes possible to theoretically determine the toolholder strain and compare it with the experimental results described in Section 3-B-1.

In the free body diagram of Figure 18, the weights of all the components and their positions along the shaft

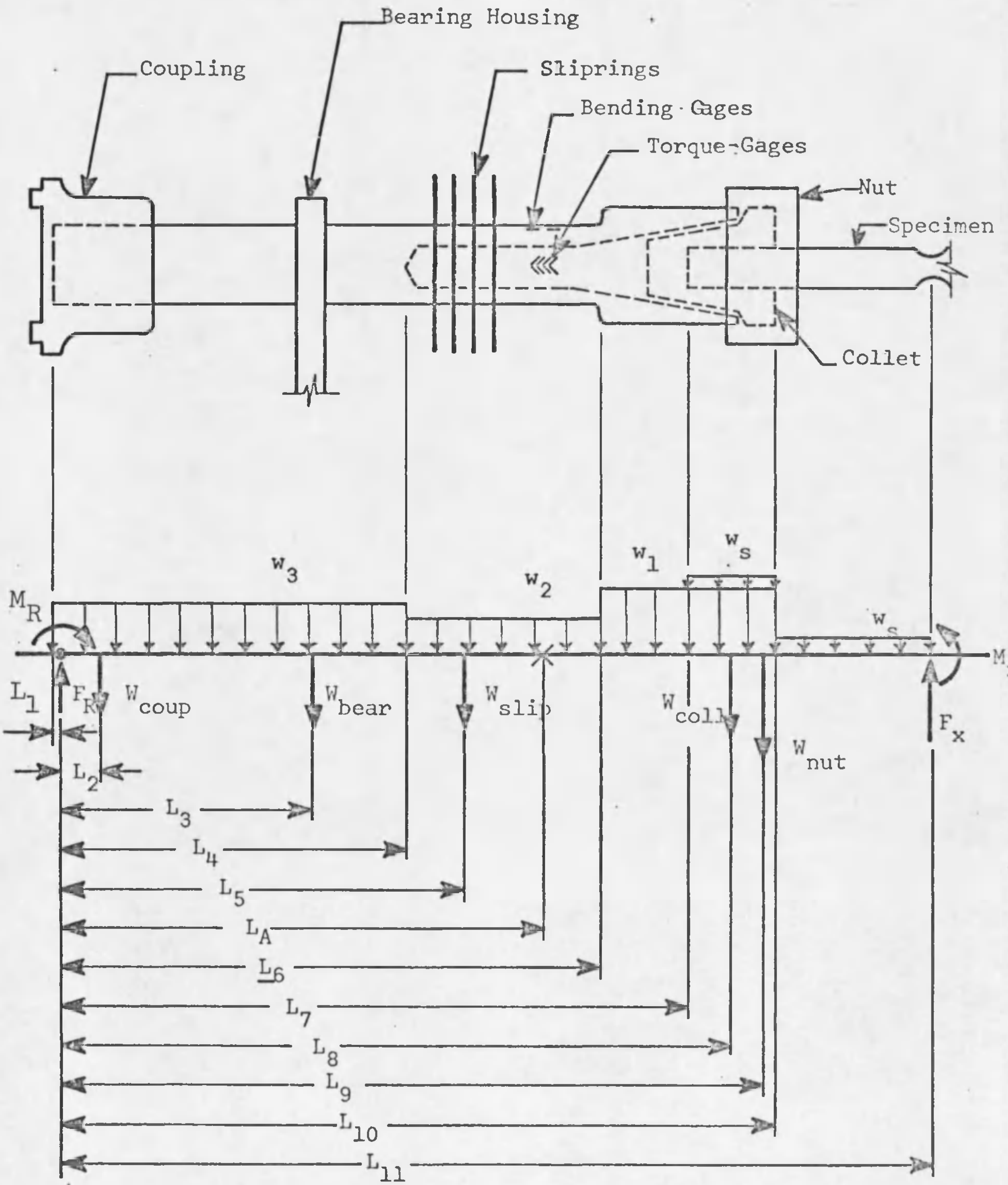

Fig. 18.--Free Body Diagram of Toolholder

can be determined easily from the design data of each machine. The loadings at the bearing housings can be expressed as a function of the pan weight if an analysis of the loading frame is undertaken.

To complete the mathematical model, the operation of the couplings at either end of the toolholder had to be fully understood. It was believed that a single-valued resisting moment, reaction force and pivot point could be associated with the coupling mechanism. An experiment was proposed and initiated to determine these three unknown parameters. A specimen was placed in the machine and the machine was set up as if it were about to be run. However, the chuck on one side was held only at one end. Then the opposite side of the machine was supported in a level position so that the linkage would exert an equal force on each section of the shaft when the machine was loaded. Next, a balance system was rigged above the machine, as shown in Figure 19. Care had to be taken to insure that the wire connected to the specimen was vertical at all times. Also, the balance bar had to be horizontal. A bubble-type level was attached to the top of the chuck with a rubber band. This was used to tell when the shaft was in a level position. Then a pointer was attached to the chuck. A scale was then connected to the opposite safety bridge and the pointer adjusted so that it

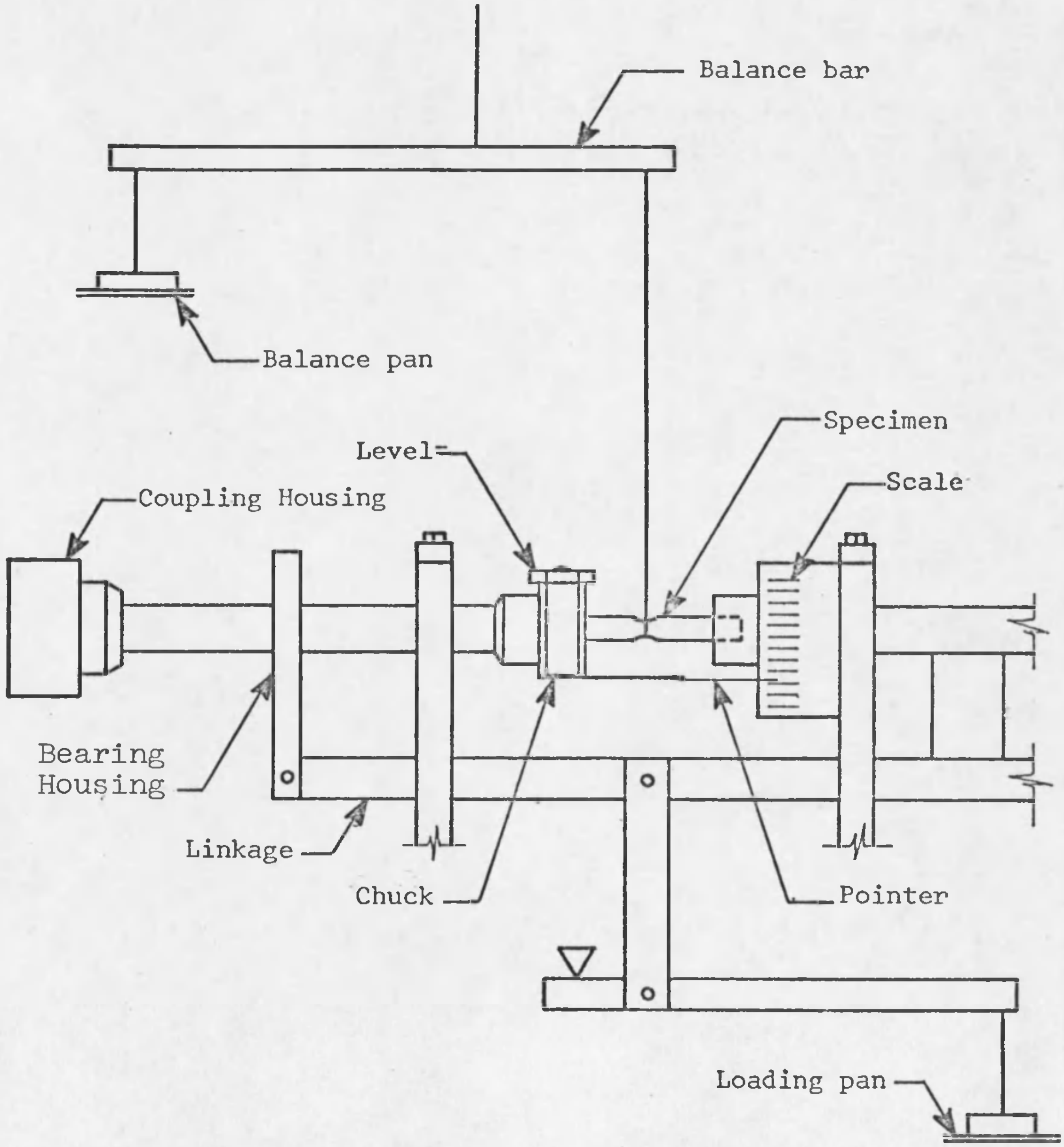

Fig. 19.--Laboratory Setup of Lever Arm, Pivot Point, Resisting Moment Measurement Experiment

would read out increments on the gage. The graduations on the scale stood for no physical quantities; they were only for reference.

Data-taking Procedure

First, the machine was loaded in the lower weight pan. Five data points were taken starting at zero loading and increasing in five-pound increments to twenty pounds. Each load was carefully centered in the loading pan so that the load was balanced at all times. Then the balance pan was loaded until the force in the wire was great enough to lift the shaft to approximately a level position as indicated by the bubble level. Then the weight in the balance pan was carefully centered and the positions of the balance pins adjusted so that all forces acted at their measured distances from the fulcrum. At this time, using the level, a zero mark (level shaft position) was recorded on the scale. Before and after each data point was taken, the zero mark was checked to see that it had not moved. Now, with the observer in a seated position so that he could line up his eye with the top of the back-shaft and the pointer to maintain the same parallax throughout the experiment, the system was displaced from the equilibrium position and allowed to return. Small weights were added or subtracted on the balance pan to reach an equilibrium point when the shaft was horizontal. Since the pivot point in the coupling was stiff (large resisting moment), there was little sensitivity to weight added to the balance pan. Thus it was found that sensitivity could be increased by following the procedure just mentioned, that is, displace the shaft up and down from the equilibrium position and allow it to return freely. An example is now given to help clarify the procedure.

Figure 20 shows the scale graduations. The dotted line, B, is the position the pointer would indicate when the shaft is level. If the shaft were displaced upward and allowed to return to the equilibrium position, it would stop, say, at line A. Now if the shaft were displaced downward, it would come to an equilibrium position at point C, or two full graduations below A. However, lines A and C are equi-distant above and below the level point, line B, and therefore the observer considered this set of circumstances to be the sought-after equilibrium position and the weight in the balance pan at this time was considered to be the weight necessary to bring the shaft to a horizontal position for a given weight in the loading pan. The problem was further complicated by the fact that the pointer would not always return to line A when the shaft was displaced upward. It would be very close to line A, and the average of the displacements upward would give line A. The same is true for line C.

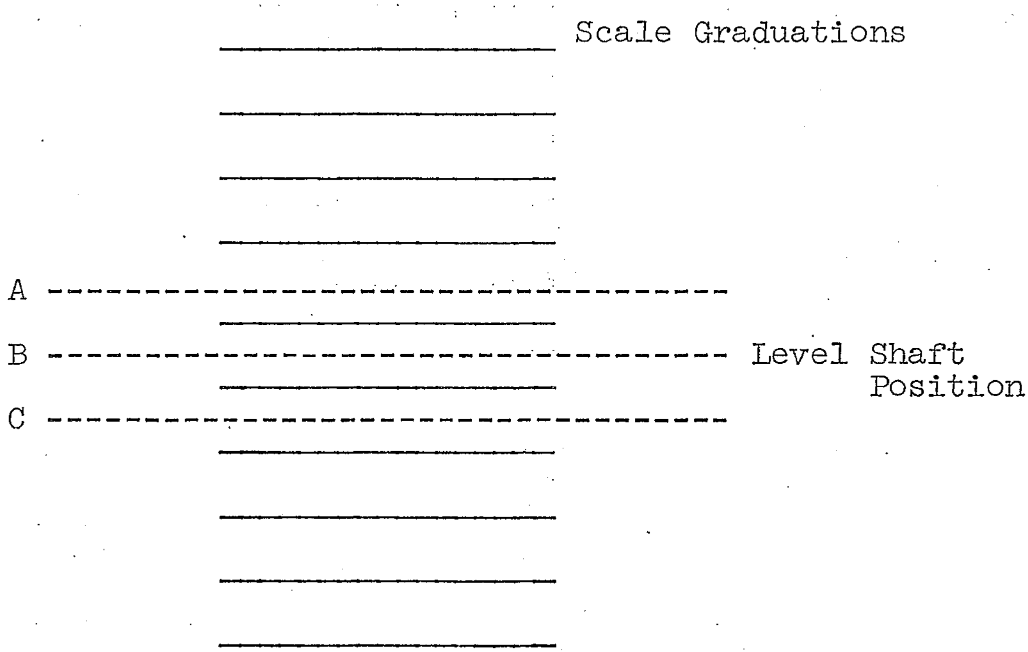

Fig. 20 Scale Graduations of Measurement Experiment

This would indicate that a great deal of time and trials were necessary to procure each data point. This was, in fact, the case.

When the data from the preceding experiment were reduced, it was found that the lever arm distance calculated was physically impossible. Since it was impossible to increase the accuracy or sensitivity of the experiment, it was concluded that:

(1) The operation of the coupling was erratic and no valid mathematical mode of its operation could be determined.

(2) Since the coupling operation was indeterminate, a full mathematical model could not be determined and some of the objectives of this study would have to be compromised.

The results of this approach indicated that the exact resisting moment at the coupling, the lever arm, and the reaction forces could not be determined with the desired accuracy. This conclusion led to the pursuit of the different calibration procedure presented in this report.

C. Torque Calibration

1. Torque load versus Visicorder output

Description of Test

As was the case in bending, it was necessary to calibrate the torque bridge on the toolholder against a known torque loading. With this calibration, any Visicorder output of the torque channel can immediately be converted to shear stress in the toolholder. Since the applied torque is constant along the toolholder shaft, shear stress in the toolholder can be converted to shear stress in the specimen groove without further calibration.

Test Setup

The test setup was identical to the system used in Section 3-B-3 to determine the torque interaction into bending. In fact, if the torque pan weights for each Visicorder run are recorded at the time the torque interaction into bending calibration is run, then the same data can be used for both tests. This procedure was followed for all three machines.

Data Reduction

The calibration data are given in Table 10. The pan weight versus torque output plots are given in Figures 21, 22, and 23. A straight line was fitted to

Table 10. Torque Output Versus Pan Weight Data for Torque Bridge Calibration

	MACHINE #1		MACHINE #2		MACHINE #3	
Data Point Number	Torque Output div.	Pan Weight lbs.	Torque Output div.	Pan Weight lbs.	Torque Output div.	Pan Weight lbs.
1	8.8	0	5.6	0	5.4	0
2	41.9	41.08	14.9	10.27	13.2	10.27
3	8.8	0	23.8	20.54	21.1	20.54
4	41.7	41.08	32.4	30.81	28.6	30.81
5	33.9	30.8	40.4	41.08	35.9	41.08
6	25.7	20.54	32.5	30.81	28.5	30.81
7	17.4	10.27	23.9	20.54	20.8	20.54
8	8.8	0	14.9	10.27	12.9	10.27
9	17.3	10.27	5.7	0	5.1	0
10	25.8	20.54	14.9	10.27	5.2	0
11	34.0	30.81	23.7	20.54	13.1	10.27
12	41.9	41.08	32.3	30.81	20.9	20.54
13	8.8	0	40.3	41.08	28.6	30.81
14			32.4	30.81	35.6	41.08
15			23.8	20.54	28.3	30.81
16			14.9	10.27	20.8	20.54
17			5.6	0	12.9	10.27
18			5.3	0	5.4	0
19			14.5	10.27		
20			23.4	20.54		
21			32.2	30.81		
22			40.2	41.08		
23			32.2	30.81		
24			23.5	20.54		
25			14.6	10.27		
26			5.3	0		

Visicorder Calibration Resistances:
Machine #1 - 304 kΩ at 45.0 divisions
Machine #2 - 304 kΩ at 44.7 divisions
Machine #3 - 304 kΩ at 44.5 divisions

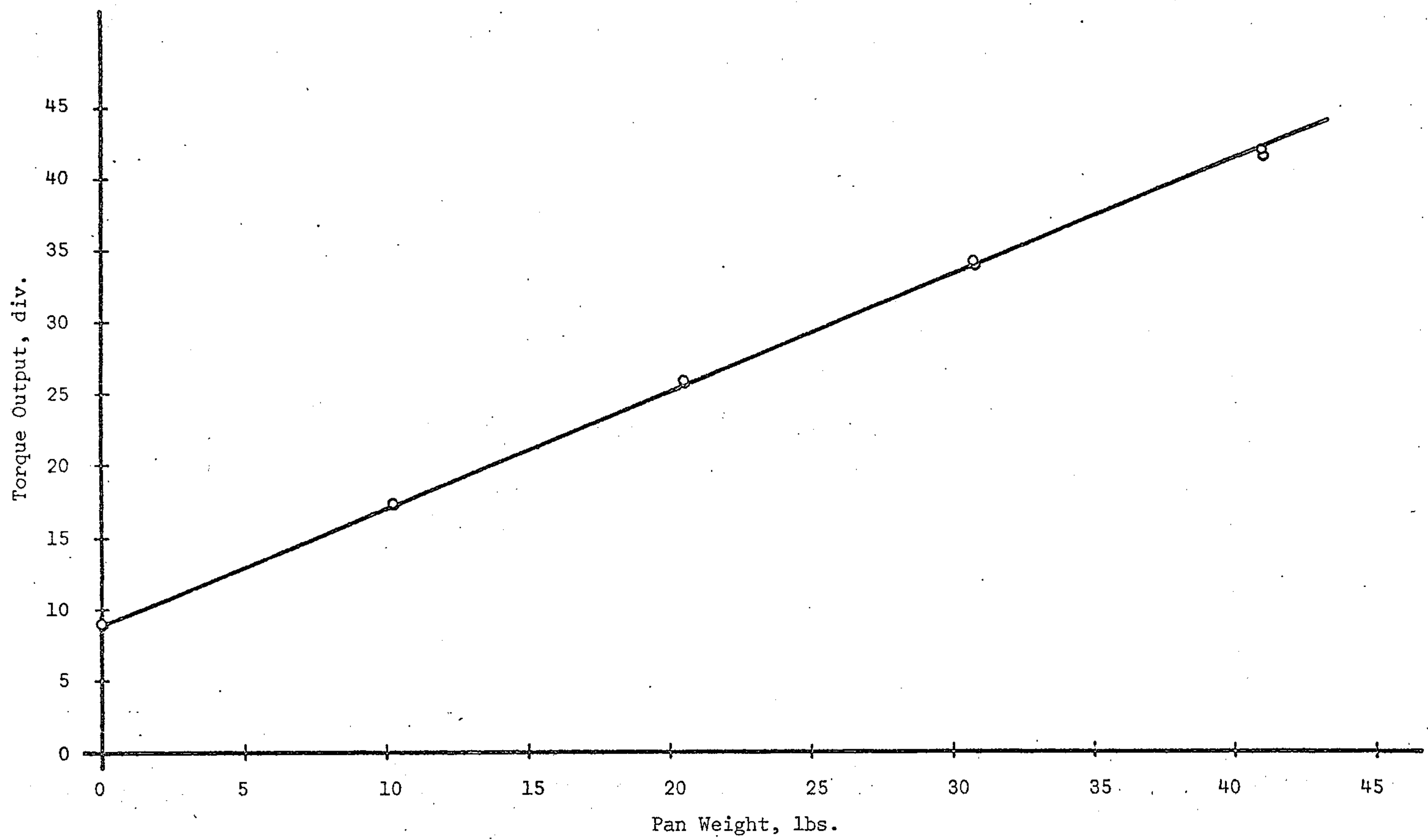

Fig. 21.--Torque Output Versus Pan Weight - Machine #1

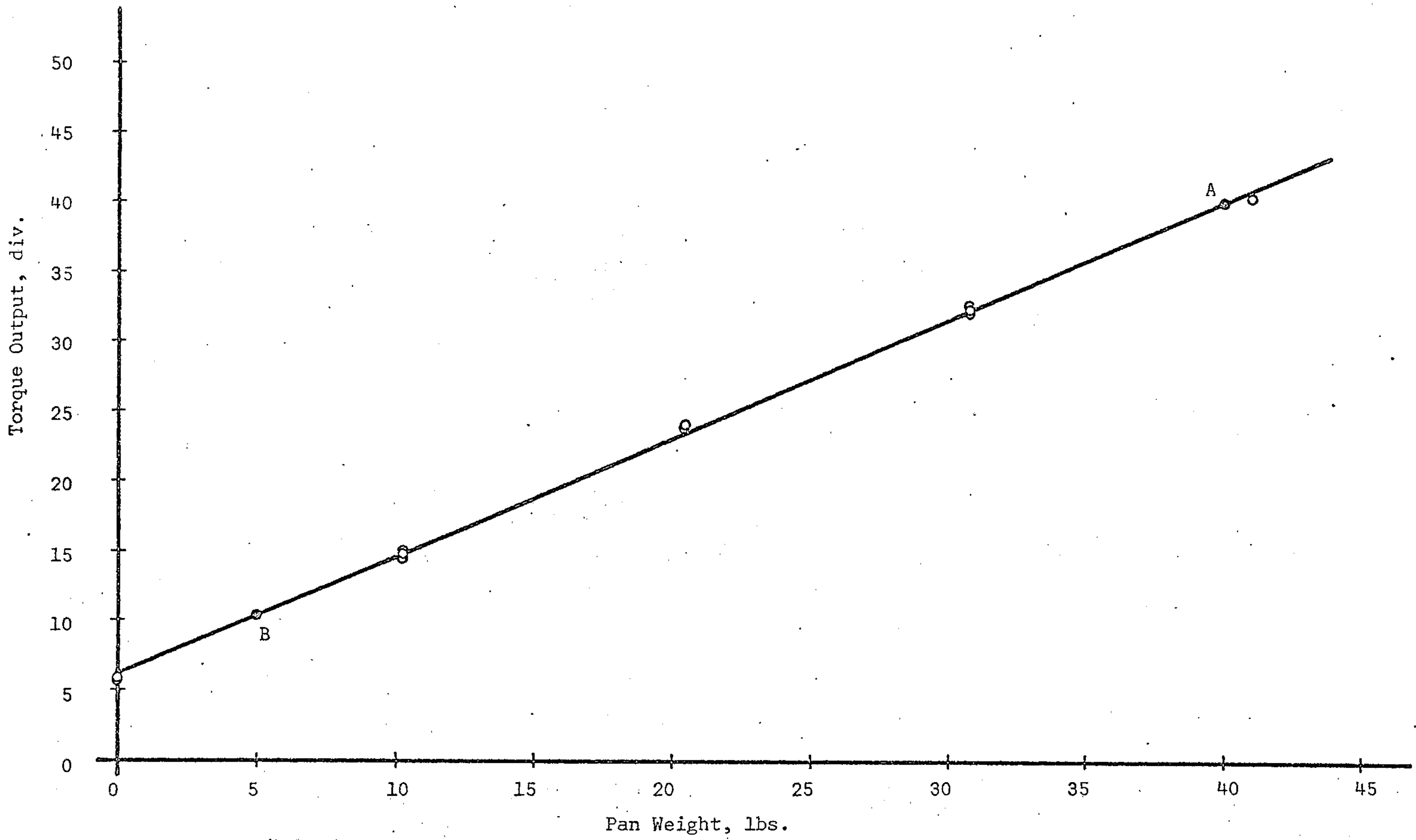

Fig. 22.--Torque Output Versus Pan Weight - Machine #2

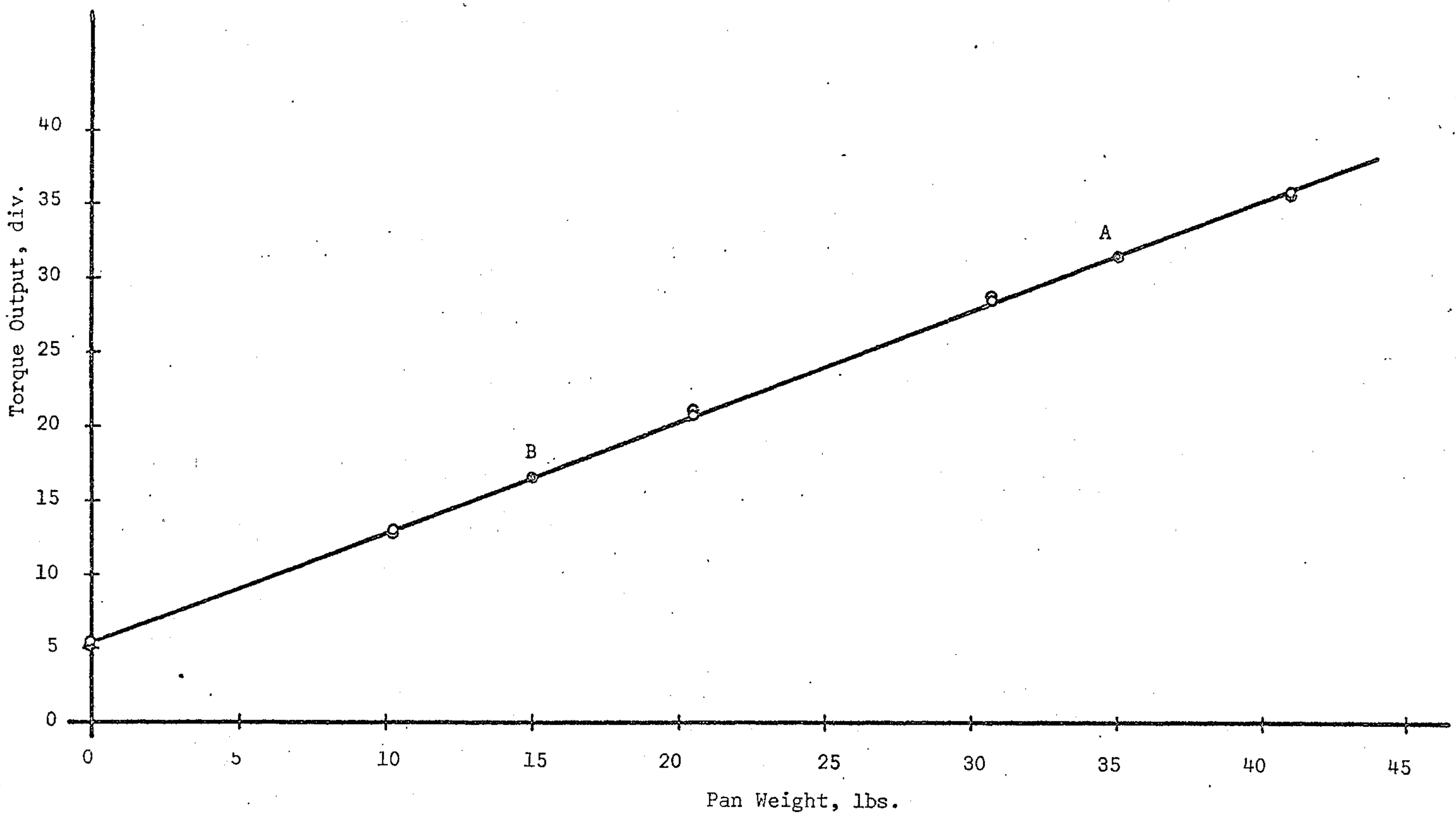

Fig. 23.--Torque Output Versus Pan Weight - Machine #3

each set of data and two points are selected off each curve. The delta values were determined; the pan weight was converted to true torque using:

$$\Delta T = \Delta WL$$

$$\Delta\tau_{true} = \frac{\Delta TC}{J}$$

where

ΔW = increment of pan weight,

L = torque lever arm distance,

ΔT = increment of torque,

C = radius of toolholder at the torque bridge,

J = polar moment of inertia at the torque bridge.

The torque output was converted to apparent shear stress using reduction Equation 1. Lastly, the slopes were determined and given the designation K_T. The results appear in Table 11.

Table 11. Torque Reduction Table from the Results of Table 10

Machine No.	Point A	Point B	ΔW lbs.	ΔN_{vis} div.	$\Delta\tau_{out}$ psi	$\Delta\tau_{True}$ psi	Slope K_T
1	(30.0, 33.0)	(10.0, 17.0)	20.0	16.0	513	452	0.882
2	(40.0, 40.0)	(5.0, 10.5)	35.0	29.5	943	792	0.840
3	(35.0, 31.5)	(15.0, 16.5)	20.0	15.0	480	452	0.944

2. Bending interaction into the torque bridge output

Description of Test

If the torque strain gages in the toolholder torque bridge were slightly misaligned during installation, then there will be an interaction between the torque bridge output and the bending load. This interaction must be determined experimentally for each torque bridge. The method used in Section 3-B-3 to determine the effect of torque on the bending bridge output was used again. The torque load was varied, and the change in the torque bridge output recorded.

Test Setup

If the torque load applied to the torque bridge is allowed to be zero, then the setup, Figure 10, used in Sections 3-B-1 and 3-B-2 can be used. Thus, three different calibration tests can be run with the same setup, greatly reducing the time necessary to complete the calibration of the fatigue machines.

In this test, the torque bridge and bending bridge outputs needed to be monitored. The cantilever system was connected electrically as described in Section 3-A.

Test Procedure

Weight was placed in the loading pan in ten-pound increments, as in Figure 10. A Visicorder run was taken after each weight increase. One hundred ten pounds was the maximum pan weight used. From twelve to thirty data points were run depending on the reproducibility of the data. Each time zero pan weight was reached, the Visicorder position was noted and compared with the previous one. If the difference was greater than 0.1 divisions, it was concluded that amplifier drift has occurred and the points between the zeroes were omitted.

Data Reduction

The calibration data are given in Table 12. For Machines #1 and #2, the data of bending bridge output were plotted against the torque bridge output, as shown in Figures 24 and 25. A straight line was fitted to the data and the slope of the line determined by taking incremental changes in torque and bending outputs and converting them to strain. Then the values were ratioed.

For Machine #1, two points on curve are:

Point A - (8, 0.15)

Point B - (0.35, - 0.1)

$$\Delta N_{vis_{bending}} = 7.65$$

$$\Delta N_{vis_{torque}} = 0.25$$

Table 12. Bending Output Versus Torque Output Data for Bending into Torque Interaction Calibration

	MACHINE #1		MACHINE #2		MACHINE #3	
Data Point Number	Torque Output div.	Bending Output div.	Torque Output div.	Bending Output div.	Torque Output div.	Bending* Output div.
1	-0.1	0.2	0	2.7	-0.3	2.4
2	+0.5	17.3	0.8	21.0	-0.5	9.0
3	-0.1	0.8	0	3.2	-0.8	20.1
4	+0.4	17.1	0.1	6.9	-0.3	9.1
5	+0.2	8.2	0.3	10.5	0	1.1
6	-0.1	0.5	0.6	14.1	-0.1	8.9
7	+0.1	8.0	0.7	17.1	-0.7	20.2
8	+0.4	16.9	0.9	22.6	-0.3	9.0
9	+0.2	7.8	1.0	25.2	+0.1	1.1
10	-0.1	0.3	0.8	21.6	-0.5	8.9
11	+0.1	7.7	0.6	18.0	-1.0	20.2
12	+0.4	16.5	0.5	14.4	-0.4	8.8
13	-0.1	0.1	0.3	10.7	+0.2	0.9
14			0.1	7.1	-0.4	8.8
15			0	3.3	-0.9	20.0
16			1.0	21.5	-0.3	8.9
17			1.2	25.2	+0.1	1.1
18			1.3	29.0	-0.4	8.8
19			1.5	32.8	-0.9	20.1
20			1.7	36.0	-0.3	9.0
21			1.8	40.0		
22			2.0	44.0		
23			2.0	44.2		
24			1.8	40.5		
25			1.6	36.0		
26			1.4	33.2		
27			1.2	29.5		
28			1.0	25.8		
29			0.8	22.0		
30						

* All bending data appears at 0.2 amplifier attenuation, therefore a 5/2 correction factor is required.

Visicorder Calibration Resistances:

Machine #1 - Bending 500 kΩ at 25.1 div.; Torque 304 kΩ at 44.9 div.
Machine #2 - Bending 500 kΩ at 24.0 div.; Torque 350 kΩ at 44.8 div.
Machine #3 - Bending 500 kΩ at 25.0 div.; Torque 350 kΩ at 44.8 div.

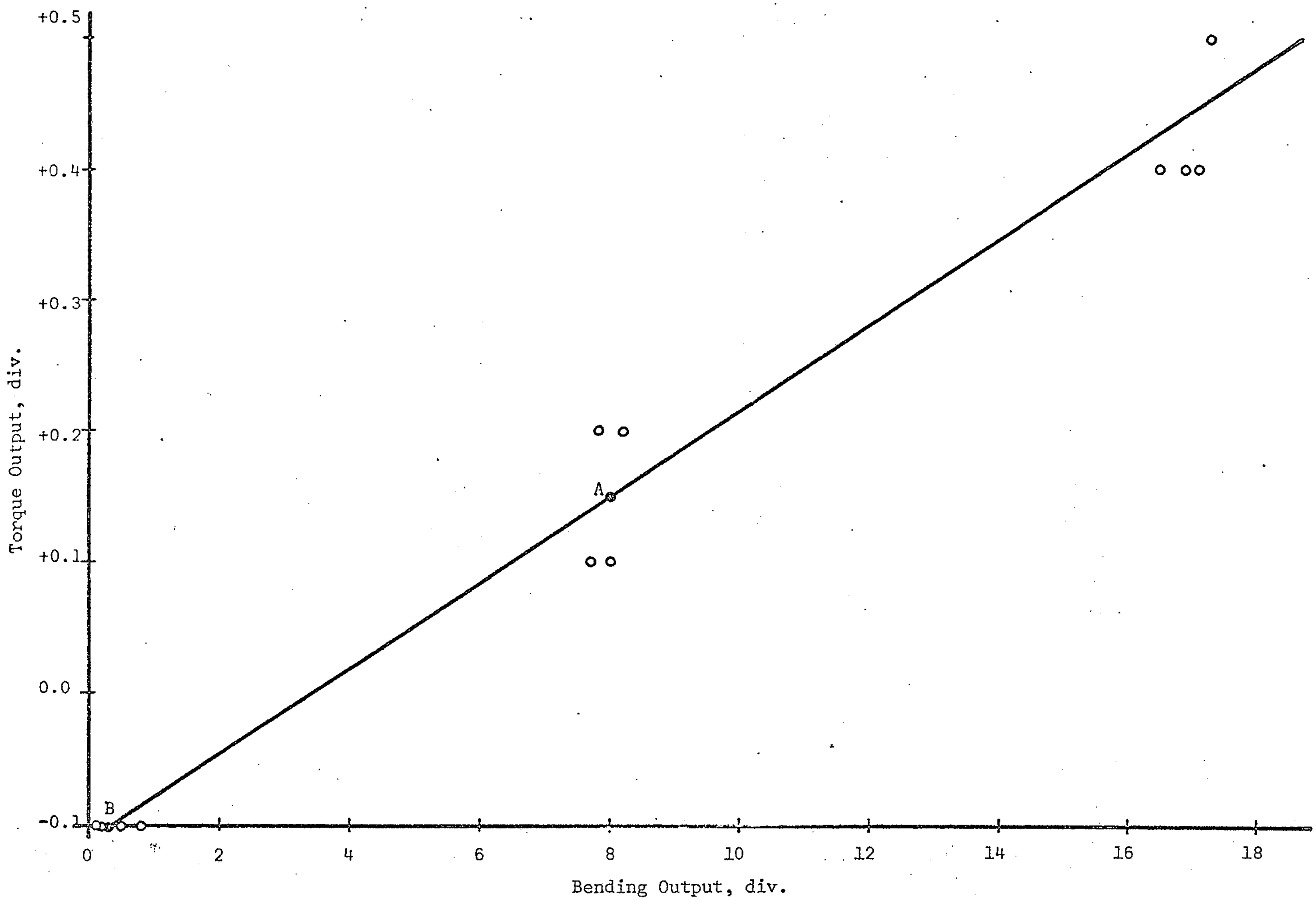

Fig. 24.--Bending Interaction into Torque - Machine #1

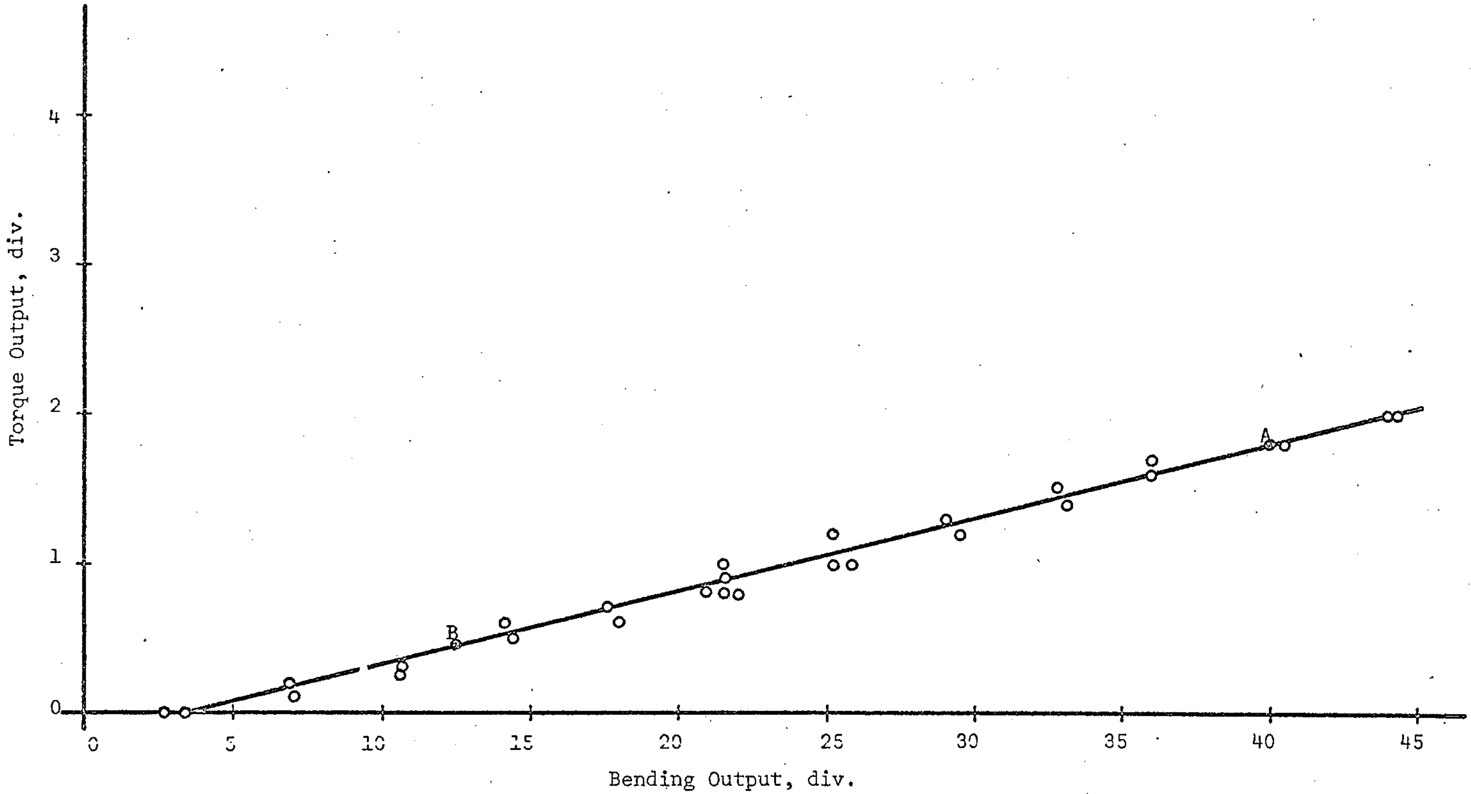

Fig. 25.--Bending Interaction into Torque - Machine #2

Using Equation 1,

$$\Delta\epsilon_B = \frac{(7.65)(190)}{(25.1)(4)(3.23)(6.5)(10^6)} = 8.97\ \mu in/in$$

$$\Delta\epsilon_T = \frac{(0.25)(120)}{(44.9)(4)(2.06)(0.304)(10^6)} = 0.267\ \mu in/in$$

$$\text{Slope} = \frac{\Delta\epsilon_T}{\Delta\epsilon_B} = \frac{0.267}{8.97} = 0.0298$$

For Machine #2, two points on curve are:

Point A - (40.0, 1.8)

Point B - (12.5, 0.45)

$$\Delta N_{vis_{bending}} = 27.5$$

$$\Delta N_{vis_{torque}} = 1.35$$

Using Equation 1,

$$\Delta\epsilon_B = \frac{(27.5)(190)}{(25.0)(4)(3.23)(500)(10^3)} = 33.58\ \mu in/in$$

$$\Delta\epsilon_T = \frac{(.135)(120)}{(44.8)(4)(2.06)(350)(10^3)} = 1.255\ \mu in/in$$

$$\text{Slope} = \frac{1.2555}{33.58} = 0.0374$$

Since for zero bending, the bending interaction into torque must also be zero; the slopes are all that are needed to completely define the interaction. The slope was given the designation $K_{B/T}$.

The Machine #3 data were reduced slightly differently. The tabulation of the data in Table 12 shows that the datum of the data shifted with each subset. Therefore, each subset was given a different plotting symbol, and the data were plotted as shown in Figure 26. A line was fitted to each subset, and the slopes were determined.

Symbol	Slope
o	- 0.02835
□	- 0.0608
x	- 0.0409
△	- 0.0591
*	- 0.0543

The dot subset was thrown out because it is far out of line. This was justified by the fact that these data were taken first, and equilibrium of the electrical equipment may not have been established. The remaining four slopes were averaged. The average slope is -0.0538. Then the conversion to strain was made.

$$\text{Slope} = \left.\frac{R_{gage}}{N_{cal}N_a GR_{cal}}\right._{T} \left.\frac{N_{cal}N_a GR_{cal}}{R_{gage}}\right._{B} \frac{N_{vis_{torque}}}{\frac{5N}{2}\,vis_{bending}}$$

$$= -0.01698$$

The coefficient of the bending Visicorder divisions is a correction factor made necessary by a change in the attenuation on the bending channel of the amplifier.

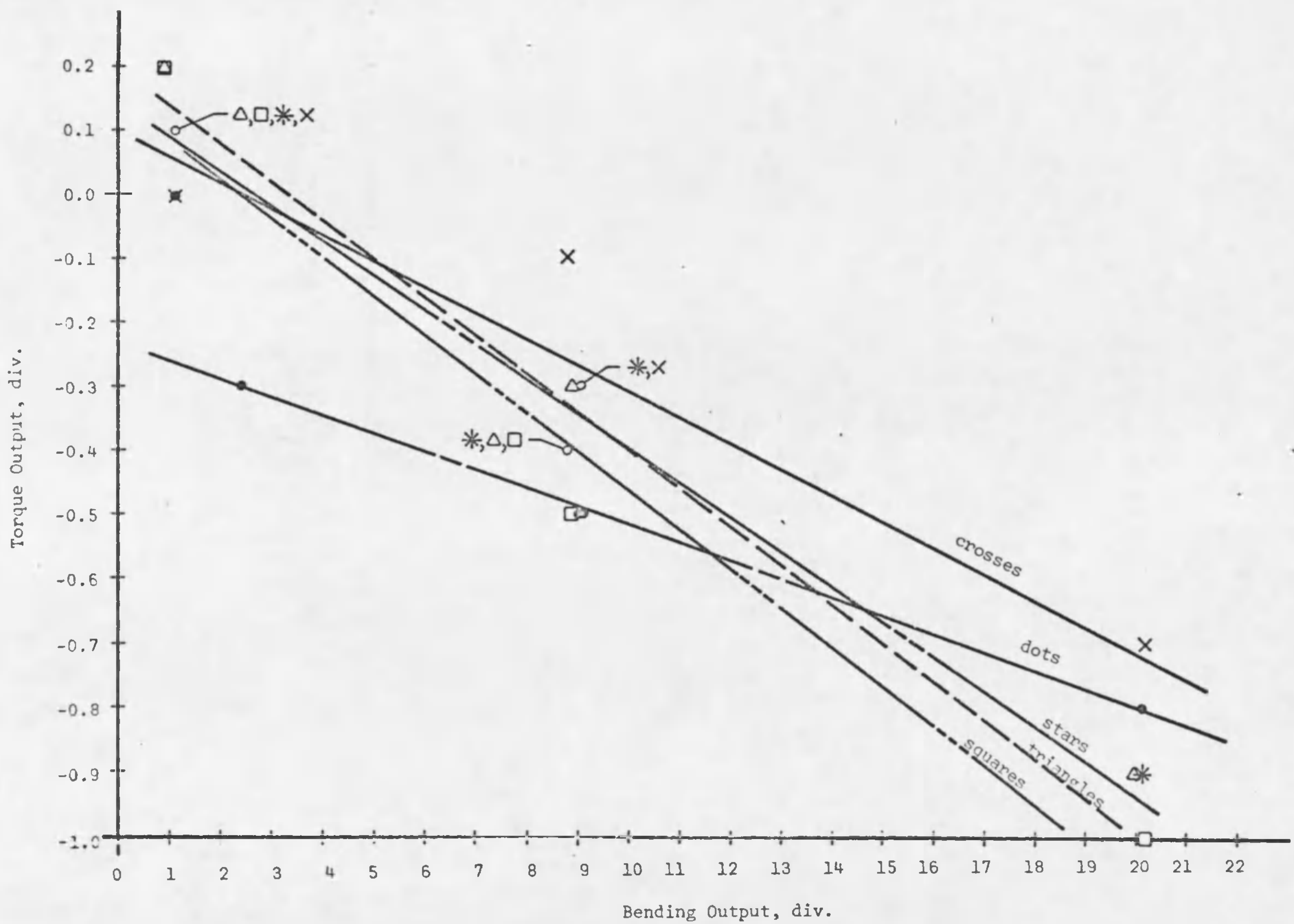

Fig. 26.--Bending Interaction into Torque - Machine #3

2a. Effect of bending on torque bridge output - additional test

Description of Test

From the definition of interaction, it is evident that the bending interaction into torque should not be a function of the mean torque load. That is, the misalignment of the torque gages does not vary with torque load; therefore, the interaction would not vary. A spot check was necessary to show that this reasoning is correct. The result can also be extended to the torque interaction into the bending bridge output. This test was applied only to Machine #2.

Test Setup

For this test, a high mean torque was applied to the cantilevered toolholder. The torque arm was required to apply this torque. The test setup was identical to that used to determine the effect of torque on the bending bridge output and is that of Figure 11.

Test Procedure

Twenty pounds was placed in the torque loading pan. This weight was left untouched for the remainder of the test. The remainder of the test proceeded in the manner described for the previous bending into torque interaction calibration.

Data Reduction

The data are given in Table 13 and plotted in Figure 27. The reduction of the data was the same as that given for the previous bending into torque interaction calibration:

From two points on fitted line:

Point A - (25.0, 26.1)

Point B - (10.0, 25.25)

$$\Delta N_{vis_{torque}} = 0.85$$

$$\Delta N_{vis_{bending}} = 15.0$$

$$\epsilon_B = \frac{N_{vis} R_{gage}}{N_{cal} N_a G\ R_{cal}} = \frac{(15.0)(190)}{(25.0)(4)(3.23)(500)(103)} = 17.65\ \mu in/in$$

$$\epsilon_T = \frac{N_{vis} R_{gage}}{N_{cal} N_a G\ R_{cal}} = \frac{(0.85)(120)}{(44.8)(4)(2.06)(350)(103)} = 0.788\ \mu in/in$$

$$\text{Slope} = \frac{0.788}{17.65} = 0.0447$$

This compares favorably with the slope presented for the zero mean torque interaction and, therefore, for Machine #2, the average of the two, 0.0410, is taken to be $K_{B/T}$.

Table 13. Bending Output Versus Torque Output Data at High Torque Level for Bending into Torque Interaction Calibration

MACHINE #2

Data Point Number	Torque Output div.	Bending Output div.
1	25.2	9.4
2	25.3	11.8
3	25.5	14.1
4	25.6	16.3
5	25.7	18.7
6	25.9	21.1
7	26.0	23.4
8	25.8	21.1
9	25.9	18.8
10	25.6	16.6
11	25.5	14.2
12	25.4	11.8
13	25.3	9.5
14	25.5	13.5
15	25.8	21.0
16	26.0	23.5
17	26.1	25.8
18	26.3	28.0
19	26.4	30.2
20	26.5	32.8
21	26.7	34.8
22	26.5	32.8
23	26.4	30.5
24	26.3	28.0
25	26.2	25.8
26	26.3	28.0
27	26.2	25.8
28	26.1	23.5
29	25.9	21.0
30	25.4	13.7

Visicorder Calibration Resistances:

Machine #2 - Bending 500 kΩ at 25.0 divisions
Torque 350 kΩ at 44.8 divisions

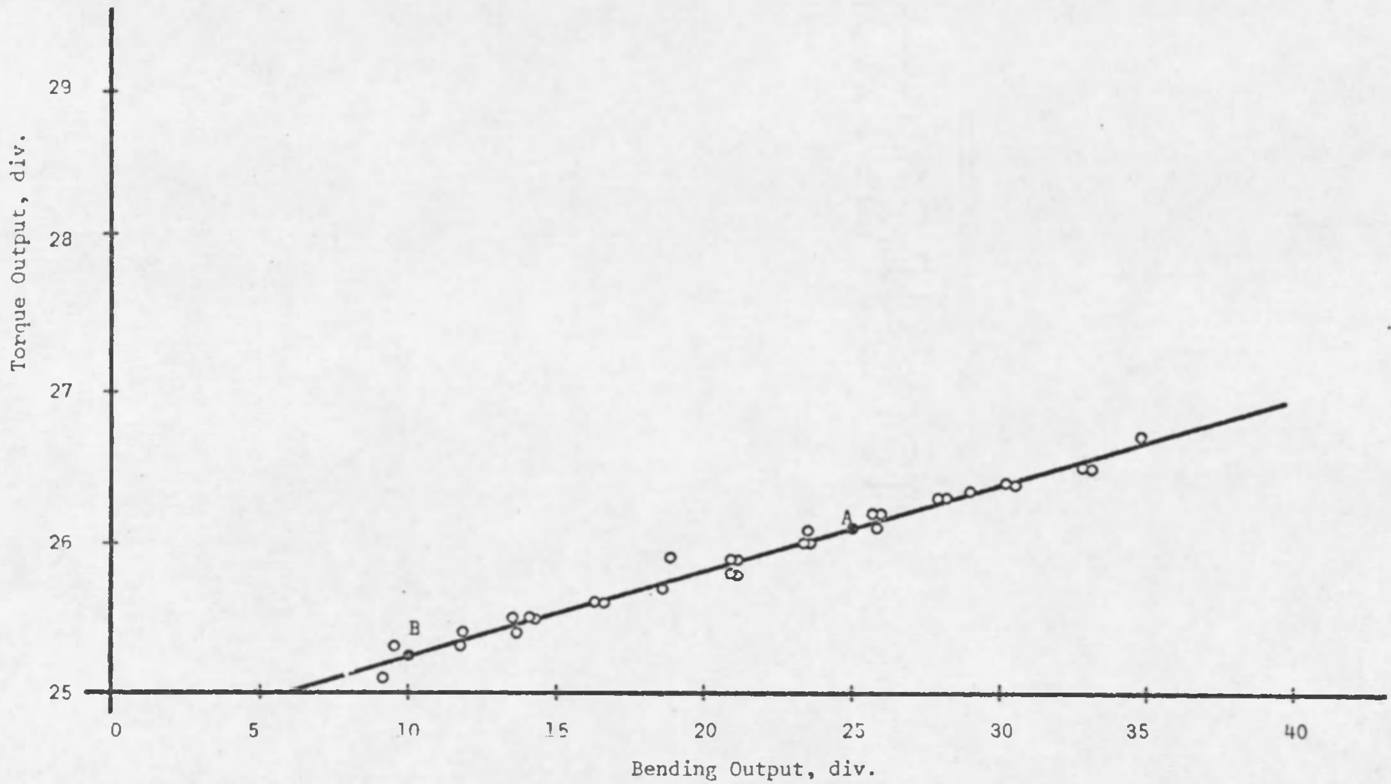

Fig. 27.--Bending Interaction into Torque at High Torque Level - Machine #2

D. Axial Effects

1. Effect of axial load on bending bridge output

Description of Test

It was not known whether the loading configuration of the fatigue machines imparts an axial stress in the test specimen. If there is such a force, then it must either be eliminated or accounted for in the determination of the stress ratio. The axial stress could be zero, a constant, a function of bending load, a function of torque load, or a function of both bending and torque loads. This axial stress must be accounted for in order to complete the calibration of the fatigue machines.

The toolholder bending bridge was set up so that it measured the bending strain and canceled any axial force applied. If two of the arms on the bridge are reversed, the bridge will now measure the axial load, cancel any bending load. A preliminary step in the measurement of the axial stress was to determine if any axial load interaction into the bending bridge output were present. If there is no interaction, then any change in the axial stress bridge, when a bending load is applied, will be a true measure of the axial stress in the specimen groove. If there is interaction, then the corrected output will be a measure of the axial force.

The test to be performed was not bending interaction into the axial bridge, but the axial interaction into the bending bridge. Since any interaction is due to misalignment of the bending gages, if one form of interaction is present, then the other must also be present.

Test Setup

The toolholder was removed from the fatigue machine and placed in a vertical position, resting the coupling end on a hard, level surface. A specimen with gages in the groove was installed in the collet. The bending bridge of the specimen was connected to the amplifier. Then the amplifier channel was balanced. A weight pan was next balanced on the end of the specimen and a Visicorder run taken. Then weight was stacked in ten-pound increments on the pan until sixty pounds was reached. The bending bridge output was recorded after each addition of weight.

Data Reduction

The Visicorder output showed that in all cases there was no measurable axial interaction into the bending bridge. From a previous discussion, it can also be concluded that there was no bending interaction into the axial bridge of the gaged specimen.

2. Measurement of the axial stress

2a. Measurement of the axial stress as a function of bending load

Description of Test

Since it was established that there was no bending interaction into the axial stress for the gaged specimen, the axial stress could be measured.

In this first test, the axial stress was investigated as a function of the bending load. The test was conducted only on Machine #1 and the results were reduced before any decision was made about extending the analysis to the other two machines.

Test Setup

The specimen which was used in the axial interaction test was installed in Machine #1 according to the installation checklist. The brush assembly which monitors the toolholder torque output was lifted from the sliprings so that they were inoperative. The long leads from the specimen were connected to the torque terminals on the brush support so that the bridge formed would measure axial stress and cancel bending. The toolholder bending bridge and the specimen axial bridge were zeroed and balanced according to the checklist.

Test Procedure

With the long arm in use, weight was added to the loading pan in five-pound increments. Between each increment a Visicorder run was taken while the toolholder was turned quickly by hand. Weight was added until twenty pounds was reached, and then the test was repeated.

Data Reduction

The data are given in Table 14. A plot of the data is given in Figure 28. It shows a non-zero axial stress which is a linear function of the bending load.

The magnitude of the axial stress was determined next. For a twenty-pound range in pan weight there was a 1.7 division range in axial groove gage bridge output. Converting this to strain,

$$\epsilon_o = \frac{N_{vis}}{N_{cal}} \frac{R_{gage}}{N_a \; G \; R_{cal}} = \frac{(1.7)(120)}{(50.0)(2)(2.09)(290{,}000)} = 3.38 \; \mu in/in$$

or in terms of stress

$$\sigma_o = E\epsilon_o = 30 \times 10^6 \times 3.38 \times 10^{-6} = 101.4 \text{ psi}$$

This is a negligible amount of axial stress. Since the pan weight range was twenty pounds on the long arm, an axial stress of about 100 psi would be the maximum that would ever be encountered in any test run. Therefore, the axial stress due to bending load can be omitted. The

Table 14. Axial Output Versus Bending Output for Axial to Bending Interaction Calibration

MACHINE #1

Data Point Number	Bending Level div.	Groove Bending Mean div.
1	20.8	-0.2
2	24.2	-0.5
3	27.9	-0.5
4	31.5	-0.6
5	35.0	-0.9
6	38.7	-1.1
7	41.9	-0.8
8	19.6	0
9	42.2	-1.4
10	19.7	+0.2
11	41.9	-1.0
12	19.4	+0.3
13	41.8	-1.0

Visicorder Calibration Resistances:
Machine #1 - Bending (toolholder) 190 kΩ at 50.0 divisions
Bending (groove) 290 kΩ at 50.0 divisions

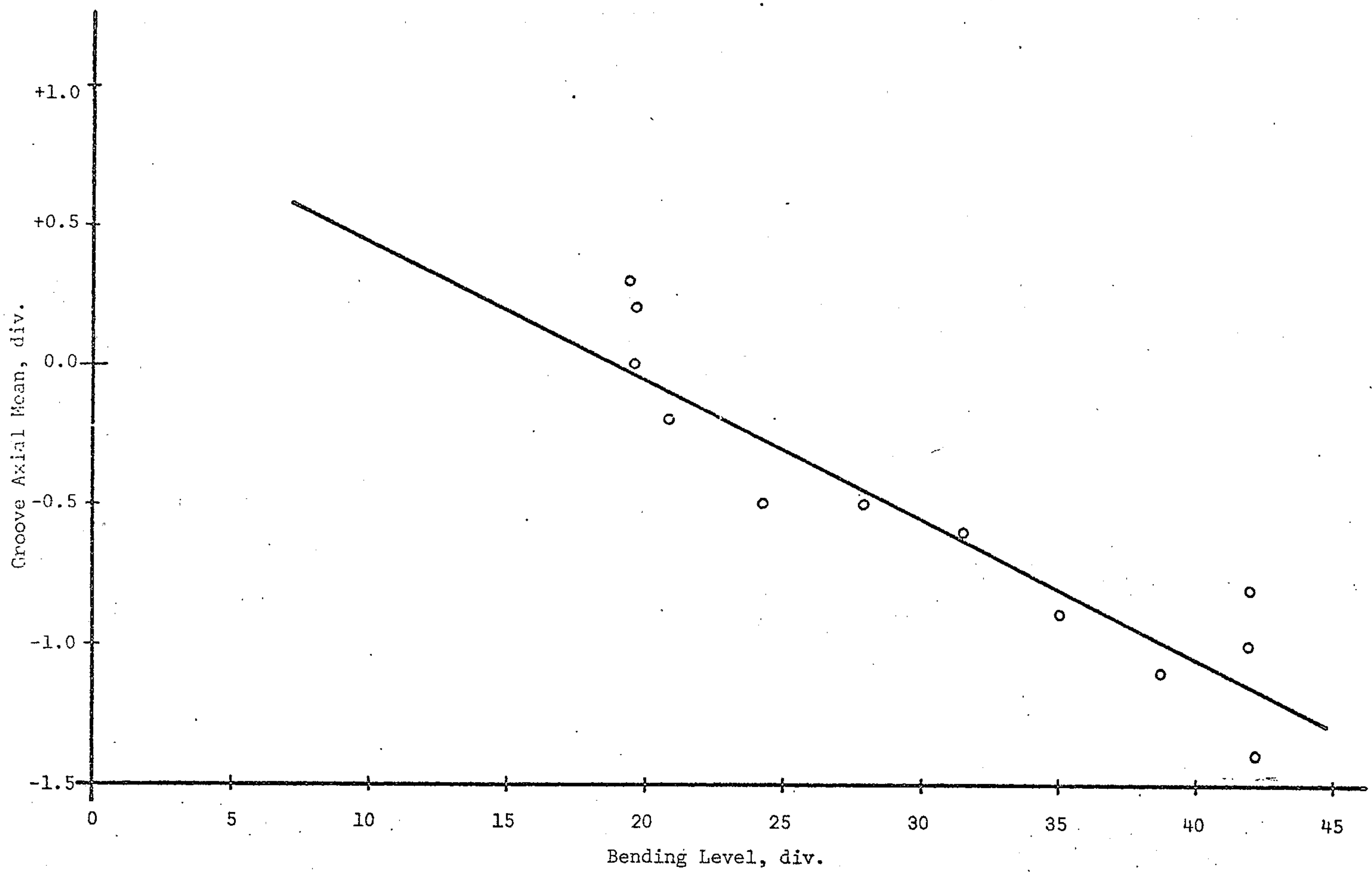

Fig. 28.--Axial Output Versus Bending Load - Machine #1

analysis was not extended to the other two machines because the axial stress was found to be so small that a value ten times as great would still be negligible.

2b. Measurement of the axial stress as a function of torque load

Description of Test

Next, the axial force was measured as a function of the torque load with the bending load held constant. This test was performed only for Machine #1.

Test Setup

The torque brushes were placed in contact with the slip-rings and the bending gages lifted. The axial bridge of the specimen was wired to the bending terminals on the brush mount. The specimen was installed according to checklist procedures. The torque bridge and the specimen axial bridge were zeroed and balanced. Five pounds was placed in the loading pan at the end of the long arm.

Test Procedure

Torque load was varied randomly through the Infinit-Indexer and a Visicorder run taken at each level. Fourteen levels were run.

Data Reduction

The data are given in Table 15. The specimen groove gage output plotted against the torque output appears in Figure 29 and is a linearly varying axial stress. The range of the stress is 2.7 divisions. The strain for this output is,

$$\epsilon_o = \frac{N_{vis}}{N_{cal}} \frac{R_{gage}}{N_a\ G\ R_{cal}} = \frac{(3.9)(120)}{(49.8)(2)(2.08)(290{,}000)} = 7.8\ \mu in/in$$

which is 233.4 psi in terms of stress.

This value, although larger than the one for bending load, is still negligible. The small value of the axial stress over a large range of torque indicated that the test did not have to be repeated for the other two machines.

E. Summary of Calibration Results

The calibration of the complex fatigue reliability research machines was thus completed. Bending, torque and axial interaction tests, calibration of the bending, torque and specimen groove bridges against a standard, and toolholder bending output versus specimen groove bending output tests were thus performed for each machine. The relationship between the variables in each case proved to be linear and a slope could be associated with each calibration. Since for all cases, the functional relationship

Table 15. Axial Output Versus Torque Output for Axial Load into Torque Interaction Calibration

MACHINE #1

Data Point Number	Torque Level div.	Groove Axial Mean div.
1	0	-0.6
2	11.8	+0.3
3	36.7	+1.8
4	27.1	+0.8
5	1.5	-1.2
6	40.0	+1.5
7	21.5	+0.5
8	7.8	-1.5
9	1.1	-1.9
10	31.3	+2.0
11	41.5	+0.8
12	27.6	+1.0
13	15.6	0
14	0.5	-1.8

Visicorder Calibration Resistances:

Bending (groove) 290 kΩ at 49.8 divisions
Torque 304 kΩ at 45.0 divisions

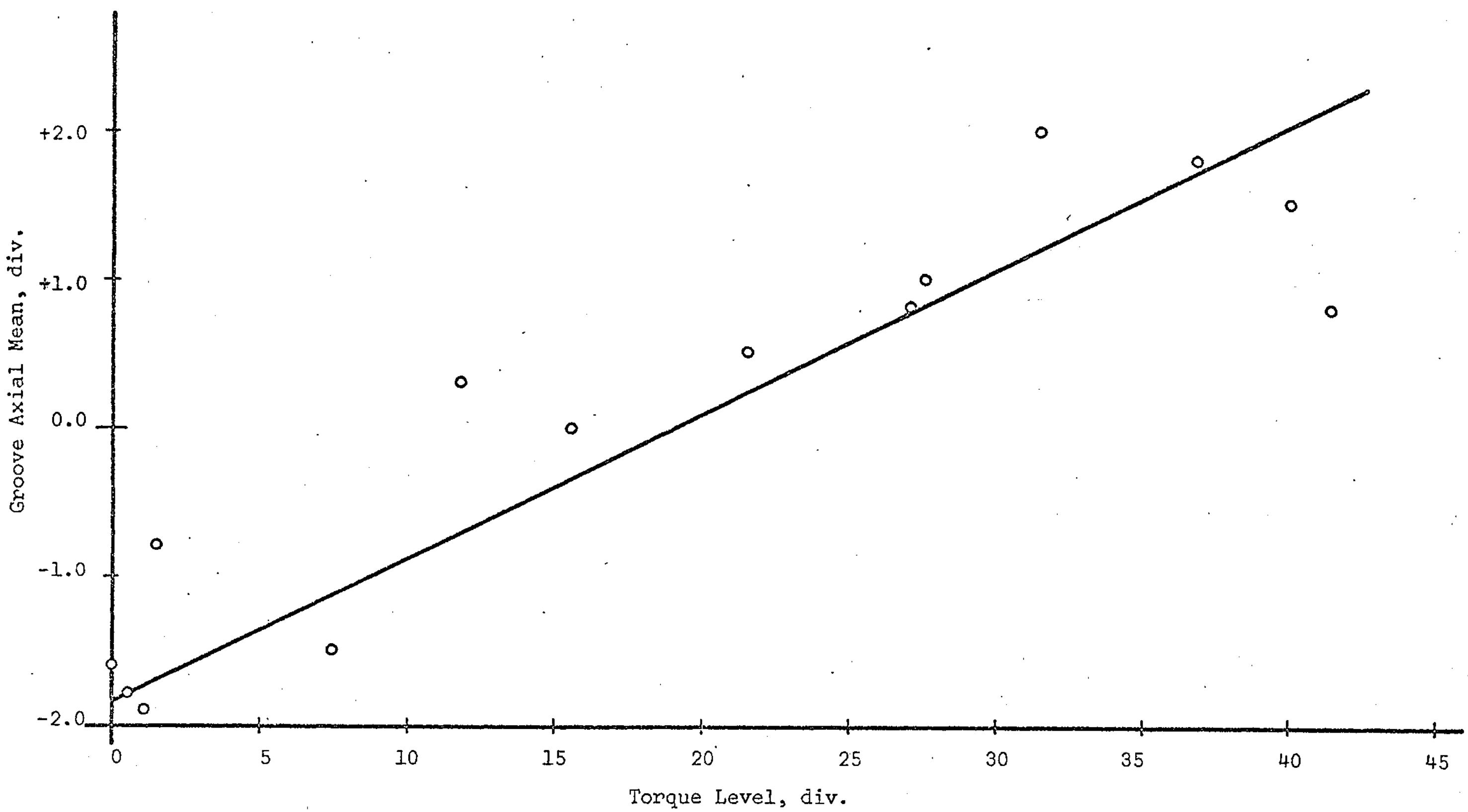

Fig. 29.--Axial Output Versus Torque Load - Machine #1

begins at the origin, the slope of each curve completely defines the function. These slopes have been given calibration coefficient designations and appear in Table 16. The two footnotes of the table are explained in Appendix E.

Table 16. The Calibration Coefficients for Each Research Machine

Machine	K_{BGR}	K_{GR-TH}	K_T	$K_{T/B}$	$K_{B/T}$
1	0.967	0.0203	0.882	0.0548	0.0298
2	0.902	0.0198	0.840	0.0343	0.0410
3	0.972	0.0215	0.944*	0.0000	-0.0170**

* After June 1, 1969 $K_T = 0.842$ because of gage replacement

** After June 1, 1969 $K_{B/T} = -0.0238$ because of gage replacement

Now, it is necessary to combine the calibration results into an orderly method of determining the true shear and bending stresses in the specimen groove given a Visicorder output, or vice versa. Actually, the calibration procedure requires that the calibration method be run in both directions. First, in any test run, the desired stress ratio and bending stress level are selected. From these, the shear stress level can be calculated and, although the use of the calibration coefficients, the number of divisions of bending and torque on the Visicorder can be determined given the machine to be used, the calibration resistance, and the calibration divisions. Next, the test is run and a Visicorder record taken. The record is then reduced. The four experimental parameters, bending divisions, torque divisions, bending calibration divisions, and torque calibration divisions, are measured. Using the calibration procedure in reverse direction, the actual bending stress, shear stress, and stress ratio are determined. When an entire stress level is run, some statistical comments can be made concerning the stress levels and stress ratios achieved. This is discussed in Section 4-A.

The calibration procedure will now be described in detail with the aid of the Calibration Flow Chart of Figure 2. Steps 1 and 2 on the flow chart require a selection of a stress ratio and a bending stress level. The true shear stress in the specimen groove to give this ratio is found in Step 3 from the relationship

$$\tau_{true_{GR}} = \frac{\sigma_{true_{GR}}}{r_s \sqrt{3}}$$

where $\sigma_{true_{GR}}$ is the true bending stress in the groove, and r_s is the desired stress ratio. Next, in Step 4, the true bending stress in the groove is converted to output stress in the groove using K_{BGR} and then K_{GR-TH}, the relationship between output bending stress in the groove, is employed. On the torque side, Step 5 gives the equation for converting shear stress in the groove to shear stress in the toolholder. This is a purely geometric relationship employing no calibration parameters. However, on the bending side an empirical relationship was necessary because the bending moment along the toolholder shaft is not constant. For torque, it is a safe assumption that the torque applied along the toolholder shaft is constant. The static stress concentration factor is shear, K_{ts}, is included in this term. A published value of K_{ts}, 1.22 [23], is used here. Also, in Step 5, the true shear stress in the toolholder is converted to output stress. Steps 6 and 7 are the corrections for interaction. The shear stress value is used to correct bending stress and vice versa. The calibration coefficients are $K_{T/B}$ and $K_{B/T}$. Steps 8 and 9 convert the corrected output stresses to Visicorder divisions, completing the procedure.

Table 17 contains the stress levels and Visicorder divisions for $r_s = 3$ and Machine #1 using the procedure just described.

Table 17. Stress Levels and Visicorder Divisions for $r_s = 3$ and Machine #1

Alternating Bending Stress psi	Bending Divisions div.	Calibration Div/Resistance div/kΩ	Mean Shear Stress psi	Shear Divisions div.	Calibration Div/Resistance div/kΩ
154,800	43.5	50/125	29,800	19.4	45/304
121,800	34.2	50/125	23,400	15.3	45/304
104,350	44.5	50/190	20,080	13.1	45/304
86,800	37.0	50/190	16,700	10.9	45/304
77,700	33.2	50/190	14,950	9.8	45/304

CHAPTER 4

RESEARCH DATA REDUCTION

A. Conversion of Visicorder Outputs to Stress Levels

Once the Visicorder divisions for bending and torque are determined according to the methods of Section 3-E, the test runs are made. A Visicorder record is made and kept for each specimen. When a stress level is complete, the shear and bending divisions, and the shear and bending calibration divisions, are measured on each Visicorder record. These four values, along with the test number, specimen number, the calibration resistances, the pan weight and the machine number, are punched on IBM cards for computer analysis. A computer program in Fortran IV has been prepared which gives the actual shear stress, bending stress and stress ratio for each run, as shown on the following pages. It also determines the mean and standard deviation of the shear and bending stresses and the stress ratio for each bending stress level assuming a normal distribution for these data.

The program contains a number of "IF" statements which select the proper machine number and mode for a data card. The mode is determined by the data on which the specimen was run.

MODE 1: For 26 July 1966 to 10 August 1967

MODE 2: For 11 August 1967 to June 1969

MODE 3: For 1 June 1969 to next gage failure

A new mode is initiated whenever a strain gage on any machine fails, necessitating recalibration. Thus, the computer program differentiates between past and present machine configurations. The program is set up so that a new configuration can be integrated into the data reduction by adding three "IF" statements and listing the new calibration parameters. In addition, the program can accommodate the stress ratio infinity as well as all finite ratios.

B. Reduction of Endurance Strength Data for $r_s = \infty$ and $r_s = 0.90$

For stress ratios of infinity and 0.90, the increment used in the staircase method [24, pp. 14-17] was one pound pan weight on the short arm. Therefore, the results of the staircase method, the mean and standard deviation of the bending stress for endurance, is in terms of pan weight. It is now necessary to convert pan weight to true stress.

Just like the finite times-to-failure runs, Visicorder records were made for the endurance limit runs. The Visicorder records were measured, the data placed on

```
      GØ TØ 50
   20 CBGR=.967
      CGRTH =.0203
      CT=.882
      CTB=.0548
      CRT=.0298
      GØ TØ 50
   30 CBGR=.902
      CGRTH =.0198
      CT=.840
      CTH=.0343
      CRT=.0410
      GØ TØ 50
   40 CBGR=.972
      CGRTH=.0215
      CT=.944
      CTB=.0
      CRT=-.01698
   50 IF(ENVIST.EQ.0.0) GØ TØ 160
      GØ TØ 51
C     CALCULATIØN ØF BENDING STRESS LEVEL FØR INFINITY
         RATIØ
  160 SØUTH=(ENVISB*E*RGAGEB)/(ENCALB*ENA*GB*RCALB)
      STRGR(I) = SØUTH / (CGRTH * CBGR)
      TAUGR(I) = 0.0
      PRINT 71.NØTEST,NØSPEC,MACHNØ,NPANWT,RCALB,ENCALB,
         ENVISB,RCALT,
     1ENCALT,ENVIST,STRGR(I),TAUGR(I)
71    FØRMAT(4X,I3,6X,I3,8X,I1,8X,I2,F14.1,F10.2,F11.2,
         F12.1,F9.2,F10.2,
     1F11.1,F11.1,2X,6HINFIN./)
      GØ TØ 120
C     CALCULATIØN ØF BENDING STRESS, SHEAR STRESS AND
         STRESS RATIØ FØR
C     ALL FINITE RATIØS
   51 SOUTHP=(ENVISB*E*RGAGEB)/(ENCALB*ENA*GB*RCALB)
      TAUTHP=(ENVIST*E*RGAGET)/(ENCALT*ENA*GT*RCALT)
      SØUTH=SØUTHP-CTB*TAUTHP
      TAUTH=TAUTHP-CBT*SØUTH
      STRGR(I) = SØUTH / (CGRTH * CBGR)
      TAUGR(I)=CT*(TAUTH/.0157)
      R(I) = STRGR(I) / (TAUGR(I) * 1.7321
      PRINT 70,NØTEST,NØSPEC,MACHNØ,NPANWT,RCALB,ENCALB,
         ENVISB,RCALT,
     1ENCALT,ENVIST,STRGR(I),TAUGR(I),R(I)
   70 FØRMAT(4X,I3,6X,I3,8X,I1,8X,I2,F14.1,F10.2,F11,2,
         F12.1,F9.2,F10.2,
     1F11.1,F11.1,F8.3/)
  120 CONTINUE
```

```
C       CALCULATIØN ØF MEAN AND STANDARD DEVIATIØN ØF
           BENDING STRESS,SHEAR
C       STRESS, AND STRESS RATIØ
        CALL MEAN (STRGR, CARDS,NCARDS, XMEAN, DEV)
        PRINT 3
3       FØRMAT (1HO)
        PRINT 130, XMEAN, DEV
130     FØRMAT (19X,31HMEAN BENDING STRESS IN GRØØVE =,
           F10.1,5H PSI.//11X,
       139HSTD. DEV. ØF BENDING STRESS IN GRØØVE =,F10.2,
           5H PSI./)
        IF(ENVIST.EQ.0.0) GØ TØ 200
        CALL MEAN (TAUGR, CARDS, NCARDS, XMEAN, DEV)
        PRINT 3
        PRINT 140, XMEAN, DEV
140     FØRMAT (20X,30HMEAN TØRQUE STRESS IN GRØØVE =,F10.1,
           5H PSI.//12X,
       138HSTD. DEV. ØF TØRQUE STRESS IN GRØØVE =,F10.2,5H
           PSI./)
        CALL MEAN (     R,  CARDS,NCARDS, XMEAN, DEV)
        DIMENSION STRGR(50), TAUGR(50), R(50)
        NCØUNT = 0
C       READ IN THE NUMBER OF STRESS LEVELS IN RUN
        READ 161, NØSTLV
  161   FØRMAT (I5)
        PRINT 90
   90   FØRMAT(1H1//)
        NCØUNT = NCØUNT + 1
        PRINT 60
C       FØRMAT FØR ØUTPUT HEADINGS
   60   FØRMAT (3X,4HTEST,3X,BHSPECIMEN,3X,7HMACHINE,5X,
           3HPAN,7X,4HRCAL,7X
       1,4HNCAL,7X,4HNVIS,6X,4HRCAL,6X,4HNCAL,6X,4HNVIS,5X,
           7HBENDING,4X,
       25HSHEAR,4X,6HSTRESS/4X,3HNØ.,6X,3HNØ.,7X,3HNØ.,5X,
           6HWEIGHT,4X,
       37HBENDING,4X,7HBENDING,4X,7HBENDING,4X,6HTØRQUE,
           4X,6HTØRQUE,4X,
       46HTØRQUE,5X,6HSTRESS,4X,6HSTRESS,4X,5HRATIØ//)
C       READ IN THE NUMBER ØF CARDS IN THE STRESS LEVEL AND
           THE MØDE
C       ØF ØPERATIØN ØF THE MACHINE
        READ 100, NCARDS,MØDE
  100   FØRMAT(2I5)
        DØ 120 I = 1, NCARDS
C       READ IN THE TEST NØ., SPECIMEN NØ., MACHINE NØ.,
           PANWEIGHT, AND THE
C       CALIBRATIØN RESISTANCE, VISICØRDER CALIBRATIØN
           DISTANCE AND VISICØRDER
```

```
C       ØUTPUT DIVISIØNS FØR BENDING AND TØRQUE
    80 READ 10,NØTEST,NØSPEC,MACHNØ,NPANWT,RCALB,ENCALB,
          ENVISB,RCALT,
      1ENCALT,ENVIST
    10 FØRMAT (4I5,6F10.2)
       CARDS = NCARDS
C      DEFINE THE ELASTIC MØDULUS, NØ. ØF ACTIVE ARMS ØF
          THE BRIDGES, THE
C      RESISTANCES ØF THE BENDING AND TØRQUE GAUGES, AND
          THE BENDING AND
C      TØRQUE GAUGE FACTØRS
       E=30000000.
       ENA=4.
       RGAGEB=190.
       RGAGET=120.
       GB=3.23
       GT=2.06
C      SELECTIØN ØF MACHINE AND MØDE
       IF(MACHNØ.EQ.1.AND.MØDE.EQ.1)  GØ TØ 21
       IF(MACHNØ.EQ.2.AND.MØDE.EQ.1)  GØ TØ 31
       IF(MACHNØ.EQ.1.AND.MØDE.EQ.3)  GØ TØ 20
       IF(MACHNØ.EQ.2.AND.MØDE.EQ.3)  GØ TØ 30
       IF(MACHNØ.EQ.3.AND.MØDE.EQ.3)  GØ TØ 32
       IF(MACHNØ.EQ.1.AND.MØDE.EQ.2)  GØ TØ 20
       IF(MACHNØ.EQ.2.AND.MØDE.EQ.2)  GØ TØ 30
       IF(MACHNØ.EQ.3.AND.MØDE.EQ.2)  GØ TØ 40
C      CALIBRATIØN PARAMETERS FØR GIVEN MØDE AND MACHINE
    31 CBGR=.902
       CGRTH=.0198
       GØ TØ 50
    21 CBGR=.972
       CGRTH=.0203
       GØ TØ 50
    32 CBGR=.972
       CGRTH=.0215
       CT=.842
       CTB=0.0
       CBT=-.0238
       PRINT 3
       PRINT 150, XMEAN,DEV
150    FØRMAT (31X,19HMEAN STRESS RATIØ =,F10.5//18X,
          32HSTD. DEV. ØF MEAN
      1 STRESS RATIØ =,F10.5)
   200 IF (NCØUNT.LT.NØSTLV) GØ TØ 170
       STØP
       END
```

computer cards, and a computer run made, just as described in Section 3-A. Only the points which were used in the staircase method (successes or failures) were used. The output contains the bending stress levels, torque stress levels ($r_s = 0.90$ only) and the stress ratios ($r_s = 0.90$ only). Also the mean and standard deviation of the data set as a whole is outputted; however, these are meaningless for endurance runs, hence are discarded. However, the stress ratio is needed.

For a given pan weight, all the bending stresses for that pan weight were averaged. This was done for each pan weight. The result was the mean true bending stress for each pan weight.

Next, the true bending stress in the groove was plotted against pan weight for both $r_s = \infty$ in Figure 30, and $r_s = 0.90$ in Figure 31. Straight lines were then fitted to the points. Since the mean, $\overline{S}_e$, and standard deviation, σ_{S_e}, of the endurance strength were determined in terms of pan weight by the staircase method [24, pp. 14-17], Figures 30 and 31 made it possible to relate pan weight to true stress. The results are as follows:

For $r_s = \infty$

$$\overline{S}_e = 25.5 \text{ lbs} = 61{,}500 \text{ psi}$$

$$\sigma_{S_e} = 1.34 \text{ lbs} = 3{,}500 \text{ psi}$$

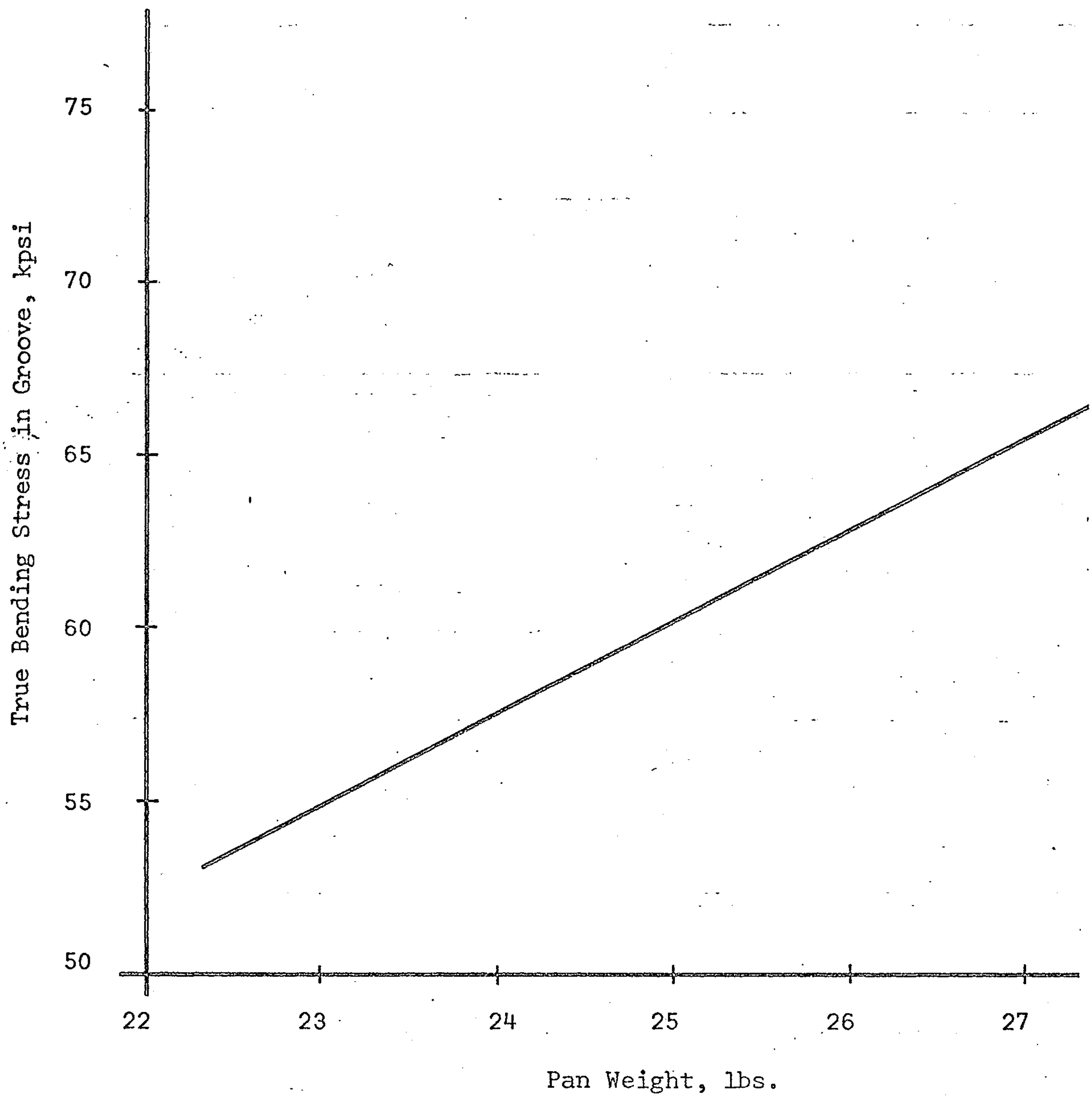

Fig. 30.--Pan Weight Versus True Bending Stress for Endurance Strength for $r_s = \infty$

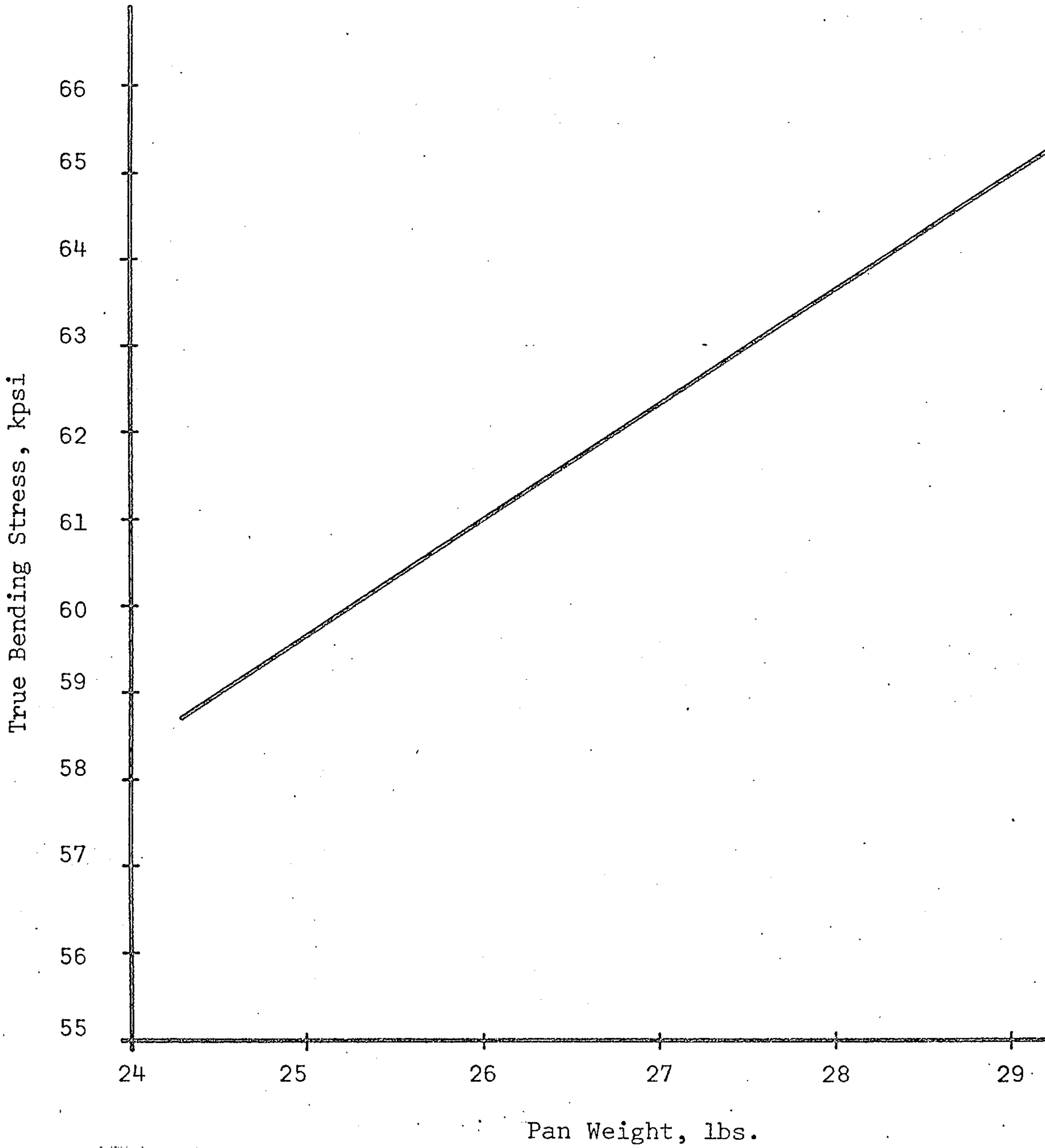

Fig. 31.--Pan Weight Versus True Bending Stress for Endurance Strength for $r_s = 0.90$

For $r_s = 0.90$

$$\bar{S}_e = 26.0 \text{ lbs} - 61{,}000 \text{ psi}$$

$$\sigma_{S_e} = 2.25 \text{ lbs} = 3{,}000 \text{ psi}$$

The mean and standard deviation of the stress ratio for $r_s = 0.90$ from the data reduction computer program, given in Appendix B, though printed out, are not intended for any use. The program is devised for finite life data; hence, it automatically calculates these and prints them out.

C. Generation of S-N Diagrams Using Distributional Stress Levels and Mean Cycles-to-Failure

The reduced data of Appendices A and B provide the mean and standard deviation of each stress level. With these distributional parameters and the corresponding mean cycles-to-failure data [28, pp. 52-54] it was possible to construct S-N curves for $r_s = \infty$, and $r_s = 0.70$, with the 3σ limits of the distribution of the actually applied bending stresses also given, assuming the stresses applied are normally distributed.

The S-N curve for $r_s = \infty$ appears in Figure 32, and for $r_s = 0.70$ in Figure 33.

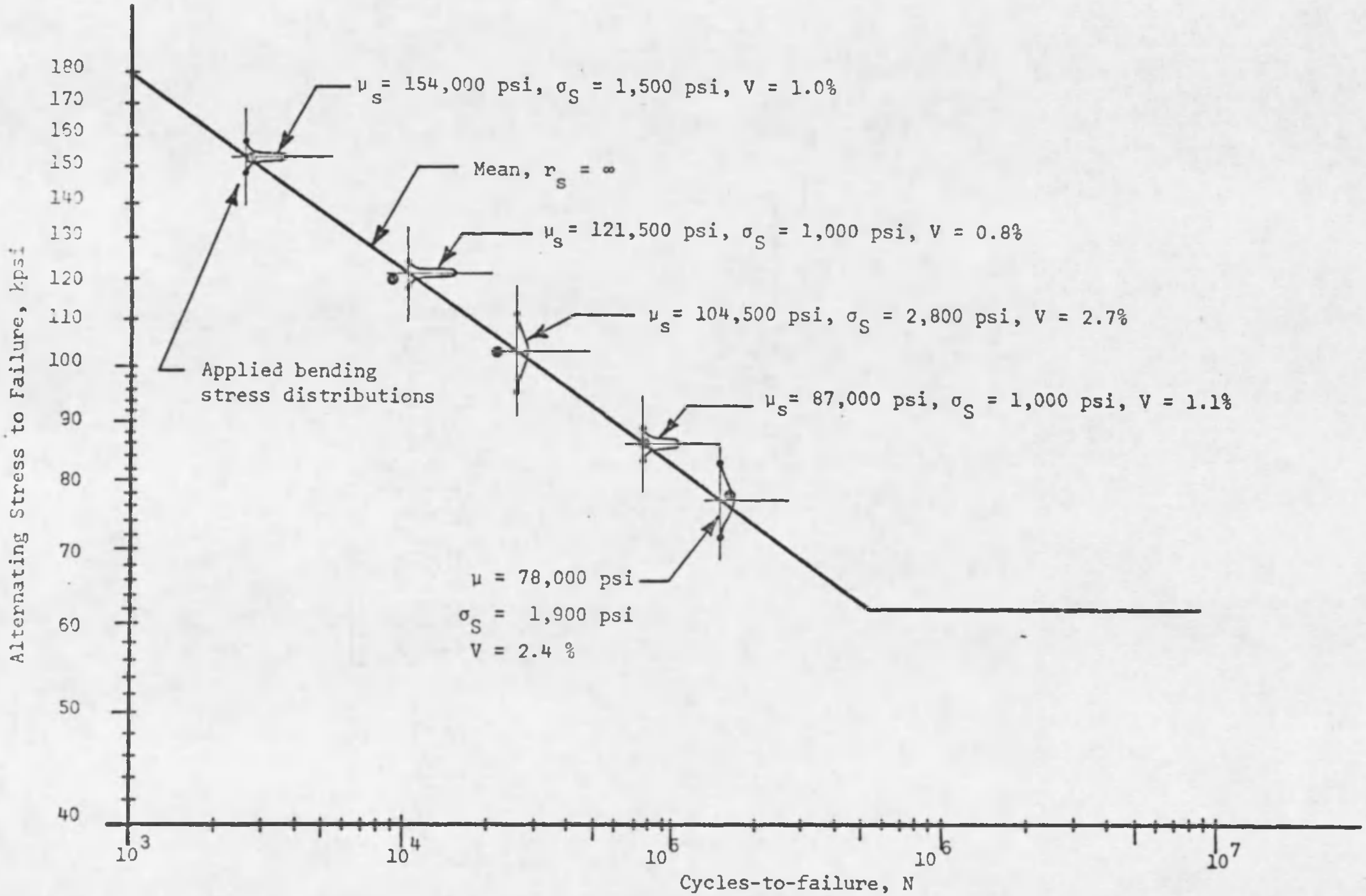

Fig. 32.--Applied Bending Stress Distributions for Stress Ratio of ∞

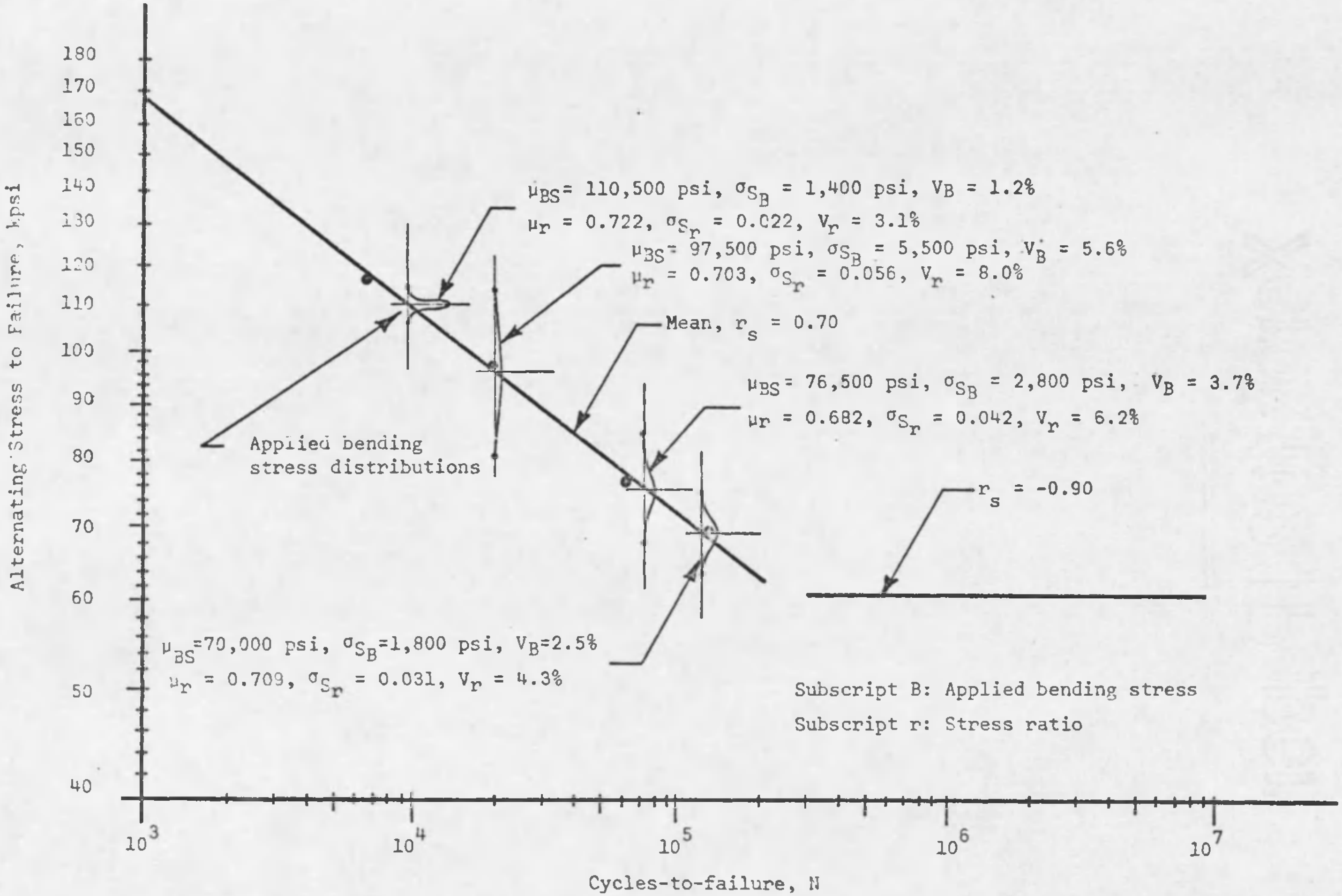

Fig. 33.--Applied Bending Stress Distribution for a Stress Ratio of 0.70 and Endurance Strength for a Stress Ratio of 0.90

D. Generation of Theoretical S-N Diagram

It would be interesting to compare the S-N diagram results generated in this research with a theoretical S-N diagram constructed according to the procedure recommended by Shigley [25, p. 162].

The fatigue strength of specimens, S_e, at 10^3 cycles $\cong 0.9S_U$

$$S_U = 178 \text{ ksi, for unnotched specimens}$$

$$S_{e_{10^3}} = 0.9 \times 178$$

$$S_{e_{10^3}} = 160 \text{ ksi}$$

The endurance strength is given by

$$S_e = k_a k_b k_d k_e k_f S_E' \tag{4}$$

For specimens used in this research,

k_a = surface finish factor = 0.89 for ground finish [25, p. 167]

k_b = size factor = 0.85 for D = 2.0 in. bending [25, p. 186]

k_d = temperature factor = 1, no temperature effect

k_e = stress concentration design factor = $\frac{1}{K_f}$ [25, p. 170]

$k_f = 1 +]\ (K_t - 1)$ [25, p. 170]

$q = 0.92$ [25, p. 171]

$K_t = 1.45$ [26, p. 49]

$K_f = 1 + 0.92\,[1.45 - 1]$

$K_f = 1.41$

$k_e = \frac{1}{1.41} = 0.709$

k_f = miscellaneous effects factor = 1

$S_e{}'$= theoretical endurance strength = 0.5 S_U [25, p. 162]

S_U = 178 ksi

Therefore,

$S_e{}' = 0.5 \times 178 = 89$ ksi

Using Equation (4)

$S_e = (0.89)(0.85)(1.0)(0.709)(1.0)(89) = 47.7$ ksi

With S_e and $S_{e_{10^3}}$ thus determined, an S-N diagram was plotted and is given in Figure 34.

E. Comparison of Theoretical and Experimental S-N Curves

In Figure 34, the theoretical and experimental S-N curves for $r_s = \infty$, and the experimental S-N for $r_s = 0.70$, are given. It can be seen that the theoretical curve is about 11% lower than the experimentally determined curve in the finite life region and the endurance strength is about 22.5% less. This indicates that the conventional approach for constructing a theoretical S-N curve is fairly pessimistic, at least for the operating conditions of this research. There is no theoretical basis for

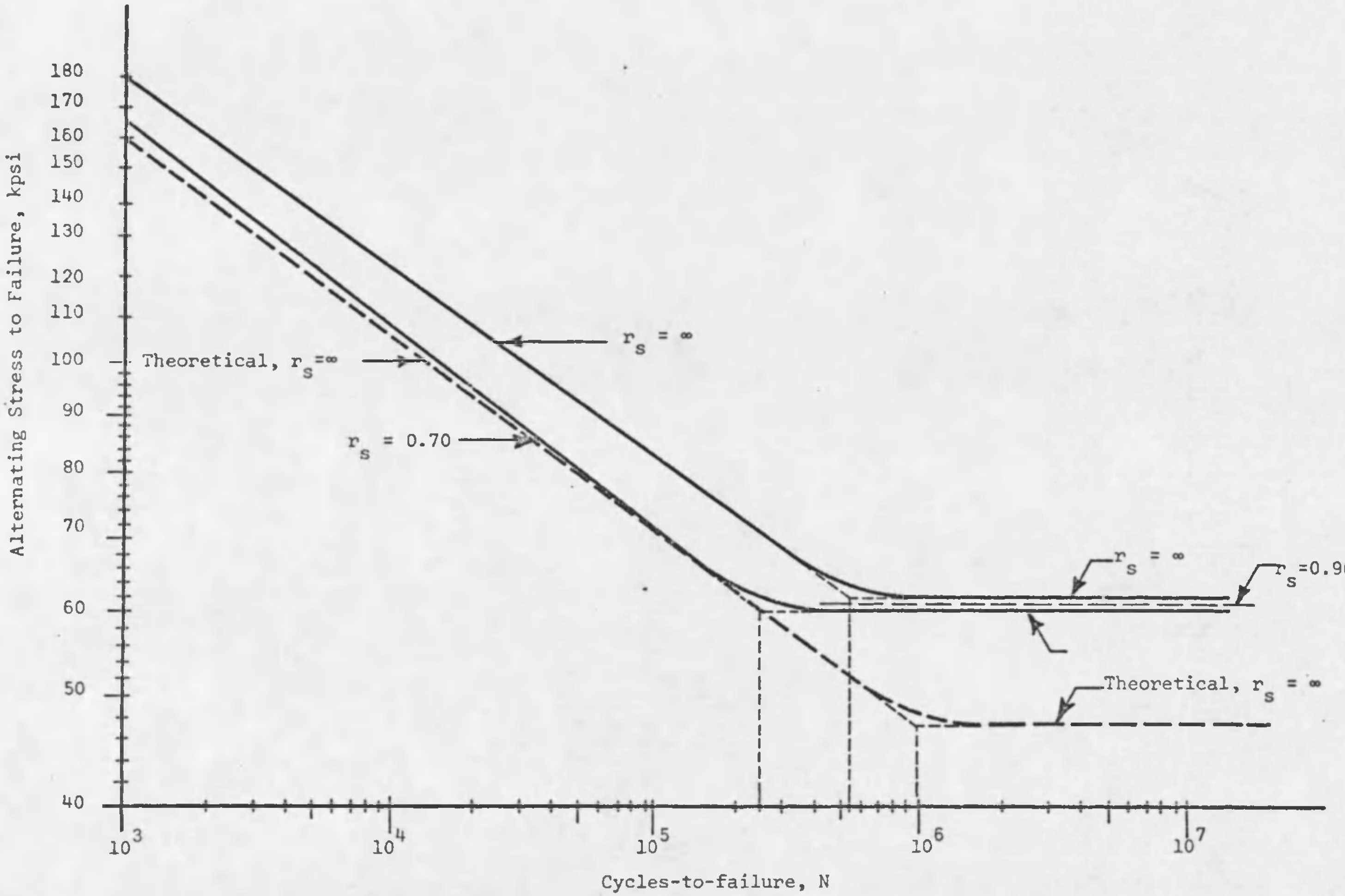

Fig. 34.--Fatigue Strength Versus Mean Cycles-to-Failure and Endurance Strength for r_s = ∞, 0.70, and 0.90, and the Theoretical S-N Diagram for r_s = ∞

$S_{e_{10^3}} = 0.90\ S_U$ relationship. It is an accepted designer's thumb rule. A more accurate multiplier to determine the $S_{e_{10^3}}$ for the steel researched here would be 1.00 instead of 0.90, using the unnotched ultimate strength. A more accurate multiplier to determine S_e' would be 0.65.

From Figure 34, it can be seen that the fatigue strength decreases as torque is added to the specimen. Also, the $r_s = \infty$ and $r_s = 0.70$ lines diverge as cycles life increases. All of these are as expected.

The small standard deviations of the bending stress distributions and the stress ratio distributions at the various levels shown in Figures 32 and 33 indicate that a given stress level and stress ratio can be maintained by the fatigue reliability research machines fairly precisely. The coefficient of variation, the ratio of the standard deviation to the mean expressed as a percentage, does not exceed 2.7% for the bending stress level of $r_s = \infty$. This is shown in Figure 32. For $r_s = 0.70$ in Figure 33, the coefficient of variation for the bending stress level is at most 5.6%, and the coefficient of variation for the stress ratio is at most 6%.

A Goodman diagram of endurance strengths for $r_s = \infty$, $r_s = 0.90$, and $r_s = 0$ is given in Figure 35 which combines the fatigue and static strength results into the

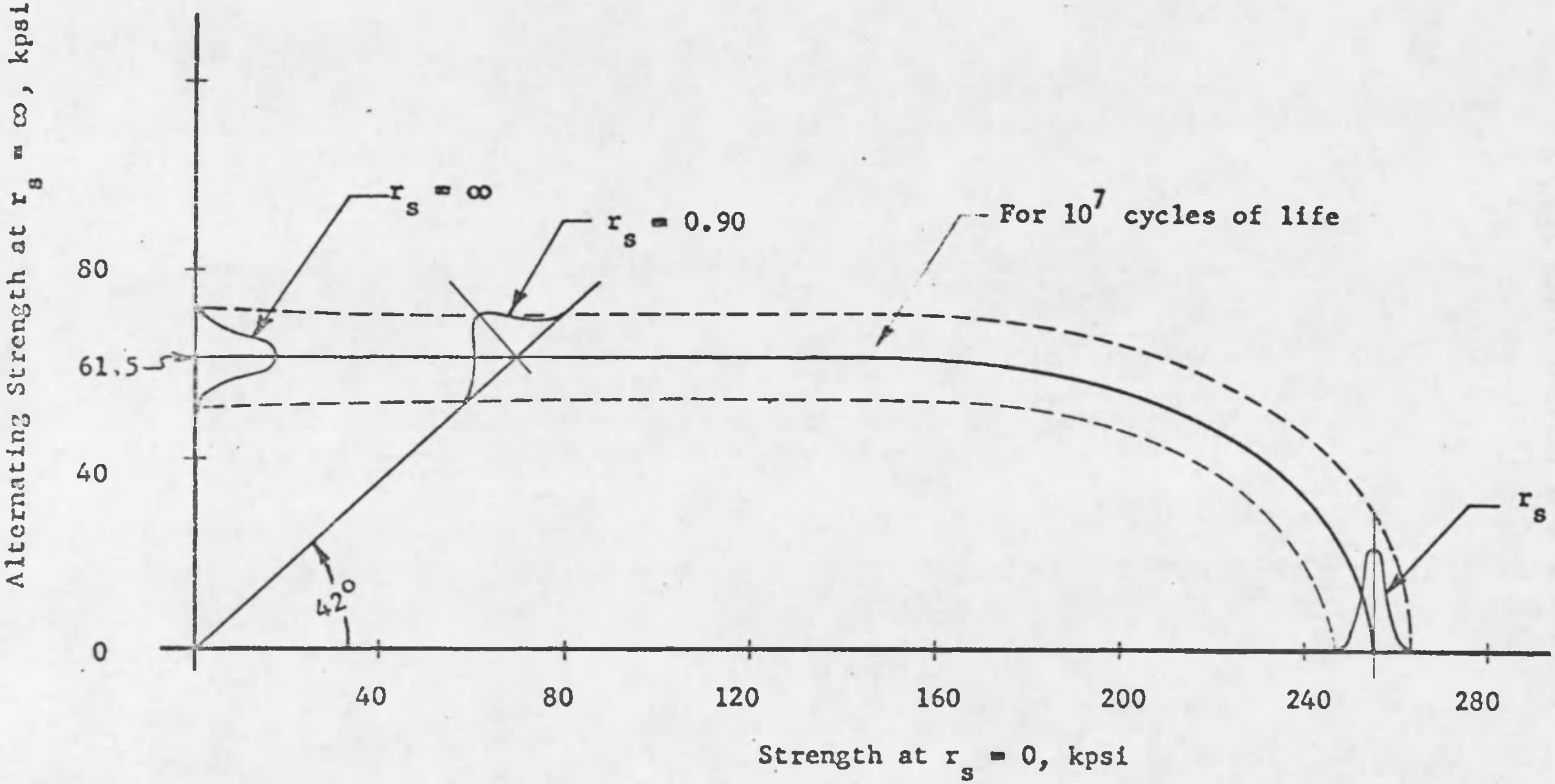

Fig. 35.--Three-dimensional Distributional Goodman Fatigue Strength Surface Based on Research Results Reported here for 10^7 Cycles of Life

most useful design information for combined-stress design situations. This diagram is made possible by the data generated by this research.

CHAPTER 5

STRESS CONCENTRATION AND NOTCH SENSITIVITY EFFECTS

A. Stress Concentration

The best published value of the static stress concentration factor for the notched specimens used in this research is 1.45 [26]. In Section 3-B-2a, an attempt was made to isolate the effective static stress concentration factor from K_{BGR}. The resulting value was 1.28. Since the experimental value was arrived at by an averaging technique rather than by a rigid procedure of measurement, there is room for error in this result. Likewise, the published values leave much to be desired since they do not take into account the test conditions. It was felt that the experimental value was a definite improvement over the theoretical value and was used in the calibration procedure to determine the bending stress in the groove. The accuracy of the result could be improved upon by outfitting more specimens with strain gages and repeating the calibration. The same reduction technique would be used but more data points would be had to average, thus increasing the accuracy of determining the effective static stress concentration factor.

For the torque strain gage bridge, a published value of the static stress concentration was used. There is an error involved in this also, as the exact stress concentration factor in shear is not known at this time. It is believed that any corrections would not be in excess of 5 percent. Nevertheless, further investigations should be initiated to obtain a better value for the static stress concentration factor in torsion.

B. Notch Sensitivity Survey

In fatigue tests, the reduction in fatigue strength is found to be less than that predicted by the static stress concentration factor, K_t [27, p. 249]. The ratio of the nominal fatigue strength of an unnotched specimen to that of a notched specimen is defined as the fatigue stress-concentration factor, K_f. K_f has also been called strength reduction factor, the fatigue notch factor, and the effective stress concentration factor. Therefore, K_f can be experimentally determined by forming the ratio [25, p. 170]

$$K_f = \frac{\text{endurance limit of notch-free specimens}}{\text{endurance limit of notched specimens}}. \qquad (5)$$

The reduction in fatigue strength is explained by the fact that the theoretical peak stress $K_t S_n$ is lowered to $K_f S_n$ by plastic flow, where S_n is the nominal stress in the corresponding unnotched specimen [28, p. 128].

It is also useful to define the notch sensitivity factor as [25, p. 170]

$$q = \frac{K_f - 1}{K_t - 1}.$$

If $q = 0$, then there is no sensitivity for the notch; while if q is unity, $K_f = K_t$, and there would be no observed reduction in the fatigue strength of notched specimens. This would be the case for perfectly elastic materials [25, p. 244].

The notch sensitivity is a very useful but also elusive parameter. As the notch radius increases, q tends toward unity as shown in Figures 36, 37, 38, 40, and 41. q also tends to unity for finegrained, relatively homogeneous materials [25, p. 172] as shown in Figure 39. Notch sensitivity is also a function of the size of the part. K_f may be higher for large parts than for small parts [27, p. 251]. Steel generally has a higher q than lower grades of iron [25, p. 172]. This can be explained by the relative grain sizes. At low cycle life, fatigue strength in notched specimens can be a little higher than notch-free specimens [26, p. 246]. Finally, q may also be a function of the stress amplitude [26, p. 246]. Peterson [23], a widely used reference on notch sensitivity, does not take this into account.

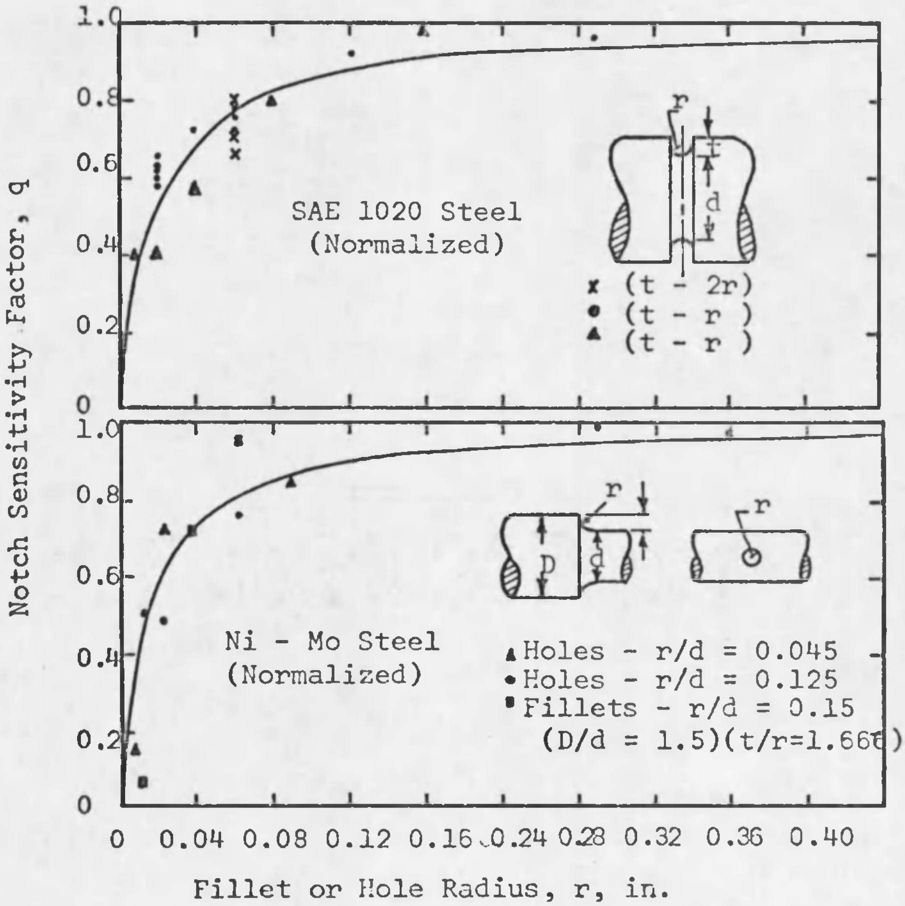

Fig. 36.--Notch Sensitivity of Normalized Steel Specimens

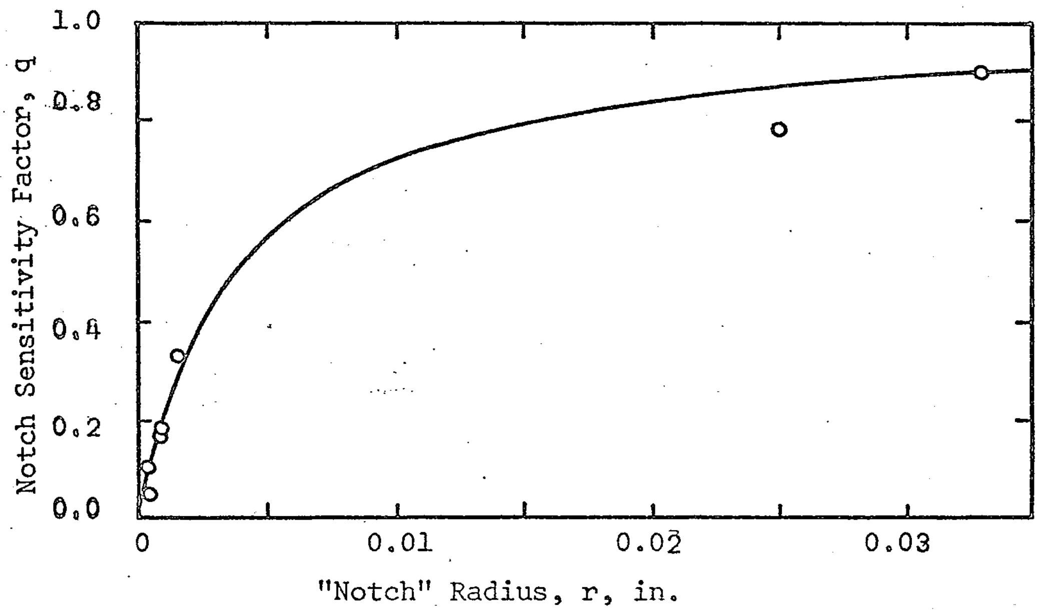

Fig. 37.--Notch Sensitivity of Quenched and Tempered Alloy Steel Specimens

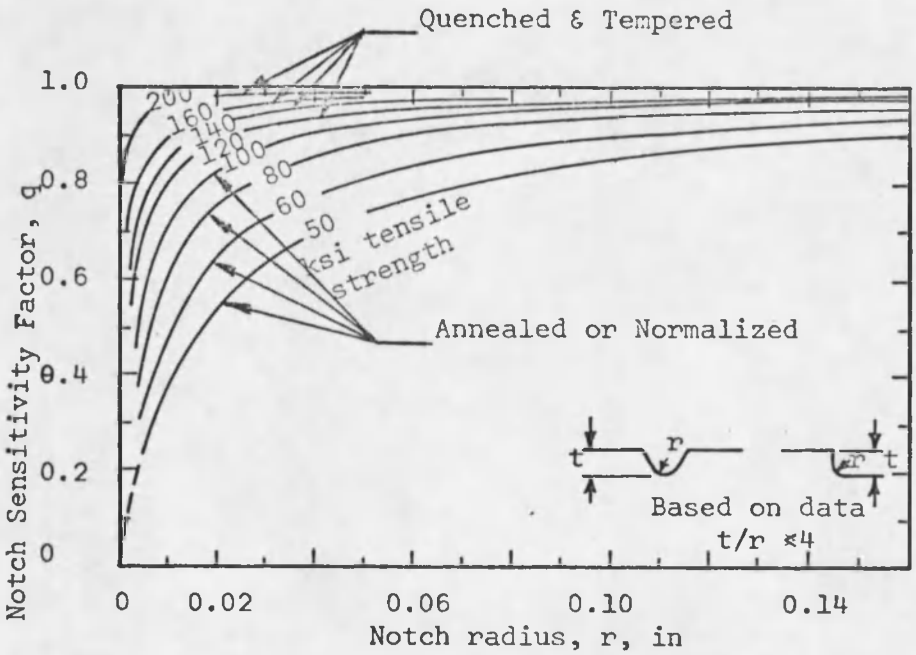

Fig. 38.--Curves of Notch Sensitivity Versus Radius for Steels, Bending or Axial Loading

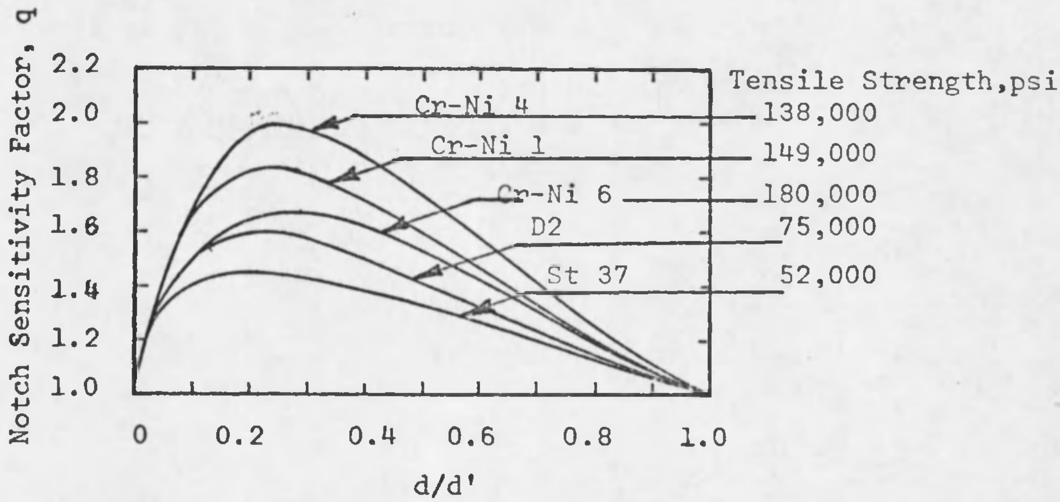

Fig. 39.--The Fatigue Notch Factor

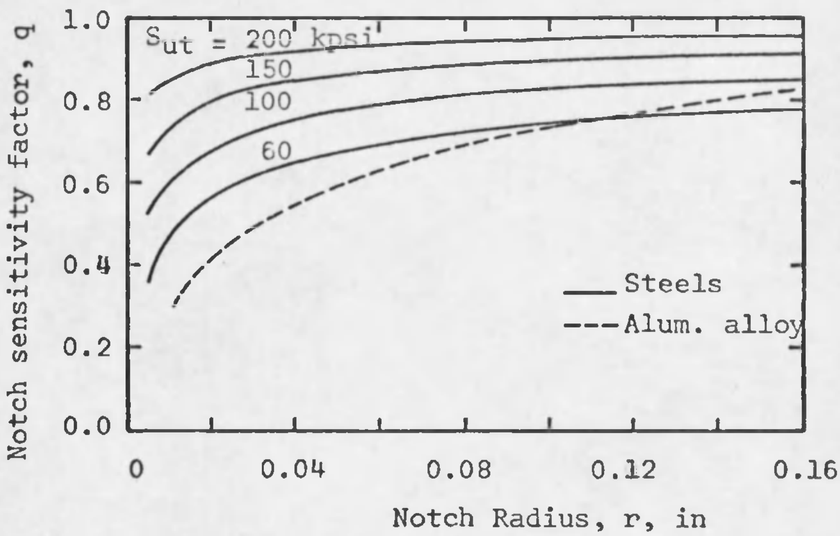

Fig. 40.--Notch Sensitivity Charts for Steels and 245-T Wrought Aluminum Alloys Subjected to Reversed Bending or Reversed Axial Loads

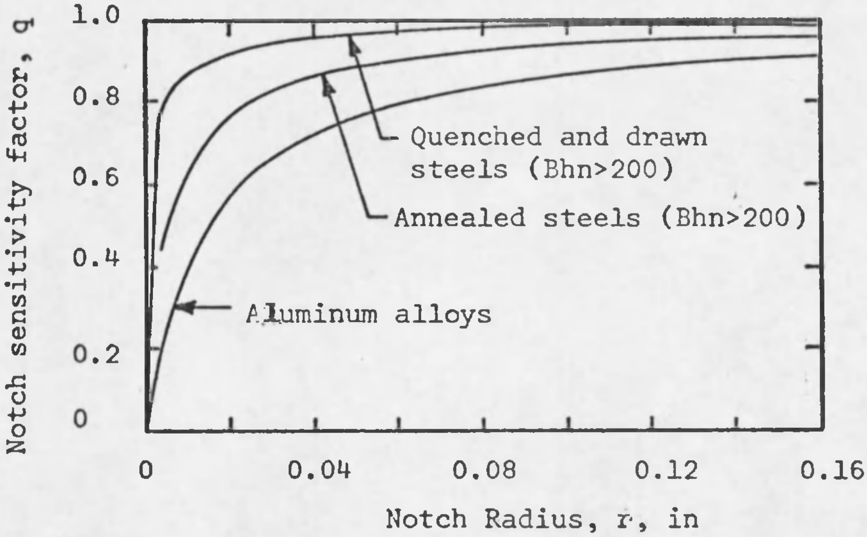

Fig. 41.--Notch Sensitivity Curves for Materials in Reversed Torsion

C. Proposed Notch Sensitivity Determination

Unlike the value of the static stress concentration factor, the notch sensitivity of the test specimen is critical. The calibration method which was used to determine the stress concentration does not incorporate notch sensitivity because it was a static test.

In the calibration procedure, the notch sensitivity effect was not included. The reasons for this are:

1. An experimental notch sensitivity determination has not as yet been carried out, and
2. The published data of Section 3-B indicate that the notch sensitivity effect will be very small, perhaps 2 or 3 percent. Such minor adjustments to the stress levels can be made at a later date if deemed appropriate.

Due to the irregularities and apparent contradictions in the notch sensitivity, the most accurate method of determining the appropriate value of q for the SAE 4340 notched steel specimens of this research is to do it experimentally. Then shape, size, and material errors would be eliminated. K_f, and consequently, q, can be determined experimentally by Equation (5).

It is proposed that unnotched specimens similar to those used in the $r_s = 0$ studies for this research be prepared. The number needed would be approximately 38.

This is the amount needed with the staircase method of endurance strength distribution determination. Only the unnotched specimen need be run since notch endurance strength for $r_s = \infty$ has already been generated. The proposed test would give an accurate value for the notch sensitivity of these specimens.

CHAPTER 6

CONCLUSIONS

1. The fatigue machines are extremely difficult to calibrate dynamically. Attempts were made over a period of one year to obtain valid dynamic calibrations but were abandoned because of large inconsistencies in the results. Finally, the static calibration procedure reported here was embarked upon and was successfully completed. Since all calibrations except one are gage calibrations, there is no error introduced by not calibrating dynamically. The determination of exact specimen groove stress from the toolholder gage bridge output does, however, require dynamic calibration so that the true fatigue stress concentration factor in bending can be determined. The determination of this factor requires extensive research and the minor improvements achieved may or may not be of the desired quality in view of the difficulties involved.

2. The calibration procedure is set up so that if a gage failure occurs, the fatigue machine may be recalibrated and put back into operation in three days.

3. Machine #1 has the following calibration equations:

$$N_{vis_B} = \frac{N_{cal} N_a GR_{cal}}{E\ R_{gage}} [(0.967)(0.0203)\sigma_{true_{GR}} + (0.0548)\tau_{out_{TH}}]$$

$$N_{vis_T} = \frac{N_{cal} N_a GR_{cal}}{E\ R_{gage}} [\frac{(0.0157)}{(0.882)}\tau_{true_{GR}} + (0.0298)\sigma_{out_{TH}}]$$

4. Machine #2 has the following calibration equations:

$$N_{vis_B} = \frac{N_{cal} N_a GR_{cal}}{E\ R_{gage}} [(0.902)(0.0198)\sigma_{true_{GR}} + (0.0343)\tau_{out_{TH}}]$$

$$N_{vis_T} = \frac{N_{cal} N_a GR_{cal}}{E\ R_{gage}} [\frac{(0.0157)}{(0.840)}\tau_{true_{GR}} + (0.0410)\sigma_{out_{TH}}]$$

5. Machine #3 has the following calibration equations:

$$N_{vis_B} = \frac{N_{cal} N_a GR_{cal}}{E\ R_{gage}} [(0.972)(0.0215)\sigma_{true_{GR}}]$$

$$N_{vis_T} = \frac{N_{cal} N_a GR_{cal}}{E\ R_{gage}} [\frac{(0.0157)}{(0.842)}\tau_{true_{GR}} + (-0.0238)\sigma_{out_{TH}}]$$

Note that there is no torque interaction into the bending channel for Machine #3, and that the bending interaction into the torque channel is negative.

6. The axial stress in the specimen was found to be negligible.

7. The effective static stress concentration factor of the specimen groove in bending was determined to be 1.28.

8. The data reduction shows that the machines were very successful in maintaining and reproducing the torque and bending loads. With other past machines, difficulty has been experienced in maintaining constant bending and torque loads.

9. From Figures 32 and 33 and Appendices A and B, it may be seen that the fatigue reliability research machines maintained the desired bending stress levels with a coefficient of variation of less than 2.7% for $r_s = \infty$ and less than 5.6% for $r_s = 0.70$.

10. From Figure 33 and Appendix B, it may be seen that the coefficient of variation did not exceed 8% and for the most part was less than 6% for the stress ratio.

CHAPTER 7

RECOMMENDATIONS

1. Calibrations, test runs, and data reduction would be greatly expedited if the amplification system were improved upon. Presently, amplifier drift must be carefully taken into account on each run; consequently, a relatively drift-free amplifying and recording system, with a very short warm-up time, should be obtained.

2. A pan weight versus true stress in the groove calibration should be conducted. Although, like the determination of K_{BTH}, this relationship would not be an integral part of the calibration procedure, it has a wide variety of uses during daily operation of the fatigue machines, e.g., in determining the pan weight directly from the required bending and shear stresses.

3. The notch sensitivity determination proposal for bending should be undertaken, thus insuring that this dynamic phenomenon has been accounted for in the calibration procedure.

4. Now that experience has been gained in running the machines, the staircase method for determining the endurance strengths can be improved. Increments of bending

stress rather than increments of pan weight should be used because they are more reproducible.

5. An additional test specimen with bending gages mounted in the groove should be prepared. Then the static stress concentration factor determination experiment can be rerun and averaged in with the previous work in order to increase the accuracy of K_t.

6. Research with these machines should be continued and expanded to include other stress ratios, notch geometries, and materials.

APPENDIX A

DATA REDUCTION RESULTS

FOR $r_s = \infty$

TEST NO.	SPECIMEN NO.	MACHINE NO.	PAN WEIGHT	RCAL BENDING	NCAL BENDING	NVIS BENDING	RCAL TORQUE	NCAL TORQUE	NVIS TORQUE	BENDING STRESS	SHEAR STRESS	STRESS RATIO
125	166	2	29	190000.0	50.20	59.30	-0.0	-0.00	-0.00	153581.2	0.0	INFIN.
126	204	2	29	90000.0	50.10	28.20	-0.0	-0.00	-0.00	154493.2	0.0	INFIN.
130	225	2	29	90000.0	49.70	27.40	-0.0	-0.00	-0.00	151318.6	0.0	INFIN.
131	133	2	29	90000.0	50.00	27.90	-0.0	-0.00	-0.00	153155.4	0.0	INFIN.
132	196	2	29	90000.0	49.40	28.00	-0.0	-0.00	-0.00	155571.2	0.0	INFIN.
133	220	2	29	90000.0	49.90	28.20	-0.0	-0.00	-0.00	155112.5	0.0	INFIN.
134	193	2	29	90000.0	49.60	28.00	-0.0	-0.00	-0.00	154943.9	0.0	INFIN.
135	191	2	29	90000.0	50.40	28.40	-0.0	-0.00	-0.00	154662.8	0.0	INFIN.
136	163	2	29	90000.0	50.20	28.40	-0.0	-0.00	-0.00	155279.0	0.0	INFIN.
425	342	1	30	150000.0	50.20	51.60	-0.0	-0.00	-0.00	153216.2	0.0	INFIN.
426	341	1	30	150000.0	50.10	50.70	-0.0	-0.00	-0.00	150844.3	0.0	INFIN.
428	365	1	30	150000.0	50.30	51.55	-0.0	-0.00	-0.00	152763.5	0.0	INFIN.

MEAN BENDING STRESS IN GROOVE = 153745.1 PSI.
STD. DEV. OF BENDING STRESS IN GROOVE = 1546.74 PSI.

TEST NO.	SPECIMEN NO.	MACHINE NO.	PAN WEIGHT	RCAL BENDING	NCAL BENDING	NVIS BENDING	RCAL TORQUE	NCAL TORQUE	NVIS TORQUE	BENDING STRESS	SHEAR STRESS	STRESS RATIO
29	63	1	20	290000.0	32.40	51.00	-0.0	-0.00	-0.00	121360.5	0.0	INFIN.
30	22	1	20	290000.0	33.20	52.10	-0.0	-0.00	-0.00	120990.6	0.0	INFIN.
31	109	1	20	290000.0	32.90	51.40	-0.0	-0.00	-0.00	120453.5	0.0	INFIN.
32	82	1	20	190000.0	50.20	51.40	-0.0	-0.00	-0.00	120491.3	0.0	INFIN.
33	42	1	20	190000.0	50.50	52.40	-0.0	-0.00	-0.00	122105.8	0.0	INFIN.
34	59	1	20	190000.0	50.50	52.70	-0.0	-0.00	-0.00	122804.9	0.0	INFIN.
35	52	1	20	190000.0	49.30	50.80	-0.0	-0.00	-0.00	121258.8	0.0	INFIN.
36	76	1	20	190000.0	50.70	51.50	-0.0	-0.00	-0.00	119535.2	0.0	INFIN.
37	64	1	20	190000.0	50.30	51.60	-0.0	-0.00	-0.00	120719.7	0.0	INFIN.
38	111	1	20	190000.0	50.40	52.00	-0.0	-0.00	-0.00	121414.1	0.0	INFIN.
39	20	1	20	190000.0	50.40	52.00	-0.0	-0.00	-0.00	121414.1	0.0	INFIN.
40	73	1	20	190000.0	49.90	51.30	-0.0	-0.00	-0.00	120979.0	0.0	INFIN.
41	69	1	20	190000.0	49.30	50.90	-0.0	-0.00	-0.00	121497.5	0.0	INFIN.
43	86	1	20	190000.0	49.30	51.40	-0.0	-0.00	-0.00	122691.0	0.0	INFIN.
44	96	1	20	190000.0	48.90	50.60	-0.0	-0.00	-0.00	121769.4	0.0	INFIN.
45	80	1	20	190000.0	49.20	51.50	-0.0	-0.00	-0.00	123179.5	0.0	INFIN.
46	101	1	20	190000.0	49.40	51.20	-0.0	-0.00	-0.00	121966.2	0.0	INFIN.
47	89	1	20	190000.0	49.00	51.10	-0.0	-0.00	-0.00	122721.7	0.0	INFIN.

MEAN BENDING STRESS IN GROOVE = 121519.6 PSI.
STD. DEV. OF BENDING STRESS IN GROOVE = 948.34 PSI.

TEST NO.	SPECIMEN NO.	MACHINE NO.	PAN WEIGHT	RCAL BENDING	NCAL BENDING	NVIS BENDING	RCAL TORQUE	NCAL TORQUE	NVIS TORQUE	BENDING STRESS	SHEAR STRESS	STRESS RATIO
10	26	1	15	290000.0	39.40	51.00	-0.0	-0.00	-0.00	99799.0	0.0	INFIN.
11	62	2	16	290000.0	41.10	49.80	-0.0	-0.00	-0.00	103212.0	0.0	INFIN.
12	88	1	15	290000.0	38.20	51.00	-0.0	-0.00	-0.00	102934.0	0.0	INFIN.
13	46	2	16	290000.0	40.00	51.00	-0.0	-0.00	-0.00	108605.7	0.0	INFIN.
14	58	1	15	290000.0	38.20	51.00	-0.0	-0.00	-0.00	102934.0	0.0	INFIN.
15	99	2	16	290000.0	40.00	50.50	-0.0	-0.00	-0.00	107541.0	0.0	INFIN.
16	33	1	15	290000.0	38.40	50.50	-0.0	-0.00	-0.00	101394.0	0.0	INFIN.
17	85	2	16	290000.0	40.00	50.00	-0.0	-0.00	-0.00	106476.2	0.0	INFIN.
18	55	1	15	290000.0	38.40	50.50	-0.0	-0.00	-0.00	101394.0	0.0	INFIN.
19	49	2	16	290000.0	39.40	49.10	-0.0	-0.00	-0.00	106151.9	0.0	INFIN.
20	110	1	15	290000.0	39.70	52.00	-0.0	-0.00	-0.00	100986.9	0.0	INFIN.
21	104	2	16	290000.0	40.60	50.40	-0.0	-0.00	-0.00	105741.9	0.0	INFIN.
22	113	1	15	290000.0	37.30	49.70	-0.0	-0.00	-0.00	102730.5	0.0	INFIN.
23	65	2	16	290000.0	40.00	50.30	-0.0	-0.00	-0.00	107115.1	0.0	INFIN.
24	39	1	15	290000.0	38.00	51.70	-0.0	-0.00	-0.00	104896.0	0.0	INFIN.
25	13	2	16	290000.0	39.40	49.50	-0.0	-0.00	-0.00	107016.7	0.0	INFIN.
26	71	1	15	290000.0	38.90	51.10	-0.0	-0.00	-0.00	101279.9	0.0	INFIN.
27	84	2	16	290000.0	39.90	50.60	-0.0	-0.00	-0.00	108024.0	0.0	INFIN.

MEAN BENDING STRESS IN GROOVE = 104346.3 PSI.
STD. DEV. OF BENDING STRESS IN GROOVE = 2801.30 PSI.

TEST NO.	SPECIMEN NO.	MACHINE NO.	PAN WEIGHT	RCAL BENDING	NCAL BENDING	NVIS BENDING	RCAL TORQUE	NCAL TORQUE	NVIS TORQUE	BENDING STRESS	SHEAR STRESS	STRESS RATIO
139	135	2	6	190000.0	49.60	30.00	-0.0	-0.00	-0.00	78636.9	0.0	INFIN.
140	167	2	6	190000.0	50.20	30.40	-0.0	-0.00	-0.00	78733.0	0.0	INFIN.
142	198	2	6	190000.0	50.20	29.20	-0.0	-0.00	-0.00	75625.1	0.0	INFIN.
143	214	2	6	190000.0	49.80	29.40	-0.0	-0.00	-0.00	76754.6	0.0	INFIN.
145	215	2	6	190000.0	49.50	29.20	-0.0	-0.00	-0.00	76694.6	0.0	INFIN.
146	134	2	6	190000.0	49.40	30.10	-0.0	-0.00	-0.00	79218.5	0.0	INFIN.
147	125	2	6	190000.0	49.20	29.60	-0.0	-0.00	-0.00	78219.2	0.0	INFIN.
148	186	2	6	190000.0	50.10	29.80	-0.0	-0.00	-0.00	77333.1	0.0	INFIN.
150	159	2	6	190000.0	49.50	30.40	-0.0	-0.00	-0.00	79846.4	0.0	INFIN.
151	148	2	6	190000.0	49.90	29.60	-0.0	-0.00	-0.00	77122.0	0.0	INFIN.
152	128	2	6	190000.0	52.20	31.20	-0.0	-0.00	-0.00	77709.0	0.0	INFIN.
153	219	2	6	190000.0	49.90	30.60	-0.0	-0.00	-0.00	79727.5	0.0	INFIN.
154	123	2	6	190000.0	50.10	31.20	-0.0	-0.00	-0.00	80966.2	0.0	INFIN.
155	121	2	6	190000.0	49.70	30.00	-0.0	-0.00	-0.00	78478.7	0.0	INFIN.
156	145	2	6	190000.0	50.00	29.90	-0.0	-0.00	-0.00	77747.8	0.0	INFIN.
157	171	2	6	190000.0	49.70	30.40	-0.0	-0.00	-0.00	79525.1	0.0	INFIN.
160	156	2	6	190000.0	49.50	27.60	-0.0	-0.00	-0.00	72492.1	0.0	INFIN.
163	183	2	6	190000.0	49.20	29.10	-0.0	-0.00	-0.00	76898.0	0.0	INFIN.

MEAN BENDING STRESS IN GROOVE = 77873.8 PSI.
STD. DEV. OF BENDING STRESS IN GROOVE = 1905.81 PSI.

TEST NO.	SPECIMEN NO.	MACHINE NO.	PAN WEIGHT	RCAL BENDING	NCAL BENDING	NVIS BENDING	RCAL TORQUE	NCAL TORQUE	NVIS TORQUE	BENDING STRESS	SHEAR STRESS	STRESS RATIO
64	87	2	25	290000.0	49.40	37.40	-0.0	-0.00	-0.00	64489.2	0.0	INFIN.
101	17	1	25	490000.0	53.40	46.80	-0.0	-0.00	-0.00	39990.7	0.0	INFIN.
102	74	2	25	490000.0	49.00	48.50	-0.0	-0.00	-0.00	49898.8	0.0	INFIN.
110	202	1	25	390000.0	49.60	47.20	-0.0	-0.00	-0.00	54556.4	0.0	INFIN.
117	182	1	25	190000.0	49.80	25.90	-0.0	-0.00	-0.00	61202.2	0.0	INFIN.
122	124	1	25	190000.0	50.20	27.50	-0.0	-0.00	-0.00	64465.2	0.0	INFIN.
141	216	1	26	190000.0	49.80	26.20	-0.0	-0.00	-0.00	61911.1	0.0	INFIN.
149	205	1	24	190000.0	49.60	22.30	-0.0	-0.00	-0.00	52907.8	0.0	INFIN.
158	199	1	25	190000.0	50.00	24.50	-0.0	-0.00	-0.00	57662.4	0.0	INFIN.
161	209	1	25	190000.0	49.10	24.00	-0.0	-0.00	-0.00	57521.0	0.0	INFIN.
169	177	1	24	190000.0	49.60	24.40	-0.0	-0.00	-0.00	57890.1	0.0	INFIN.
175	168	1	25	190000.0	49.80	25.80	-0.0	-0.00	-0.00	60965.9	0.0	INFIN.
185	190	2	26	190000.0	50.00	25.40	-0.0	-0.00	-0.00	66046.6	0.0	INFIN.
186	207	2	27	190000.0	50.10	25.40	-0.0	-0.00	-0.00	65914.8	0.0	INFIN.
190	142	2	25	190000.0	49.90	26.80	-0.0	-0.00	-0.00	69826.7	0.0	INFIN.
195	208	2	23	190000.0	50.10	24.40	-0.0	-0.00	-0.00	63319.7	0.0	INFIN.

ENDURANCE

APPENDIX B

DATA REDUCTION RESULTS

FOR $r_s = 0.7$ AND $r_s = 0.9$

TEST NO.	SPECIMEN NO.	MACHINE NO.	PAN WEIGHT	RCAL BENDING	NCAL BENDING	NVIS BENDING	RCAL TORQUE	NCAL TORQUE	NVIS TORQUE	BENDING STRESS	SHEAR STRESS	STRESS RATIO
411	354	1	19	190000.0	50.10	47.75	200000.0	45.20	32.50	108353.6	84677.9	.739
412	395	1	21	190000.0	50.35	49.65	200000.0	45.20	34.30	112014.6	89444.6	.723
413	345	1	21	190000.0	50.45	49.90	200000.0	45.10	33.55	112460.8	87595.7	.741
415	335	1	22	190000.0	50.10	49.30	200000.0	45.15	33.30	111900.3	86833.5	.744
416	358	1	21	190000.0	49.95	48.45	200000.0	45.10	32.90	110286.0	85898.5	.741
417	406	1	20	190000.0	50.50	48.60	200000.0	45.10	34.30	109198.5	89743.7	.703
418	387	1	21	190000.0	50.10	49.25	200000.0	45.10	33.60	111736.6	87755.5	.735
419	356	1	21	190000.0	50.45	48.75	200000.0	45.30	35.50	109521.9	92571.8	.683
420	397	1	22	190000.0	50.25	49.60	200000.0	45.30	33.90	112193.1	88149.6	.735
421	432	1	21	190000.0	50.35	49.15	200000.0	45.15	34.55	110801.1	90267.2	.709
422	392	1	21	190000.0	50.30	48.65	200000.0	45.10	35.50	109606.4	92995.5	.680
423	390	1	21	190000.0	49.80	48.75	200000.0	45.15	33.75	111234.3	88078.5	.729

MEAN BENDING STRESS IN GROOVE = 110775.6 PSI.
STD. DEV. OF BENDING STRESS IN GROOVE = 1358.99 PSI.

MEAN TORQUE STRESS IN GROOVE = 88667.7 PSI.
STD. DEV. OF TORQUE STRESS IN GROOVE = 2483.41 PSI.

MEAN STRESS RATIO = .72187
STD. DEV. OF MEAN STRESS RATIO = .02275

TEST NO.	SPECIMEN NO.	MACHINE NO.	PAN WEIGHT	RCAL BENDING	NCAL BENDING	NVIS BENDING	RCAL TORQUE	NCAL TORQUE	NVIS TORQUE	BENDING STRESS	SHEAR STRESS	STRESS RATIO
223	295	3	15	190000.0	50.00	41.60	304000.0	45.00	42.60	92443.7	83775.7	.637
226	274	3	15	190000.0	50.00	41.64	304000.0	45.00	42.14	92532.6	82894.3	.644
228	262	3	15	190000.0	49.80	43.70	304000.0	45.00	43.10	97500.3	84843.8	.663
230	261	3	15	190000.0	50.06	46.00	304000.0	45.30	43.33	102098.9	85042.3	.693
232	312	3	15	190000.0	49.50	51.20	304000.0	45.10	42.30	114926.1	83499.2	.795
233	256	3	15	190000.0	49.90	43.50	304000.0	45.10	43.40	96859.6	85221.4	.656
235	258	3	15	190000.0	50.00	43.40	304000.0	45.08	41.60	96443.7	81799.1	.681
236	254	3	15	190000.0	49.60	44.10	304000.0	44.88	42.10	98789.5	83167.2	.686
237	237	2	15	190000.0	50.10	40.70	304000.0	45.00	46.50	102767.3	75428.9	.787
238	292	2	15	190000.0	49.70	39.60	304000.0	44.84	42.96	100947.5	69713.3	.836
239	307	3	15	190000.0	49.80	41.90	304000.0	45.00	38.80	93484.3	76500.9	.706
240	314	3	15	190000.0	49.80	40.90	304000.0	44.80	41.20	91253.2	81415.2	.647
241	227	3	15	190000.0	49.90	41.30	304000.0	44.80	40.30	91961.0	79694.3	.666
403	426	1	16	190000.0	50.10	43.75	250000.0	44.90	36.20	99361.1	75887.5	.756
405	408	1	16	190000.0	50.00	42.90	250000.0	44.60	37.50	97388.1	79346.4	.709
406	367	1	16	190000.0	50.00	42.70	250000.0	45.00	37.90	96908.1	79501.1	.704
407	370	1	16	190000.0	50.55	43.25	250000.0	44.80	39.00	96957.8	82279.2	.680
408	379	1	16	190000.0	50.15	42.70	250000.0	44.90	37.80	96607.6	79476.5	.702

MEAN BENDING STRESS IN GROOVE = 97735.0 PSI.
STD. DEV. OF BENDING STRESS IN GROOVE = 5464.49 PSI.
MEAN TORQUE STRESS IN GROOVE = 80527.0 PSI.
STD. DEV. OF TORQUE STRESS IN GROOVE = 4082.99 PSI.
MEAN STRESS RATIO = .70266
STD. DEV. OF MEAN STRESS RATIO = .05601

TEST NO.	SPECIMEN NO.	MACHINE NO.	PAN WEIGHT	RCAL BENDING	NCAL BENDING	NVIS BENDING	RCAL TORQUE	NCAL TORQUE	NVIS TORQUE	BENDING STRESS	SHEAR STRESS	STRESS RATIO
207	172	1	10	190000.0	49.80	32.20	304000.0	44.30	32.50	73539.3	56814.4	.747
209	200	1	10	190000.0	50.10	34.60	304000.0	45.10	36.90	78408.5	63480.5	.713
210	185	1	10	190000.0	50.20	33.90	304000.0	44.80	35.10	76735.6	60733.9	.729
211	176	1	10	190000.0	49.80	33.00	304000.0	45.00	36.00	75173.2	62118.9	.699
212	141	1	10	190000.0	49.80	29.70	304000.0	44.60	37.00	67216.2	64769.9	.599
213	154	1	10	190000.0	50.00	34.00	304000.0	44.80	35.30	77273.8	61076.7	.730
215	218	1	10	190000.0	49.90	33.70	304000.0	44.90	36.00	76668.3	62213.6	.712
217	277	3	10	190000.0	49.90	34.70	304000.0	44.00	36.60	77265.0	73527.6	.607
218	326	3	10	190000.0	50.00	35.30	304000.0	44.50	37.50	78443.8	74492.8	.608
222	285	3	10	190000.0	49.90	36.50	304000.0	45.00	35.60	81273.0	70095.5	.669
384	363	1	10	190000.0	50.30	34.30	304000.0	45.10	37.50	77324.9	64590.2	.691
386	427	1	10	190000.0	50.10	33.75	304000.0	45.20	37.65	76342.4	64741.9	.681
387	404	1	10	190000.0	50.20	34.90	304000.0	45.25	37.80	78883.8	64851.7	.702
390	441	1	10	190000.0	50.10	34.10	304000.0	44.95	37.80	77136.7	65359.3	.681
391	416	1	10	190000.0	49.70	33.45	304000.0	45.00	37.80	76241.5	65313.2	.674
392	405	1	10	190000.0	50.15	34.20	304000.0	44.90	37.40	77324.3	64709.4	.690
393	382	1	10	190000.0	50.15	33.60	304000.0	45.00	37.60	75898.7	64965.7	.675
433	471	1	10	190000.0	49.80	33.95	304000.0	45.00	38.50	77206.8	66537.4	.670

MEAN BENDING STRESS IN GROOVE = 76575.3 PSI.
STD. DEV. OF BENDING STRESS IN GROOVE = 2833.46 PSI.
MEAN TORQUE STRESS IN GROOVE = 65021.8 PSI.
STD. DEV. OF TORQUE STRESS IN GROOVE = 4275.40 PSI.
MEAN STRESS RATIO = .68211
STD. DEV. OF MEAN STRESS RATIO = .04200

TEST NO.	SPECIMEN NO.	MACHINE NO.	PAN WEIGHT	RCAL BENDING	NCAL BENDING	NVIS BENDING	RCAL TORQUE	NCAL TORQUE	NVIS TORQUE	BENDING STRESS	SHEAR STRESS	STRESS RATIO
245	287	2	7	190000.0	49.80	29.10	304000.0	44.60	32.30	73972.6	52788.3	.809
252	228	3	7	190000.0	49.60	30.70	304000.0	44.80	27.80	68771.9	55089.1	.721
253	230	3	7	190000.0	49.80	30.50	304000.0	44.60	28.70	68049.4	57057.8	.689
254	327	3	7	190000.0	49.50	30.20	304000.0	44.80	28.00	67788.5	55453.8	.706
256	304	3	7	190000.0	49.60	31.00	304000.0	44.50	29.20	69443.9	58183.5	.689
257	321	3	7	190000.0	49.40	30.70	304000.0	44.80	28.20	69050.3	55866.5	.714
258	232	3	7	190000.0	49.20	30.20	304000.0	44.80	30.10	68201.8	59513.2	.662
259	255	3	7	190000.0	49.80	30.30	304000.0	44.60	28.60	67603.2	56854.6	.687
260	272	3	7	190000.0	49.50	31.60	304000.0	44.70	29.20	70931.0	57961.5	.707
261	247	3	7	190000.0	49.70	30.80	304000.0	45.00	28.70	68857.0	56580.8	.703
262	231	3	7	190000.0	49.60	30.90	304000.0	44.80	29.10	69219.9	57606.1	.694
263	229	3	7	190000.0	49.30	31.70	304000.0	44.60	29.10	71444.1	57905.3	.712
264	268	3	7	190000.0	49.50	32.00	304000.0	44.80	28.90	71828.8	57276.0	.724
394	385	1	7	190000.0	49.90	30.55	304000.0	44.80	32.70	69489.7	56646.9	.708
396	337	1	7	190000.0	50.10	30.00	304000.0	44.85	33.10	67869.5	57354.5	.683
398	442	1	7	190000.0	50.15	31.05	304000.0	44.80	33.35	70429.8	57793.3	.702
400	413	1	7	190000.0	50.15	31.15	304000.0	45.00	33.00	70530.1	56889.0	.716
402	360	1	7	190000.0	49.95	31.70	304000.0	45.00	32.80	72144.6	56477.1	.738

MEAN BENDING STRESS IN GROOVE = 69747.0 PSI.
STD. DEV. OF BDNEING STRESS IN GROOVE= 1765.29 PSI.
MEAN TORQUE STRESS IN GROOVE = 56849.9 PSI.
STD. DEV. OF TORQUE STRESS IN GROOVE = 1453.79 PSI.
MEAN STRESS RATIO = .70895
STD. DEV. OF MEAN STRESS RATIO = .03052

TEST NO.	SPECIMEN NO.	MACHINE NO.	PAN WEIGHT	RCAL BENDING	NCAL BENDING	NVIS BENDING	RCAL TORQUE	NCAL TORQUE	NVIS TORQUE	BENDING STRESS	SHEAR STRESS	STRESS RATIO
280	248	3	27	390000.0	50.15	50.15	304000.0	45.15	24.30	54130.6	47662.4	.656
317	288	2	27	190000.0	50.10	25.95	304000.0	44.55	25.15	65783.9	40830.9	.930
318	267	2	26	190000.0	49.70	24.35	304000.0	44.45	24.30	62189.7	39599.0	.907
321	300	2	27	190000.0	49.60	23.15	304000.0	44.65	24.10	59191.7	39183.8	.872
323	275	2	26	190000.0	49.60	24.85	304000.0	44.10	22.25	63745.0	36297.4	1.014
330	409	2	25	190000.0	49.90	23.90	304000.0	44.95	23.60	60821.7	37987.6	.924
339	364	2	24	190000.0	53.05	23.55	304000.0	45.00	22.40	56341.6	36067.8	.902
348	372	2	26	190000.0	49.65	24.55	304000.0	45.20	25.00	62759.8	40070.0	.904
377	362	2	28	190000.0	49.80	25.75	304000.0	45.00	26.30	65612.5	42368.6	.894
378	429	2	27	190000.0	50.00	24.75	304000.0	45.00	25.45	62795.5	41026.6	.884
381	359	2	27	190000.0	50.00	24.65	304000.0	45.10	24.60	62590.9	39489.0	.915
383	417	2	26	190000.0	49.55	23.15	304000.0	44.60	24.30	59238.9	39573.3	.864
385	336	2	26	190000.0	50.30	22.95	304000.0	45.15	26.15	57721.5	42273.0	.788
395	435	2	26	190000.0	50.10	23.65	304000.0	47.10	23.40	60002.2	35850.4	.966
397	401	2	25	190000.0	49.95	24.00	304000.0	45.00	23.40	61033.5	37592.7	.937
430	400	2	29	190000.0	50.10	25.30	304000.0	44.65	24.75	64125.4	40109.9	.923
431	386	2	28	190000.0	50.10	24.65	304000.0	47.15	25.50	62475.8	39137.7	.922
432	402	2	27	190000.0	50.00	24.45	304000.0	47.10	24.80	62123.1	38052.9	.943

MEAN STRESS RATIO = .89701 ENDURANCE

STD. DEV. OF MEAN STRESS RATIO = .07582

APPENDIX C

OPERATING CHECKLIST FOR COMBINED BENDING-TORSION FATIGUE RESEARCH MACHINES

To Install Specimen

1. Turn power off at the wall - block up loading arm.
2. Choose correct specimen for test using data book.
3. Prepare specimen for test.
   a) Inspect specimen for defect or damage.
   b) Clean any oil or foreign matter off specimen.
4. Clean inside of toolholders.
5. Clean collets.
6. Use WD-40 on collets - insure there is no binding.
7. Block up one side of loading arm with support bolt.
8. Insert specimen and install collets.
9. Block up other side of loading arm with support bolt.
10. Level the toolholder arms using the support bolts.
11. Place coupling gauges over the flex couplings. Be sure the coupling gauges fit snugly.
12. Check the toolholder arms to see if they are still level. If not, adjust the support bolts to make the arms level.
13. Install keys in specimen.

14. Center specimen in toolholder.

15. Tighten outboard side (with strain gages) of specimen by hand.

16. Tighten outboard side of specimen using the wrench. Make sure it is very tight as it cannot be tightened again after this step.

17. With the inboard side (without strain gages) still loose, place brushes on the slip-rings. They should be firm against the rings, but not bent tight.

18. Zero the instrumentation.

    a) Turn milliammeter to "in".

    b) Check B^+ (5 volts) - Bridge Balance Switch to "B^+".

    c) Check GV (5 volts) - Bridge Balance Switch to "GV".

    d) Turn Bridge Balance Switch to "BB".

    e) Turn Channel Selector to desired channel.

    f) Set Atten Switch to desired level.

    g) Use C. Bal. to "dip" voltmeter.

    h) Use R. Bal. to "zero" milliammeter.

    i) Repeat (g) and (h) until minimum voltmeter reading and zero milliammeter readings are obtained simultaneously.

    j) Lock C. Bal. and R. Bal. controls

    k) Take a short Visicorder run.

l) Repeat (e) through (k) for each channel to be used in the test.

m) Turn milliammeter switch to "out".

19. Calibrate the instrumentation.

a) Connect to Ext. Cal. the appropriate value of calibration resistance.

b) Using the gain control, obtain the appropriate deflection on the Visicorder (some adjustment of the R. Bal. may be necessary) - do not change C. Bal.

c) Take a short Visicorder run for each deflection - be sure instrumentation is calibrated for both bending and torque.

20. Tighten the inboard side of the test specimen.

21. Remove flex coupling gages.

22. Clean the specimen and specimen groove.

23. Lower support bolts. Make sure horizontal link is not resting on a support bolt (check both sides).

24. Lower the loading arm - no pan load.

25. Check to see if pins are loose and all nuts are tight.

26. Check to see if bearings are vertical.

27. Check to see if vertical link is vertical.

28. Check to see if brushes are still correctly set on the slip-rings.

29. Rotate machine by hand.

30. Turn the power on at the wall.

31. Clean the slip-rings (with machine running).
32. Turn the machine off.
33. Apply the appropriate load to the pan.
34. Set microswitch.
35. Record static bending.
36. If torque is to be applied, see Procedure for Operating NASA Complex Fatigue Research Machines with Bending and Torque Loads.
37. Set the clock to zero.
38. Put on the bridges.
39. Record dynamic conditions.
40. Check lubrication and oil level.

<u>To Remove Specimen</u>

1. Turn power off at the wall.
2. Block up loading arm.
3. Remove the brushes from the slip-rings - <u>this step is very important</u>.
4. Loosen both collets so the specimen is free to slide.
5. Remove the bridges.
6. Remove the keys.
7. Raise one side of the toolholder using a support bolt.
8. Remove collets and specimen.

APPENDIX D

PROCEDURE FOR OPERATING COMBINED BENDING-TORSION FATIGUE RESEARCH MACHINES WITH COMBINED BENDING AND TORQUE LOADS

1. Install specimen and balance Visicorder as per "Checklist."
2. Apply the torque to the required number of divisions, including the bending interaction divisions, using the Infinit-Indexer.
3. Stabilize the torque divisions as follows:
   a) Turn the machine by hand for at least five cycles. You will probably observe a decrease in the torque divisions.
   b) Re-torque machine to desired divisions and repeat the process until the mean torque level remains constant.
4. Start the run and observe the mean torque divisions insuring that it does not decrease. If no more than 2 divisions of downward shift in the mean torque divisions is observed, continue the run.
5. If more than 2 divisions of shift in the mean torque level in the downward direction is observed or if excessive upwards drift in the mean torque divisions

is observed, particularly 10 or more divisions, stop machine, remove pan weight, block up bending load train, block up loading arm until level, and remove torque by loosening in-board collet only (the side without the strain gages). Check to see where the new torque zero is. If the shift in the zero is within one division of the drift in the mean of the torque divisions, re-zero the torque channel, re-tighten the specimen and repeat Steps 3, 4, 5, and 6 until torque is stabilized.

6. If the zero shift is in excess of the drift in the mean torque divisions initiate an investigation as to its cause. Probable causes may be the following:
   a) True change in torque beyond the intended level.
   b) Change in strain gage characteristics, perhaps indicating a strain gage deterioration.
   c) Deterioration of amplifier components.
7. If the drift in the mean torque divisions is not in excess of 10 divisions, and a few specimens at the same stress level check out favorably in Steps 1 through 4, do not re-check the zero; finish run.

APPENDIX E

CALIBRATION OF NEW TORQUE GAGES FOR MACHINE #3, JUNE 1969

In May 1969, one of the strain gages in the torque bridge of the toolholder of Machine #3 failed. The gage was replaced and it was necessary to recalibrate. Since the bending bridge was left untouched, the only tests which had to be conducted were the torque load versus Visicorder output calibration and the bending interaction into torque calibration.

The results of these tests are presented below.

Torque Load Versus Visicorder Output

The procedure used is identical to the one presented in Section 3-C-1. The data appear in Table 18.

Data Reduction

The same data reduction technique that was used in Section 3-C-1 is used. Figure 42 gives the plot of the data of Table 18.

Table 18. Torque Output Versus Pan Weight Data for New Torque Gages, Machine #3, June 1969

Data Point Number	Torque Output div.	Pan Weight div.
1	3.3	0
2	13.1	10.27
3	22.6	20.54
4	31.3	30.81
5	40.6	41.08
6	31.9	30.81
7	22.6	20.54
8	13.2	10.27
9	3.4	0
10	13.2	10.27
11	11.7	10.54
12	31.9	30.81
13	40.7	41.09
14	31.9	20.54
15	22.7	20.54
16	13.3	10.27
17	3.4	0

Visicorder Calibration Resistance:
Machine #3 - 304 kΩ at 44.8 divisions

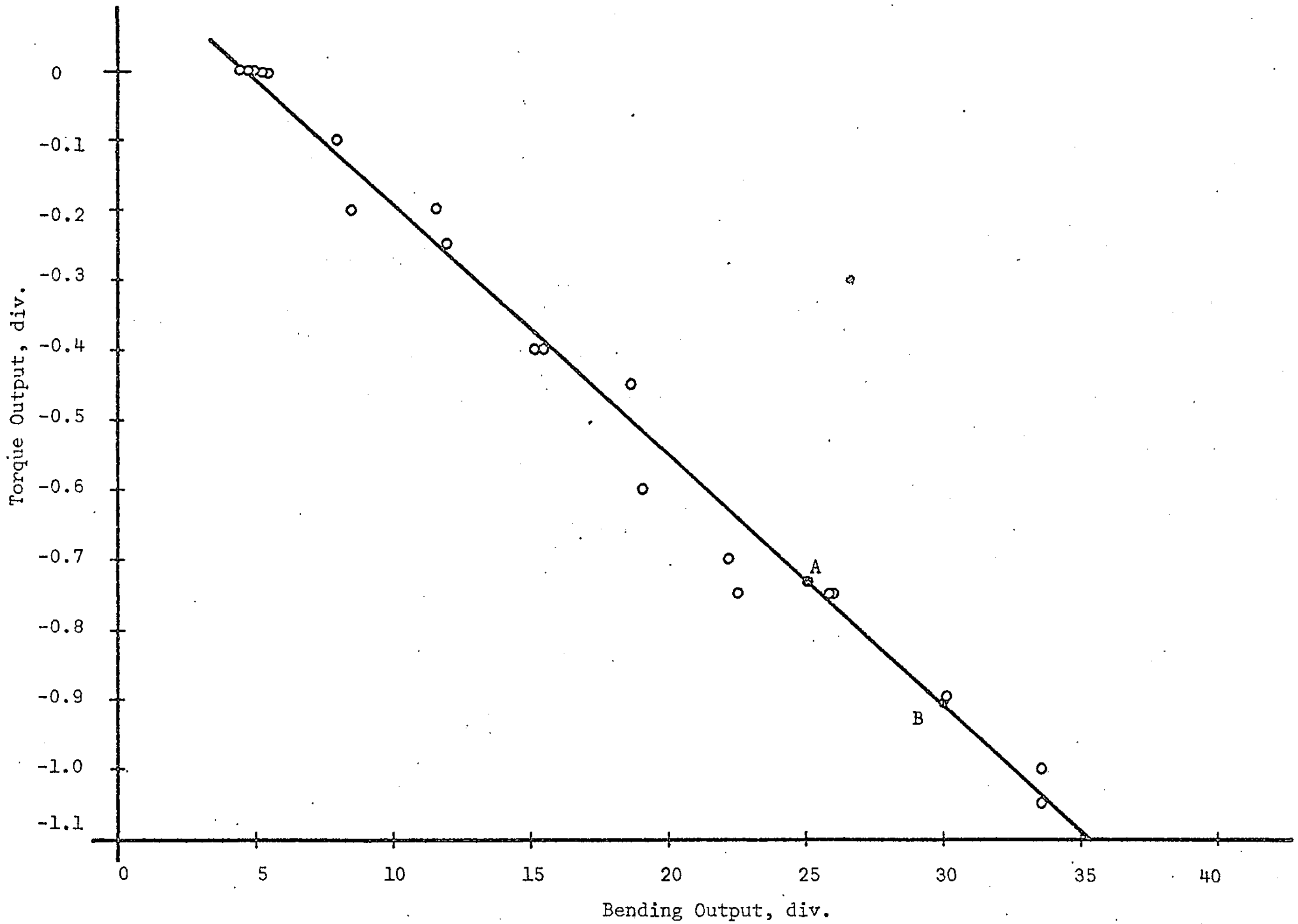

Fig. 42.--Bending Interaction into Torque - Machine #3, June 1969

Machine	Point	Point	W lbs	N_{vis} div	τ_{out} psi	τ_{true} psi	slope K_T
3	(40.0,40.0)	(2.5,6.0)	37.5	34.0	1008	848	0.842

Therefore,

$$K_T = 0.842$$

Bending Interaction Into Torque

For the bending interaction into torque procedure, consult Section 3-C-2. The method given there was followed exactly for this test. The data appear in Table 19.

Data Reduction

Using the graphical reduction technique from Figure 43,

Point A = (25.0, 0.73)

Point B = (35.0, 1.00)

$$N_{vis_B} = -\ 10.0$$

$$N_{vis_T} = +\ 0.27$$

$$\epsilon_B = \frac{N_{vis_B}}{N_{cal_B}} \frac{R_{gage}}{N_a \ G \ R_{cal}} = \frac{(-10.0)(190)}{(25.0)(4)(2.23)(490)(10^3)} = \begin{array}{l} 12.00 \\ \mu in/in \end{array}$$

$$\epsilon_T = \frac{N_{vis_T}}{N_{cal_T}} \frac{R_{gage}}{N_a \ G \ R_{cal}} = \frac{(0.27)(120)}{(45.3)(4)(2.06)(304)(10^3)} = \begin{array}{l} -.2855 \\ \mu in/in \end{array}$$

Table 19. Bending Output Versus Torque Output Data for New Torque Gages, Machine #3, June 1969

Data Point Number	Bending Output div.	Torque Output div.
1	4.4	0
2	7.9	-0.10
3	11.5	-0.20
4	15.1	-0.40
5	18.6	-0.45
6	22.2	-0.70
7	25.8	-0.75
8	30.0	-0.90
9	33.5	-1.00
10	30.0	-0.90
11	26.0	-0.75
12	22.5	-0.75
13	19.0	-0.60
14	15.4	-0.40
15	11.9	-0.25
16	8.4	-0.20
17	4.8	0
18	4.9	0
19	33.5	-1.00
20	5.5	0
21	33.5	-1.00
22	5.3	0
23	33.5	-1.05
24	5.5	0

Visicorder Calibration Resistances:
Machine #3 - Bending 490 kΩ at 25.0 divisions
Torque 304 kΩ at 45.3 divisions

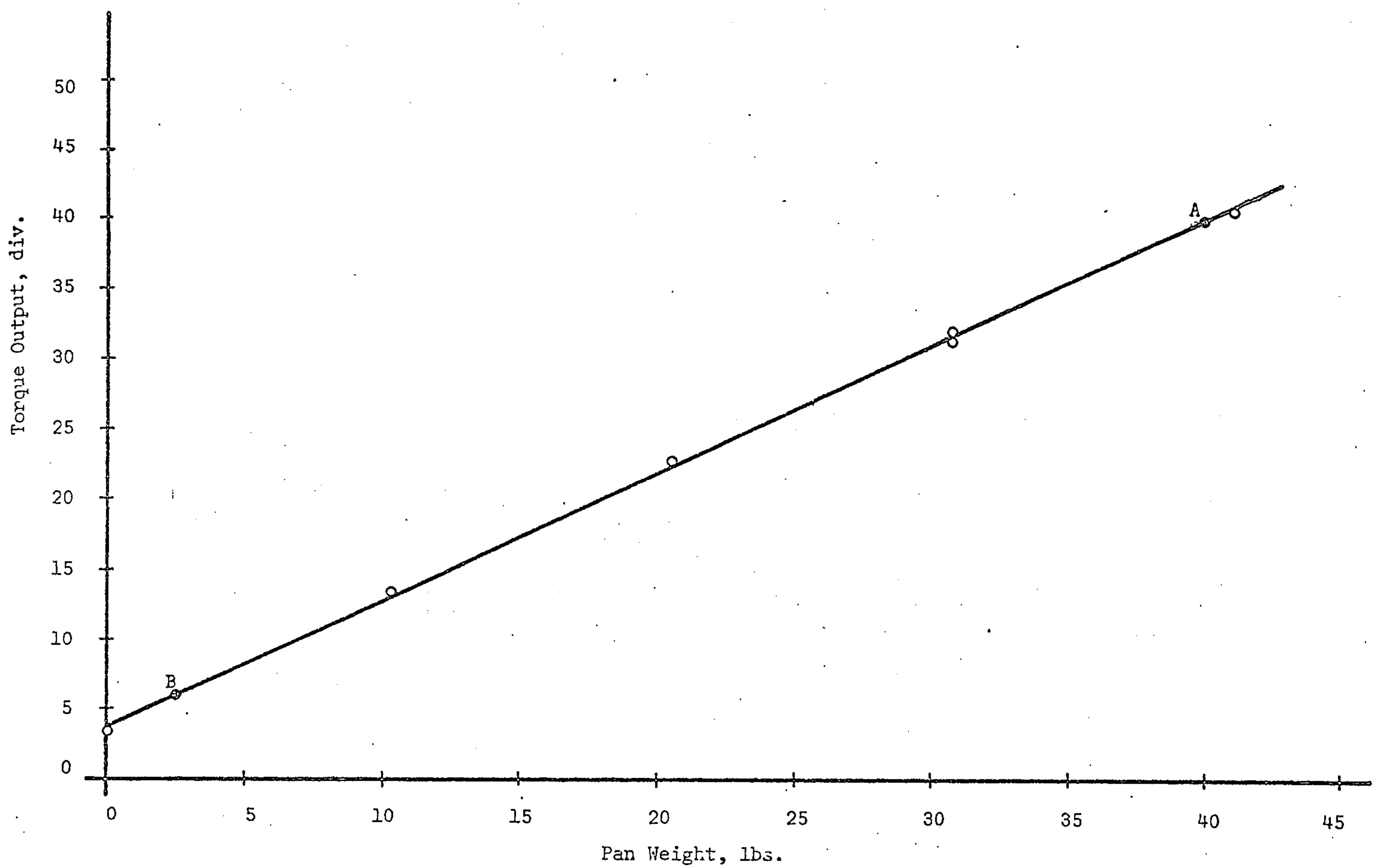

Fig. 43.--Torque Output Versus Pan Weight - Machine #3, June 1969

Therefore,

$$K_{B/T} = \frac{-0.2855}{12.00} = -0.0238.$$

APPENDIX F

MAINTENANCE CHECKLIST FOR COMBINED BENDING-TORSION FATIGUE RESEARCH MACHINES

Each Run

The level of the grease in the front shaft couplings and the level of oil in the gear box shall be checked and lubrication added if needed. The oil to be used in the gear box is Mobil D. T. E. Oil - BB.

Log the hours each machine has been run.

Every Month

Check front shaft couplings for proper amount of Marfak #1 grease.

Every Four Months

Front and back shaft couplings shall be cleaned, inspected and regreased with Texaco Marfak #1.

SYMBOLS

Arabic

Symbol	Meaning
C	Radius of shaft, in
div	Divisions
E	Young's Modulus, psi
F	Force, lbs
G	Strain gage factor
I	Moment of inertia of cross-section, in^4
in	Inches
k_a	Surface finish factor
K_{ave}	Experimentally determined static stress concentration factor
k_b	Size factor
K_{BGR}	Groove bending calibration coefficient
$K_{B/T}$	Bending into torque interaction coefficient
K_{BTH}	Toolholder bending calibration coefficient
k_d	Temperature factor
k_e	Stress concentration design factor
K_f	Dynamic stress concentration factor
k_f	Miscellaneous effects factor
K_{GR-TH}	Groove-toolholder calibration coefficient
K_T	Toolholder torque calibration coefficient

Symbol	Meaning
K_t	Static stress concentration factor
K_{ts}	Static stress concentration factor in shear
$K_{T/B}$	Torque interaction into bending calibration coefficient
L	Lever arm distance, in
lbs	Pounds
M	Moment, lb-in
N_a	Number of active arms in strain gage bridge
N_{cal}	Visicorder calibration divisions, div
N_{vis}	Visicorder output, div
q	Notch sensitivity factor
r_s	Stress ratio
R_{cal}	Calibration resistance, ohms
R_{gage}	Resistance of strain gage, ohms
$\overline{S}_e$	Mean of endurance strength, psi
S_e	Endurance strength, psi
$S_{e_{10^3}}$	Fatigue strength for 10^3 cycles, psi
S	Ultimate strength, psi
S_U	Ultimate strength, psi
V	Coefficient of Variation, %
W	Pan weight, lbs
w	Loading, lbs/in
W_{bear}	Weight of the bearing, lbs
w_{col}	Weight of the collet, lbs

Symbol	Meaning
W_{coup}	Weight of the coupling, lbs
W_{nut}	Weight of the collet assembly nut, lbs
W_{slip}	Weight of the slip-ring assembly, lbs

Greek

ϵ	Normal strain, micro in/in
μ	Mean
σ	Normal stress, psi
σ_S	Standard deviation of normal distribution
σ_{S_e}	Standard deviation of endurance data, psi
τ	Shear stress, psi

Subscripts

B	Bending
GR	Specimen Groove
out	Output
TH	Toolholder
T	Torque
vis	Visicorder

REFERENCES

1. Kececioglu, Dimitri, and David Cormier, "Designing a Specified Reliability Directly Into a Component," Proceedings of the Third Annual SAE-ASME-AIAA Aerospace Reliability and Maintainability Conference, Washington, D. C., pp. 546-565, June 29-July 1, 1964.

2. Freudenthal, A. M., "Safety, Reliability and Structural Design," American Society of Civil Engineers Transactions, Vol. 127, Part II, pp. 304-323, 1962.

3. Freudenthal, A. M., J. M. Garrelts, and M. Shinozuka, "The Analysis of Structural Safety," Institute for the Study of Fatigue and Reliability, Columbia University, New York, N. Y., 129 pp., June 1965.

4. Mittenbergs, A. A., "Fundamental Aspects of Mechanical Reliability from Mechanical Reliability Concepts," ASME Design Engineering Conference, New York, N. Y., pp. 17-33, May 17-20, 1965.

5. Clover, A. H., A. R. Rosenfield, A. A. Putnam, R. E. Mesloh, L. M. Cassidy, R. Simon, and A. A. Mittenbergs, "Sixth Progress Report to MRRC Members," Battelle Memorial Institute, Columbus, Ohio, March 31, 1965.

6. Bush, T. L., A. P. Meyers, and D. F. Semonaitis, "Methods for Prediction of Electro-Mechanical System Reliability," IIT Research Institute Technology Center, Chicago, Ill., 173 pp., May 1965.

7. Bratt, M. J., G. Reethof, and G. W. Weber, "A Model for Time Varying and Interfering Stress-Strength Probability Density Distributions with Considerations for Failure Incidence and Property Degradation," Proceedings of the Third Annual SAE-ASME-AIAA Conference on Aerospace Reliability and Maintainability, Washington, D. C., pp. 566-575, June 29-July 1, 1964.

8. Lipson, C., J. J. Sheth, and R. L. Disney, "Reliability Prediction - Mechanical Stress/Strength Interference," Rome Air Development Center, Griffiss Air Force Base, New York, 450 pp., 1967.

9. American Society for Testing Materials, "References on Fatigue - ASTM STP 9G-9N," Philadelphia, Pa., 1955-1963.

10. American Society for Testing Materials, "Proceedings of the Symposium on Large Fatigue Testing Machines and Their Results" - ASTM STP No. 216, p. 151, Philadelphia, Pa., p. 151, 1957.

11. American Society of Mechanical Engineers, "Seventy-Seven Year Index," New York, 1957.

12. The H. W. Wilson Company, "Applied Science and Technology Index," New York, 1958 to December 1965.

13. Society for Experimental Stress Analysis, "Proceedings of the Society for Experimental Stress Analysis," Cambridge, Mass., 1943-1960.

14. Journal of the Society for Experimental Stress Analysis, "Experimental Mechanics," Easton, Pa., 1961-December 1965.

15. Mabie, H. H., and M. S. Gjesdahl, "A Fatigue Testing Machine for Reversed Bending and Steady Torque," Proceedings of the Society for Experimental Stress Analysis, Vol. 14, No. 1, Cambridge, Mass., pp. 83-88, 1956.

16. Falk Corporation - Photographs and Correspondence submitted to Dr. Dimitri B. Kececioglu, NASA NGR-02-002-044, University of Arizona, Tucson, Arizona, Milwaukee, Wisconsin, October 1965.

17. Mabie, H. H., Correspondence, Professor of Mechanical Engineering, Virginia Polytechnic Institute, Blacksburg, Virginia, Sept. 1965.

18. Burr, Arthur H., Professor in charge, Department of Machine Design, Sibley School of Mechanical Engineering, Cornell University, Ithaca, New York, Correspondence, October 1, 1965.

19. Burr, Arthur H., Professor in Charge, Department of Machine Design, Sibley School of Mechanical Engineering, Cornell University, Ithaca, New York, Correspondence, September 1965.

20. Mabie, H. H., "Four-Square Test Machine," D/N 100, Department of Mechanical Engineering, Pennsylvania State College, August 10, 1951.

21. Sibley School of Mechanical Engineering, "Four-Square Test Machine Modified," D/N 100, Cornell University, Ithaca, New York, September 13, 1957.

22. Mabie, H. H., Professor of Mechanical Engineering, Virginia Polytechnic Institute, Correspondence, Blacksburg, Virginia, January 1966.

23. Peterson, R. E., Stress Concentration Design Factors, John Wiley and Sons, Inc., New York, 155 pp., 1953.

24. Kececioglu, D. B., M. J. Saroni, H. W. Broome, and J. McConnell, "Design and Development of and Results from Combined Bending-Torsion Fatigue Reliability Research Machines," NASA, Washington, D. C., p. 57, July 15, 1969.

25. Shigley, J. E., Mechanical Engineering Design, McGraw-Hill Book Company, Inc., New York, 631 pp., 1963.

26. Yokobori, T., Strength, Fracture, and Fatigue of Materials, P. Noordhoff, Ltd., Groningen, The Netherlands, 372 pp., 1964.

27. Juvinall, R. C., Stress, Strain, and Strength, McGraw-Hill Book Company, Inc., New York, 580 pp., 1967.

28. Madayag, A. F., Metal Fatigue: Theory and Design, John Wiley and Sons, Inc., New York, 425 pp., 1969.